universität wien

MASTERARBEIT | MASTER'S THESIS

Titel | Title

Tectonostratigraphic evolution of the Eastern Alps-Danube Basin transition using high-resolution lake seismic data from Neusiedler See (Eastern Austria)

verfasst von | submitted by

Sebastian Keglovits BSc

angestrebter akademischer Grad | in partial fulfilment of the requirements for the degree of

Master of Science (MSc)

Wien | Vienna, 2025

Studienkennzahl lt. Studienblatt | Degree programme code as it appears on the student record sheet:	UA 066 815
Studienrichtung lt. Studienblatt | Degree programme as it appears on the student record sheet:	Masterstudium Erdwissenschaften
Betreut von | Supervisor:	Mag. Dr. Erich Draganits Privatdoz.
Mitbetreut von | Co-Supervisor:	Dr. Katerina Schöpfer

ABSTRACT

2D lake seismic data consisting of two seismic surveys from the northern area of Lake Neusiedl were analyzed. The main software used for preparing and interpreting the seismic dataset was Schlumberger Petrel (2023). A quality assessment revealed offsets between the two seismic surveys and internal inconsistencies within the multichannel survey. After refining the dataset, seismic horizons and faults were manually interpreted and mapped. The geometries of identified features were categorized and selected features further correlated to the broader stratigraphic context of the region. Finally, a tectono-stratigraphic model was developed for the westernmost part of the Danube Basin linking the findings of this study to well logs and vintage seismic data situated east of the survey and the Leitha Mountains to the west respectively.

ZUSAMMENFASSUNG

2D Seeseismische Daten, bestehend aus zwei seismischen Untersuchungen aus dem nördlichen Bereich des Neusiedler Sees, wurden analysiert. Die Hauptsoftware zur Aufbereitung und Interpretation der Daten war Schlumberger Petrel (2023). Eine Qualitätskontrolle der Daten ergab Versätze der Daten zueinander sowie innerhalb. Nach einer Korrektur und Qualitätskontrolle wurden seismische Horizonte und Störungen kartiert und interpretiert. Geometrien identifizierter Strukturen wurden kategorisiert, wobei einige Strukturen weiter für die Erstellung eines tektono-stratigraphischen Modells verwendet wurden, welches Bohrlochdaten und ältere seismische Daten im Seewinkel, östlich des Neusiedler Sees, mit geologischen Beobachtungen des Leithagebirges verknüpft.

ACKNOWLEDGEMENT OF THE USAGE OF AI

I acknowledge the use of the AI tool Perplexity (https://www.perplexity.ai/) to help me in the refinement of my academic language and to generally identify improvements in the writing style. I confirm that I have read and understood the AI usage guidelines from the University of Vienna and that this thesis complies with them.

ACKNOWLEDGEMENTS

I want to thank first and foremost my supervisor, Kateřina Schöpfer, Mgr., PhD, for her sheer endless motivation and energy to teach me and help me create this work. Her guidance and support were and will be invaluable. I also want to thank my principal supervisor Erich Draganits, PD Mag. Dr, for giving me the opportunity of writing a thesis and his always supportive suggestions. This work would have not been possible without the generous provision of the seismic data by Gabor Tari, Msc., PhD (OMV). Finally, I want to thank all the people that helped me in other but not less important ways to finish this path: My family for supporting me through this journey and my friends and colleagues for always being there.

Table of Contents

1. INTRODUCTION

This study uses high-resolution 2D seismic data in the area of Lake Neusiedl (German: Neusiedler See, Hungarian: Fertő-tó), which is located in Burgenland, Austria (Fig. 1), to unravel tectono-stratigraphic evolution of the western part of the Danube Basin. This area is characterized by a low-lying, low-relief landscape, dominated by Quaternary fluvial and lacustrine sediments, deposited on top of Upper Pannonian (= Tortonian, Upper Miocene) lacustrine sediments (Fuchs and Schreiber, 1985). This region is situated at the tectonic and geomorphological boundary between the Alps, Carpathians and the Pannonian Basin (Székely et al., 2009). The Vienna Basin towards the west (Fig. 2) has been intensely explored based on data from decades of hydrocarbon prospection (e.g. Harzhauser et al., 2022, 2026). Although the Danube Basin has been studied for many years (Tari, 1996; Šujan et al., 2016; Zámolyi et al., 2017; Tari et al., 2024), the westernmost lying sub-basin, which lies adjacent to the Leitha Mountains, is still relatively poorly understood and drew little attention (Hodits, 2006; Zámolyi et al., 2017; Loisl et al., 2018, 2025). It is owing to the lack of modern deep boreholes and absence of good quality seismic data. In May 2013, 2D multichannel and single-channel seismic data was acquired in the northern part of the Lake Neusiedl, for details on setup, data acquisition and interpretation see Loisl et al., (2018). This multinational campaign resulted in the first high-resolution seismic survey in the area and revealed a more complex structural regime than previously recognized. The seismic data enabled to identify key geological features including progradational clinoforms and paleochannel systems, providing unprecedented insight into the subsurface architecture beneath the lake. The work also discussed gas seeps and subhorizontal flat spots possibly indicating biogenic gas.

The goal of this thesis is to revisit the seismic data and analyzed structural setting, lateral extent of individual seismic surfaces and external/internal geometries of seismic features in greater detail to achieve more refined tectonostratigraphic model of the area. The analysis of data can possibly lead to an alternative interpretation of the features such as flat spots identified in Loisl et al. (2018).

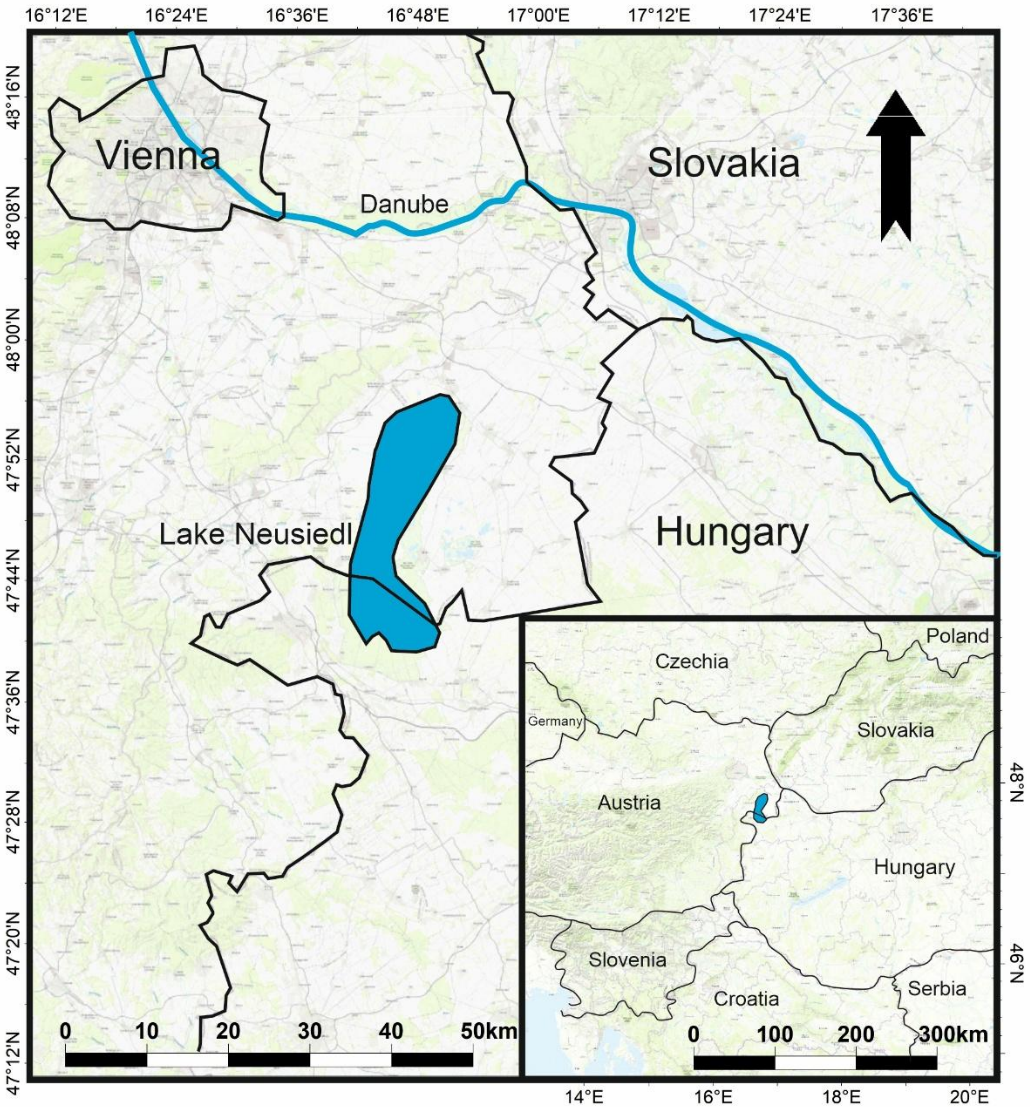

Figure 1. Local and regional geographic overview of Lake Neusiedl, stretching over two countries: Austria in the north and Hungary in the south.

The goals of this master´s thesis are:

- To achieve alignment between shallow single-channel and deeper multichannel seismic data.
- To map thickness of individual seismic package to identify sedimentary depocenters and their shift during the Miocene.
- To map faults and define their age – syn-sedimentary activity or reactivation of older structures.
- To map deltaic and fluvial features in detail to estimate the main flow direction and their distribution in the study area.
- To analyze the deltaic structures and their position in the seismic stratigraphy, which could help to establish more precise age estimates of individual seismic packages. This is vital as no deep boreholes exist in the area.
- To refine the existing tectono-stratigraphic model of the westernmost sub-basin of the Danube Basin (Loisl et al., 2018) to improve our understanding of the deeper parts of the basin, fault activity in the area and the connection to the sedimentary area west and east of Lake Neusiedl, the latter recently studied by Loisl et al. (2025).

2. GEOLOGIC SETTING

Lake Neusiedl is located southeast of Vienna in Burgenland at the border between Austria and Hungary (Fig. 1). The exact age of Lake Neusiedl is still not clear, but it has been estimated to some 12-14 thousand years (Löffler, 1980). At present the lake is less than 1.8 m deep and the lake level always has been showing strong variations; changes in its appearance and morphology became accelerated in the last centuries due to human activity (Draganits et al., 2022) The thickness of Lake Neusiedl sediments overlaying Pannonian strata is usually less than 0.7 m only (Heine et al., 2016).

The study area is located in a basin, which is bound by the eastern Alps to the west, the Leitha mountains to the NW the western Carpathians to the NE and the Transdanubian Range to the SW (Fig. 2). Name of this basin in the literature varies: the Danube Basin (DB)(Šujan et al., 2021), little Hungarian plain (geographic) (Zámolyi et al., 2017) and the Danube/Kisalföld Basin (DKB)(Sztanó et al., 2016). For consistency, the name Danube Basin is used throughout the thesis. The seismic surveys used in this study are located in the NW part of the Danube basin, which is considered a transitional zone between the eastern Alps and the Pannonian basin (Zámolyi et al., 2017).

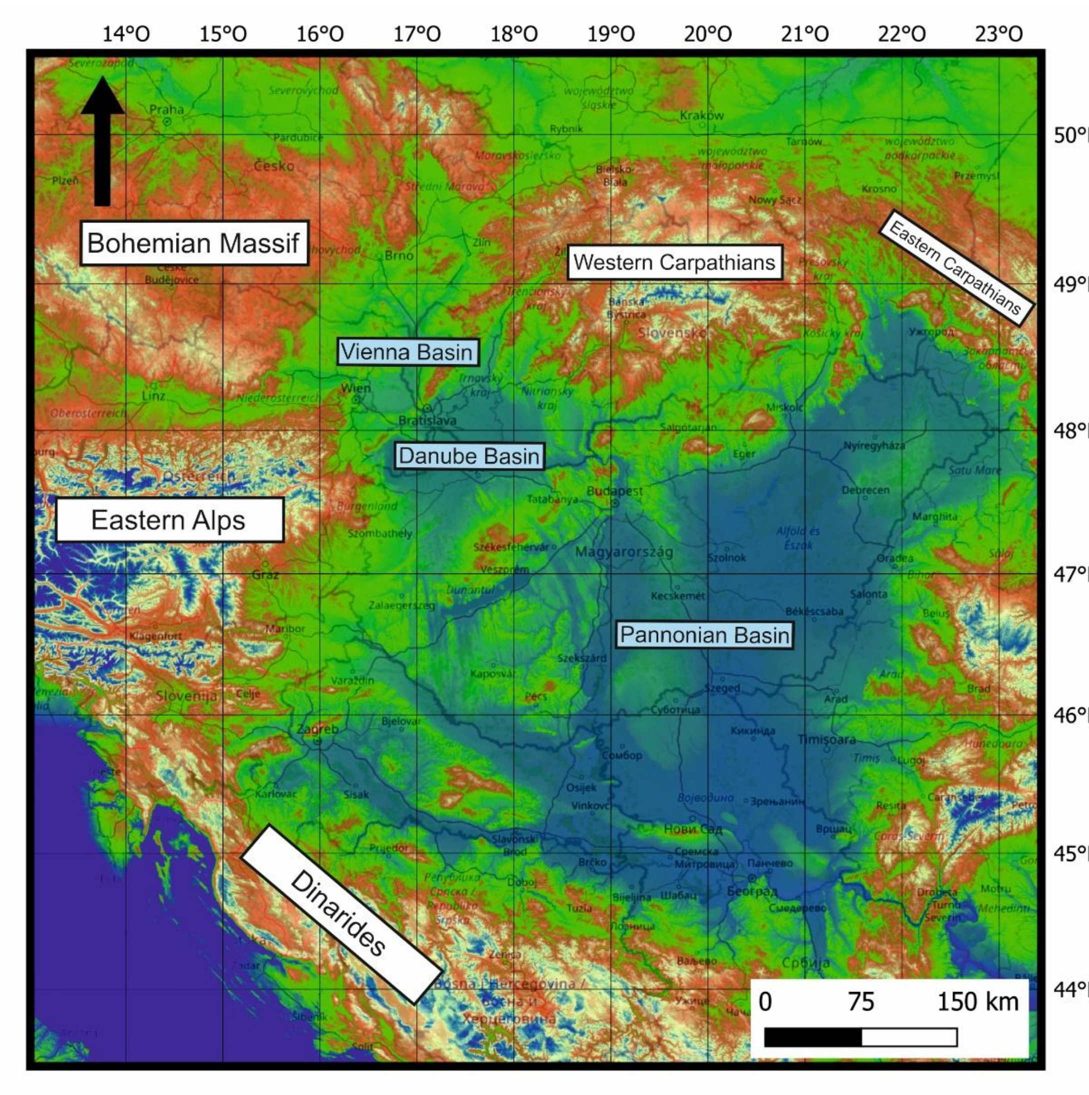

Figure 2. Regional setting of the Pannonian Basin and its subbasins: the Danube Basin and the Vienna Basin, bounded by surrounding orogens (Eastern Alps, Western Carpathians, and Dinarides) and the Bohemian Massif.

The Danube basin itself is the western part of the Pannonian Basin System (PBS) or often just Pannonian Basin, that was formed during the Miocene as part of the lateral extrusion of the Eastern Alps following thermal subsidence (Csontos and Vörös, 2004; Tari et al., 2024; Sztanó et al. 2025).The Pannonian Basin transitioned from the marine environments of the Paratethys, to the lacustrine environment Lake Pannon, as a result of tectonic isolation at the end of the Sarmatian. This environmental shift was accompanied by significant changes in sedimentary deposition and water input.

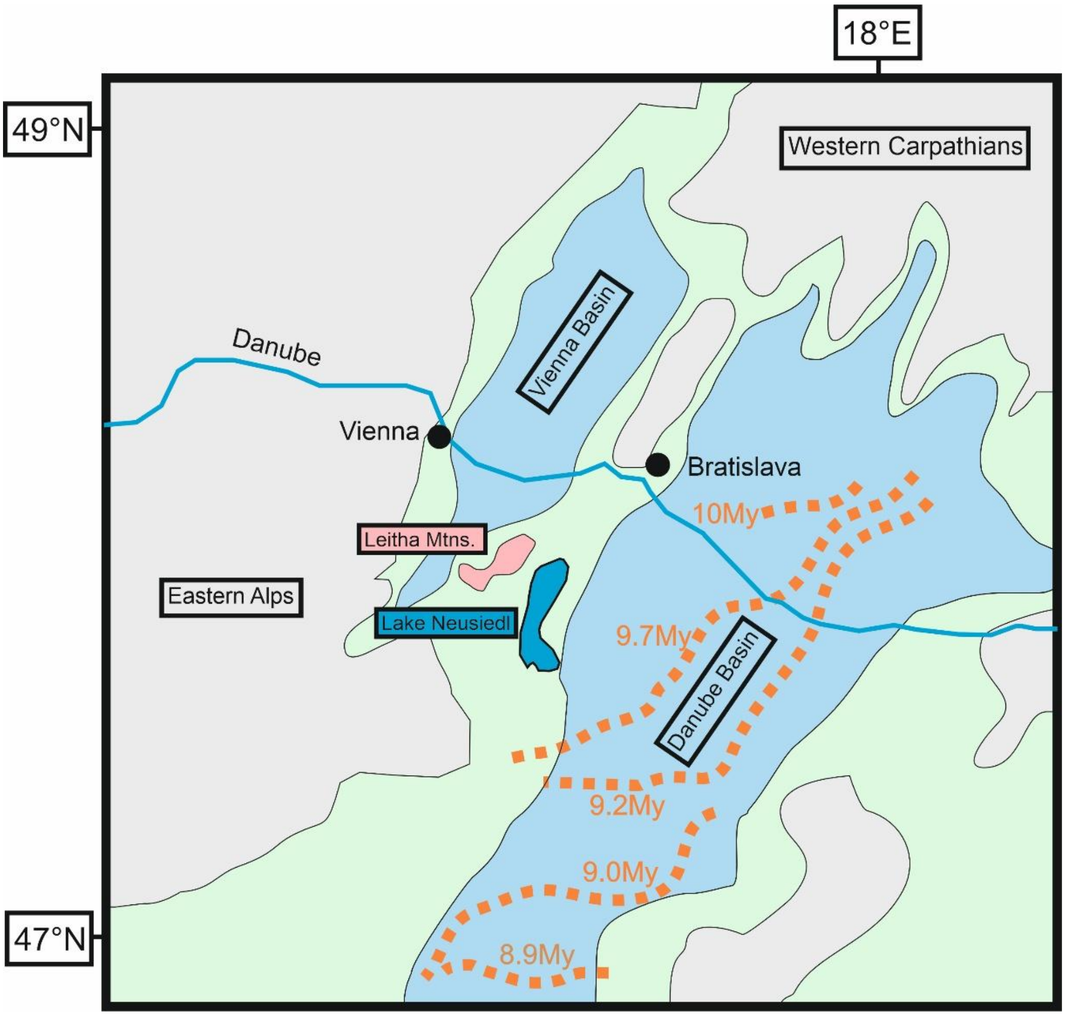

Figure 3. Schematic overview of basement units surrounding Lake Neusiedl and proximal sub-basins (grey: pre-Cenozoic units; blue: basins, green: Miocene sediments). Orange dots highlight the shelf margins of the Paleo-Danube delta system, with ages indicating progressive southward migration. Modified from Magyar et al., 2013.

The lake expansion was probably related to increased precipitation during the early Late Miocene (Böhme et al., 2011). When precipitation rate decreased, progradation began to take over at around 10 Ma and advanced across the basin. This progradation lead to the first clinoforms (Fig. 3; Magyar et al., 2013) marking the beginning of the infill and change in environment from lacustrine to alluvial of Lake Pannon that lasted until 4 Ma with the closing of the lake altogether c. The Danube Basin was affected by basin inversion at around 6 Ma (Šujan et al., 2021).

The Danube Basin is generally divided into three stratigraphic units: pre-rift, syn-rift, and post-rift. Pre-rift unit consists of the pre-Cenozoic basement. Rifting began in the middle-late Miocene and is characterized by multiple phases, as described by (Šujan et al., 2021)These phases span from the Early Badenian to the Early Late Miocene (approx. 15.2-9.5 Ma), with the later phases particularly affecting the middle parts of the basin. Post-rift phase was characterized by thermal subsidence and consequent accumulation of thick sedimentary strata of Upper Miocene age (Magyar et al., 2020) until 6 My ago, followed by basin inversion that is still ongoing (Šujan et al., 2021)

In the vicinity of the high-resolution lake seismic survey used in this study, the deep wells Podersdorf 001 and Frauenkirchen 001, situated east of the studied region, serve as the only direct stratigraphic information sources (Fig. 4). Unfortunately, these are not located directly within the studied region and their correlation is problematic. The deepest deposits seen in the seismic surveys could be correlated to Middle and Upper Miocene sediments that crop out in the Leitha Mountains, west of the study area (Schmid, 1968; Wiedl et al., 2014).

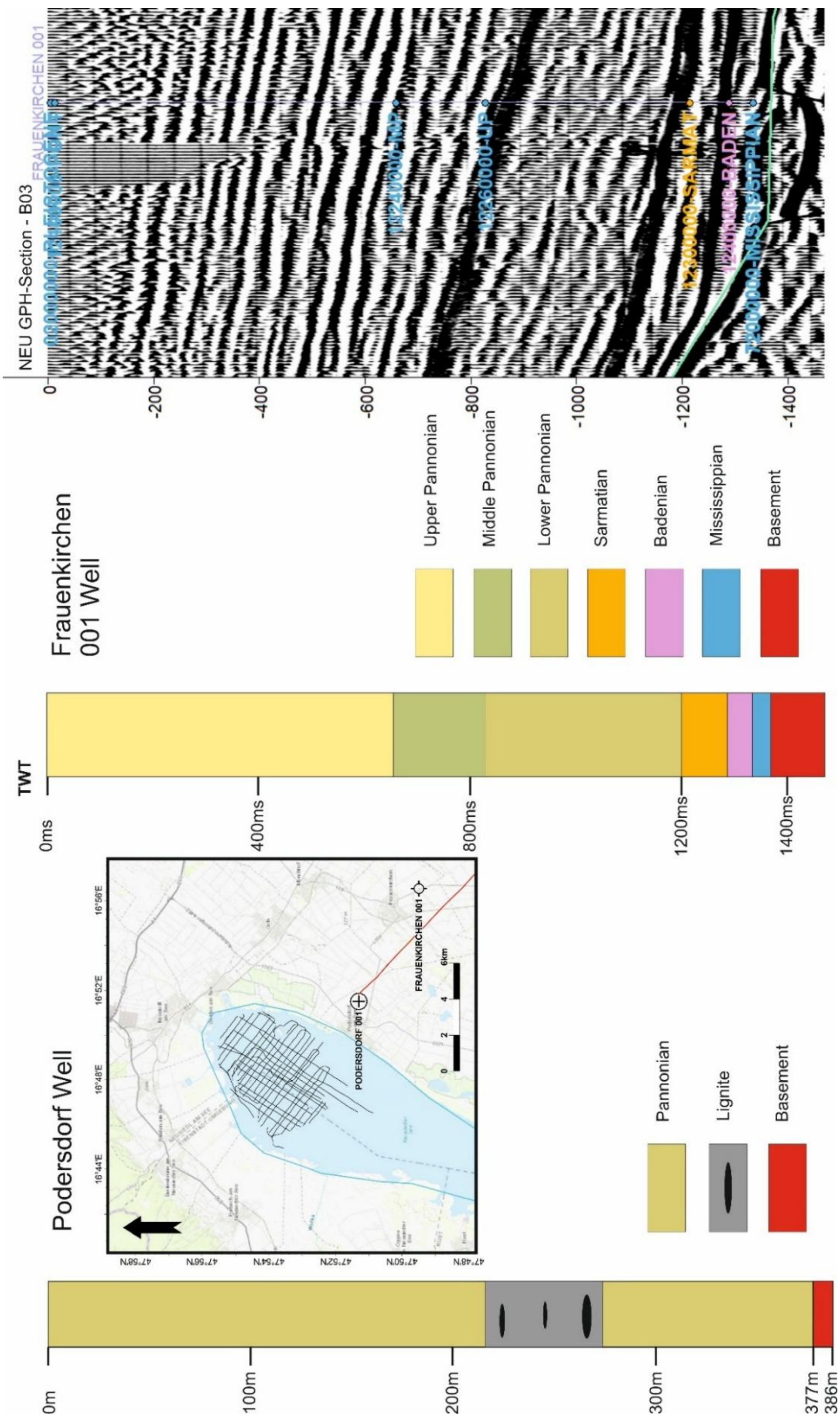

Figure 4. The two most important wells that are used for the newly derived tectonostratigraphic model as well as and representthe stratigraphy of the region. The Podersdorf Well (left, in meters) was adapted from well log data from 1947 from the Kohle-Öl-Union. The Frauenkirchen 001 well (center, in ms two-way-travel time,TWT) was adapted from data already in the dataset (right). A map overview is given depicting both wells, the multichannel seismic lines (in black) and the B03 Vintage seismic line from OMV (in red), with the right image showing a part of the seismic line and projected well top data.

3. METHODOLOGY

3.1. General Information

The analyzed dataset comprises two different seismic surveys, measured in May 2013, located in the northern part of lake Neusiedl, with a combined length of over 400 km. Both surveys are presented in two-way travel time (TWT) with an average velocity of 2500m/s (Loisl et al., 2018). The multichannel seismic data reaches depths of up to 700 ms TWT with a line spacing of 250 m to 500 m. The vertical resolution of the multichannel is in the order of tens of meters. The single-channel seismic data, offering a super high-resolution of tens of decimeters, reaches depths of 60 TWT with a line spacing of approximately 50 meters. The seismic resolution of multichannel data generally allows for interpretation down to the top of the acoustic basement, while coherent features of the single-channel data can be interpreted down to c. 40 TWT; below that the seismic resolution is too low. Changes in seismic resolution of the multichannel data were also observed horizontally, with a general trend of decreasing seismic resolution towards the southeast. The study area and the coverage of the two seismic surveys is shown in Figure 5. The main program used for preparing and interpreting the seismic dataset was Schlumberger Petrel (2023). Horizons as well as faults were interpreted manually, in order to follow correct seismic reflectors. Additionally, surfaces and time thickness maps were generated using Petrel 2023.

In this study, the seismic stratigraphic framework follows the methodology and terminology of (Mitchum et al.,1977). The seismic character, reflector geometries, bounding relationships and external/internal geometry of layers and bodies led to the identification of different seismic packages and features.

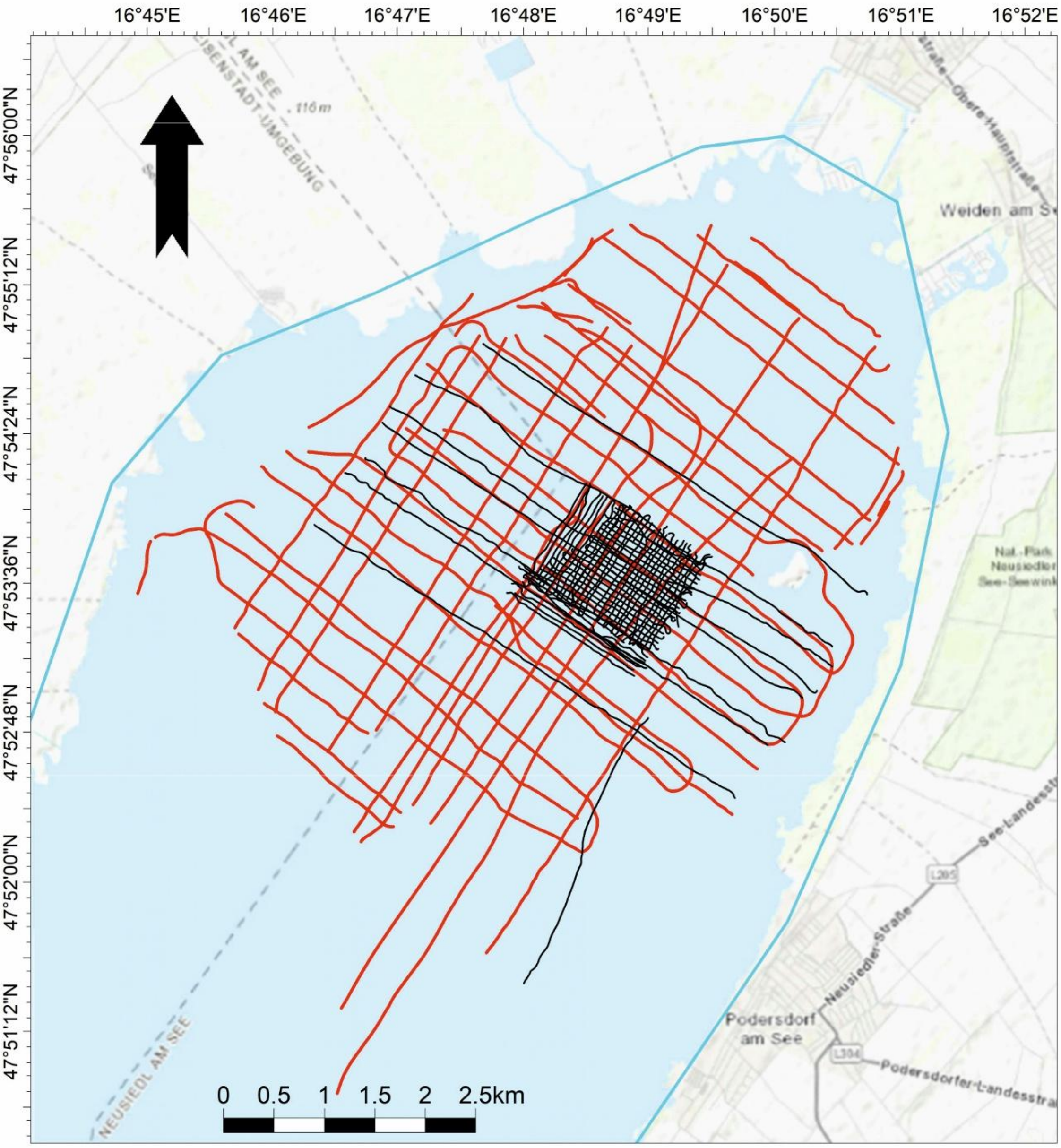

Figure 5. Regional map showing the northern part of lake Neusiedl with its seismic coverage. Seismic lines of single-channel data are shown in black and multichannel survey is shown in red. Map data from (Esri, 2025)

3.2 Data Preparation and Quality Check

At the beginning of this thesis, the correct import of the seismic data into the program was checked. The multichannel seismic data required various adjustments vital for reliable horizon and fault interpretation as well as a precise correlation with the a single-channel survey. As seen in Figure 7. the top of the multichannel data seemed incorrectly vertically aligned, resulting in offsets ranging from 20 to 30 TWT. Some seismic images of the multichannel seismic lines appear to have a cutoff of the uppermost section (Fig. 8). Figure 8 also displays an example, where an internal vertical offset between two multichannel seismic lines is observed. These smaller offsets within the multichannel survey were in the range of 5 TWT. The single-channel survey seemed to be correctly aligned in the Petrel project and was therefore picked as reference datum for the multichannel survey.

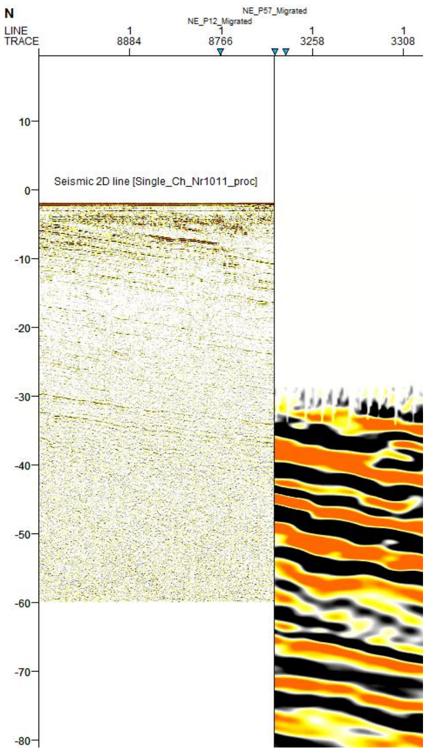

Figure 6. Visible vertical offset between two seismic lines of the single-channel and multichannel data respectively. Single-channel shown on the left, multichannel on the right side.

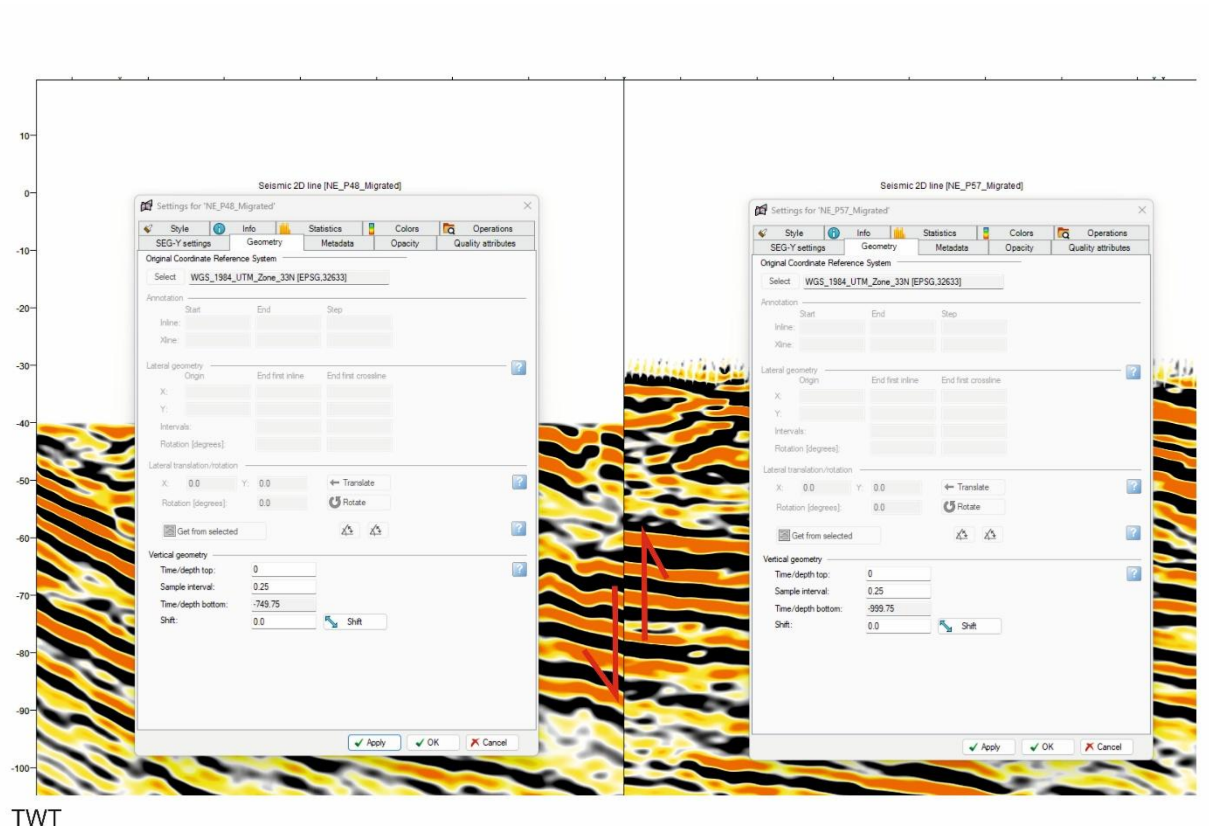

Figure 7. Visible vertical offset between two seismic lines of the multichannel survey; with depths set to 0. Left seismic image lacks the uppermost part. Red arrows mark the offset.

Assuming the highest parts of the multichannel is close to the surface (lake bottom), a random seismic image was picked and shifted up so that the first seismic reflector matches the starting level of the seismic of the single-channel data. This first multichannel seismic line then served as an “anchor” for all other seismic lines in the multichannel survey and was used to calibrate the depth respectively to the alignment of the internal structures of the dataset. After calibration, the seismic image with the highest seismic reflector was picked as the new “anchor” and its altitude adjusted accordingly with the depth of the start of the single-channel survey. This height difference was then applied to the whole survey. This process assured, that no seismic image was above 0 TWT whilst alignment of the inner features (e.g., continuation of individual seismic reflectors throughout the survey without artificially created offsets due to improper alignment) was still maintained throughout the whole survey. The result was a clean and interpretable set of seismic images that were more realistic and correctly vertically aligned (Figure 8). As a result, a realistic geometrical relationship between the single- and the multichannel seismic surveys was established as well. Figure 9 shows an example of a composite image of both seismic surveys now being correctly aligned to reflect horizon lateral coherence.

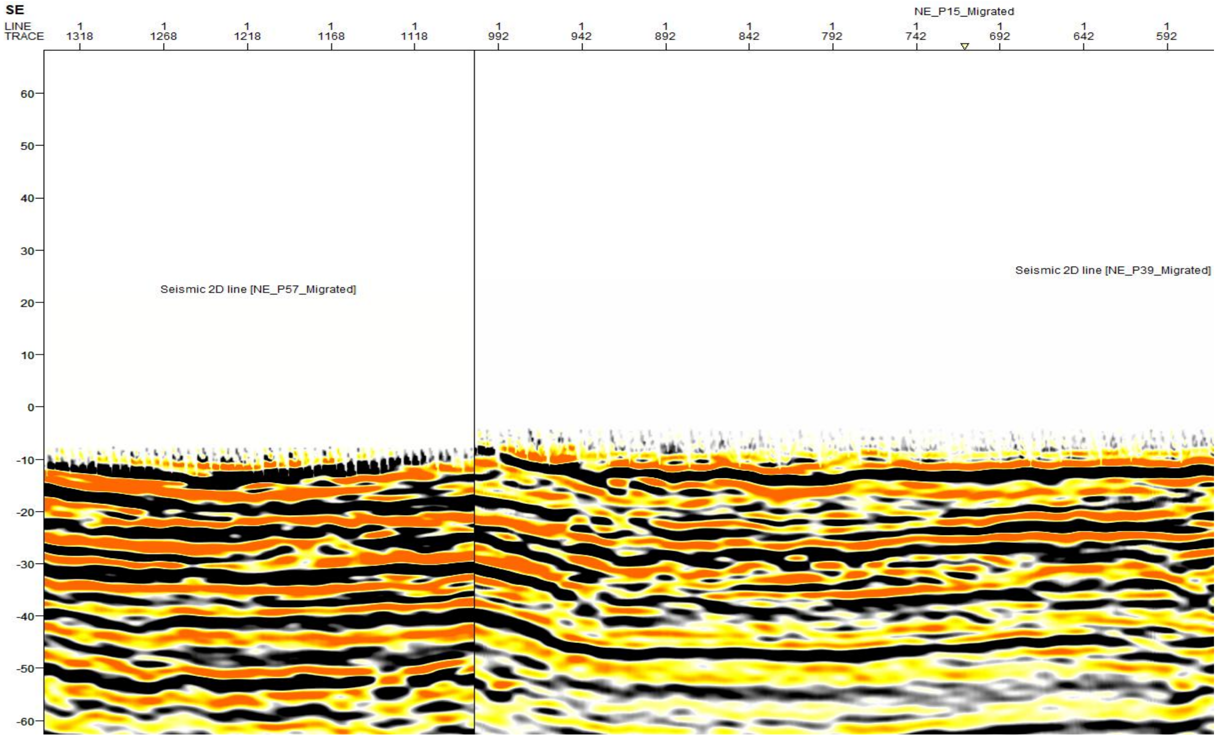

Figure 8. Composite section of two multichannel seismic images after the depth calibration and internal offset adjustment.

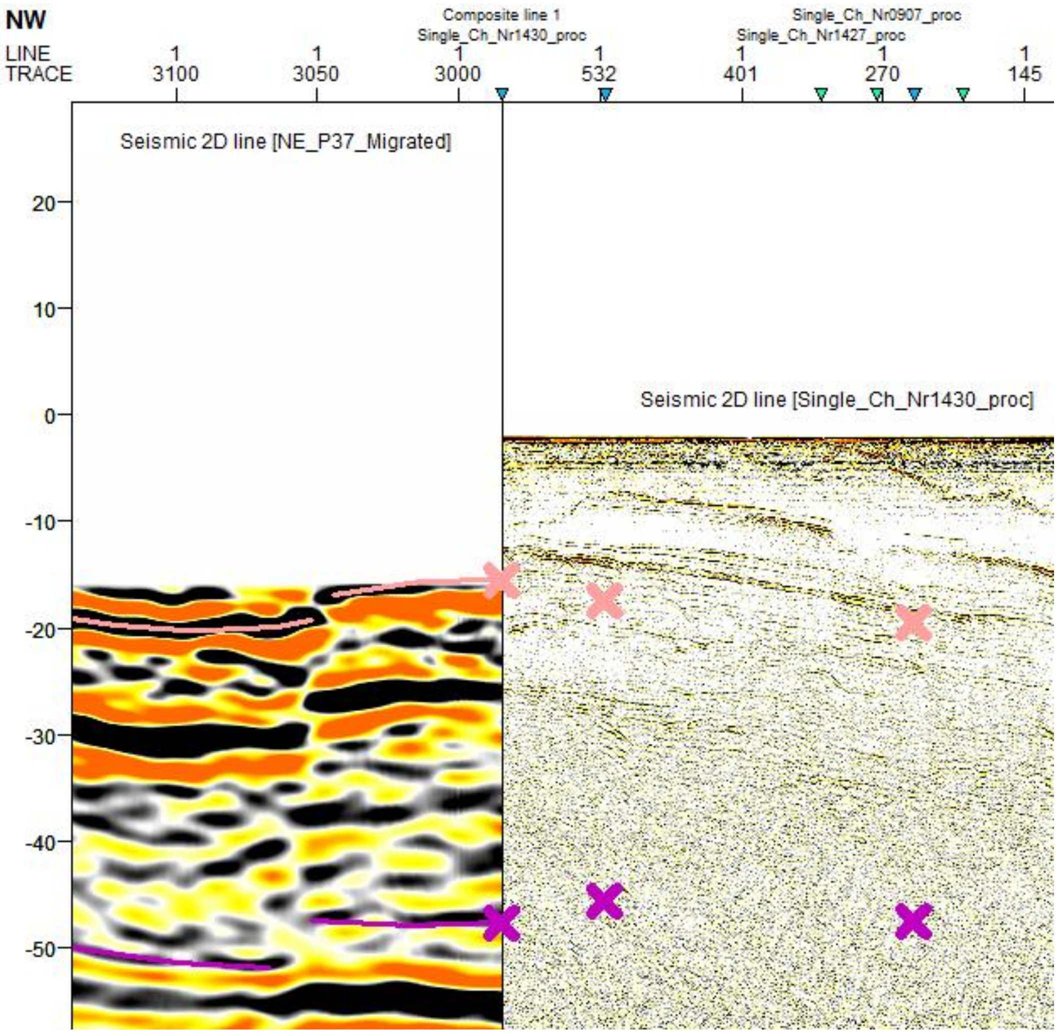

Figure 9. Composite section of single and multichannel seismic lines. Mapped horizons 1 (light pink) and horizon 2 (purple) are visible in both seismic images and correlate well.

After described data processing, a good correlation of seismic features between multichannel and single-channel surveys was achieved (Figure 10).

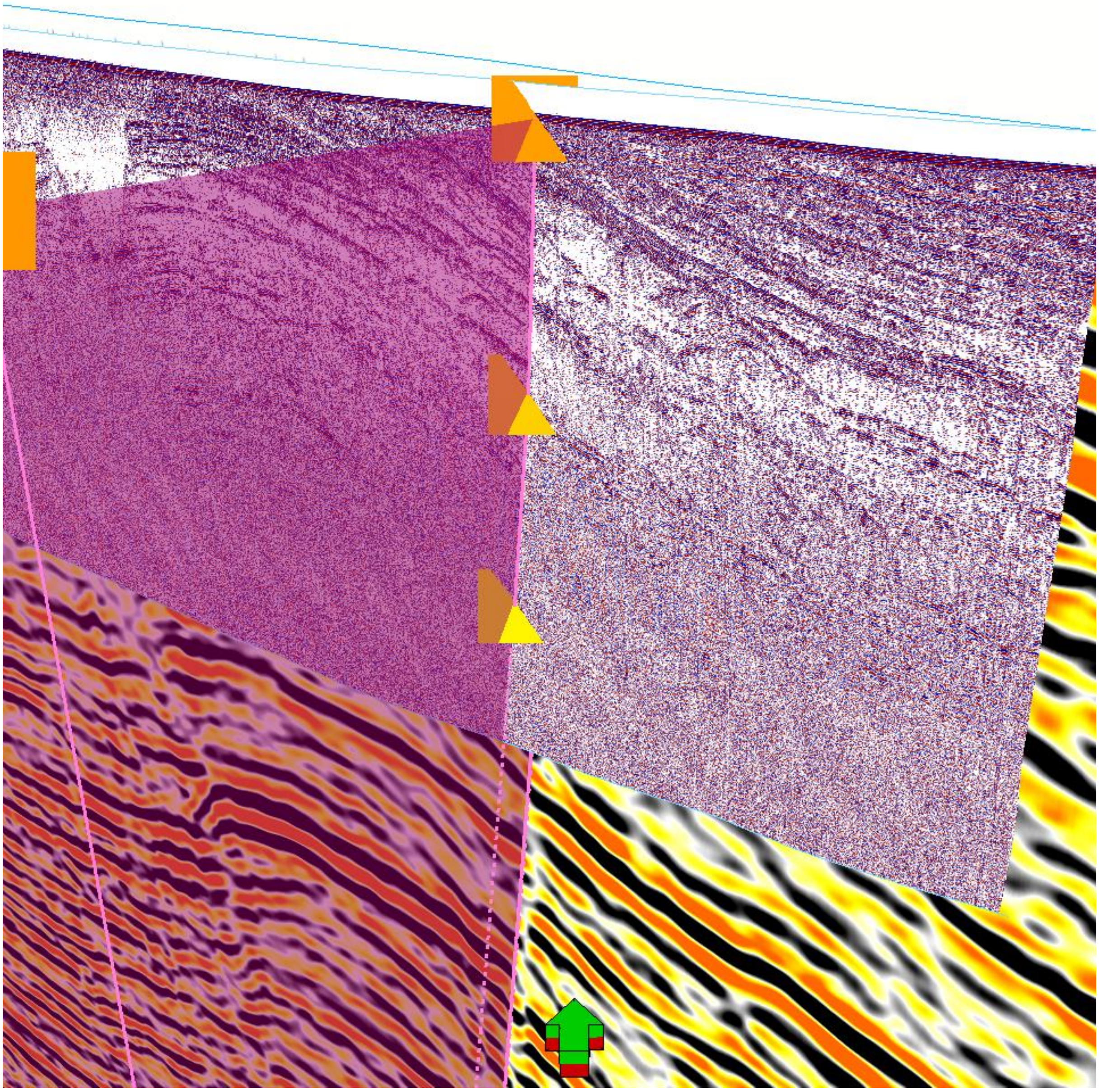

Figure 10. A single-channel seismic line (in the front) and multichannel seismic line (in the background) both display a single fault. The fault is clearly visible in both seismic lines and correlates very well. At the top, both seismic lines are now aligned correctly.

3.3. Horizon mapping

Mapping of the horizons was an iterative process involving the identification of key seismic reflectors, mapping portions of those seismic reflectors, re-evaluating their consistency throughout the dataset. The "flatten horizon" tool in Petrel was used to analyze the consistency of reflectors. All horizons were mapped manually without automation tools and they were selected in such way that they mark significant seismic changes (e.g., internal geometry of packages, thickness, seismic appearance). There are no deep wells in the study area, so they cannot be used to tie the horizons. The result of the mapping yielded 6 regionally occurring horizons, which are persistent through the whole dataset (Figure 11). Furthermore, local horizons and seismic features were picked throughout the study area.

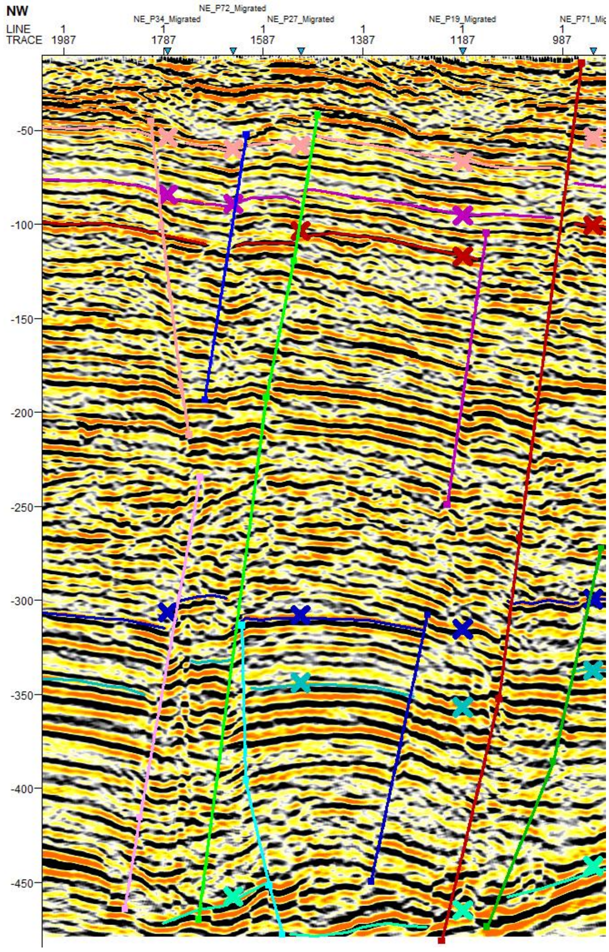

Figure 11. Overview of the 6 mapped regionally occurring horizons and some faults. Note that the package between 200 and 300 ms TWT is seismically noisier and does not always display the fault propagation.

3.4. Fault mapping

Similar to the process of horizon mapping, manual fault interpretation also proved to be of iterative nature. Locally, due to distances between seismic lines of up to 500 m, assigning individual fault segments into the fault surfaces proved a challenging task. This was especially true in areas with high fault density, e.g., the NW part of the study area. Keeping track of major faults required intense reevaluation. Note that not all faults cross-cut the entire vertical section. Some faults in the lower part of the seismic section have similar counterpart located in the upper section, but the link of these two is not clear. As mentioned above, the seismically poorly imaged seismic package between 200-300 ms TWT does not always allow a clear interpretation. Consequently, some faults were not connected and rather split into two independent faults (Fig.11). The initial mapping resulted in the interpretation of over 100 faults. This number was then reduced by removing duplicate interpretations, eliminating single outliers and merging faults into fault planes to be more coherent. This process reduced the final number of faults to approximately 60.

4. RESULTS

4.1 Seismic Horizons

A total of 7 prominent seismic horizons were defined and mapped mainly across the multichannel survey, with selection criteria focused solely on observable extent of reflectors, their amplitude and geometry rather than based on well ties due to limited deep well coverage in the surveys area. An overview of all of these horizons is given in Figure 12 and Table1. Horizons are additionally shown as individual surface maps in Figures 13-16.

Name	**Extent**	**Depth [ms]**	**Colour**
Mid	localized in the W. Only used for analysis of clinoforms	286-145	Dark Pink
Horizon 1	discontinuous in the NW due to truncation	140-0	Pink
Horizon 2	whole survey	150-2	Purple
Horizon 3	whole survey	183-5	Red
Top	discontinuous in the NW due to complex faulting and SE due to seismic resolution	289-119	Green
Horizon 4	whole survey	367-214	Dark blue
Horizon 5	whole survey	401-244	Blue
Basement	whole survey	573-365	Turquoise

Table 1. An overview of the interpreted seismic horizons.

Most horizons are mapped throughout the entire seismic volume, with notable exceptions: Horizon 1 (Figs. 12 and 16), which is restricted to the central and southeastern area due to erosional truncation and general dip direction, and the “Top” horizon (Figs. 12 and 14), which was later mapped as the upper boundary of a specific clinoform package described in Chapter 4.4 and was not mapped in the southeasternmost part of the survey. This horizon is also discontinuously traced in the northwestern parts due to complex faulting in that area (Fig. 14). "Mid" is a local horizon interpreted to analyze the internal structure of the distinct clinoform package (Fig. 12 and Table 1.). Across the area, horizon traceability generally decreases towards the southeast, except for the acoustic basement, whose high-amplitude character diminishes in the southwest, where it is deepest (Fig. 12 and 13). Aside from “Mid,” each horizon serves as a boundary for six distinct seismic packages also presented in Fig.12 That will be presented in chapter 4.3.

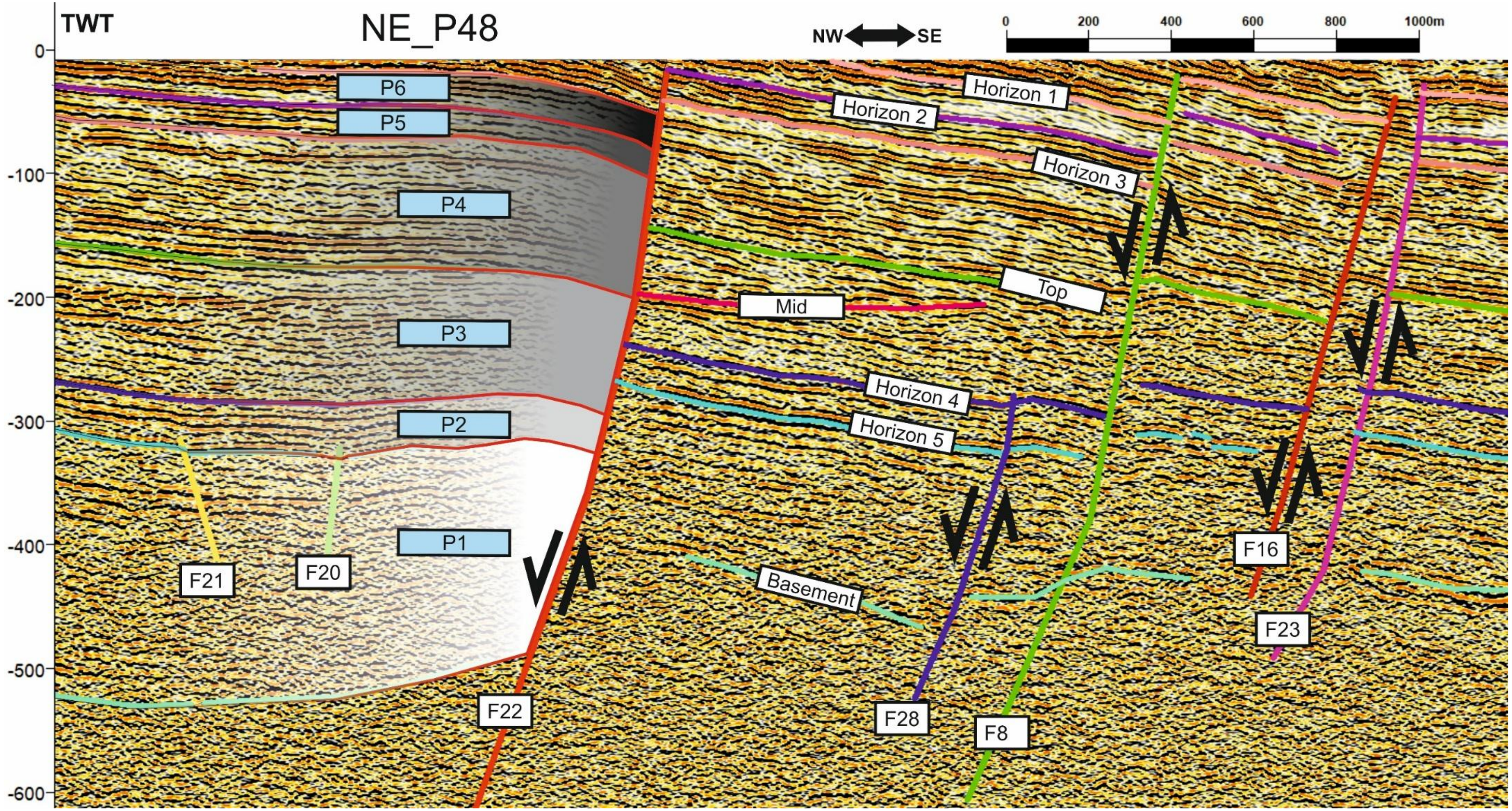

Figure 12. Overview of structural elements interpreted on seismic profile NE_P48, including main horizons (Basement, Horizons 1-5), a clinoform-associated local horizon (Mid), normal faults (F8, F16, F22, F23, F28), and seismic packages (P1-P6). Black arrows indicate fault kinematics. For the location see Fig. 24. Vertical exaggeration (VE): 3.

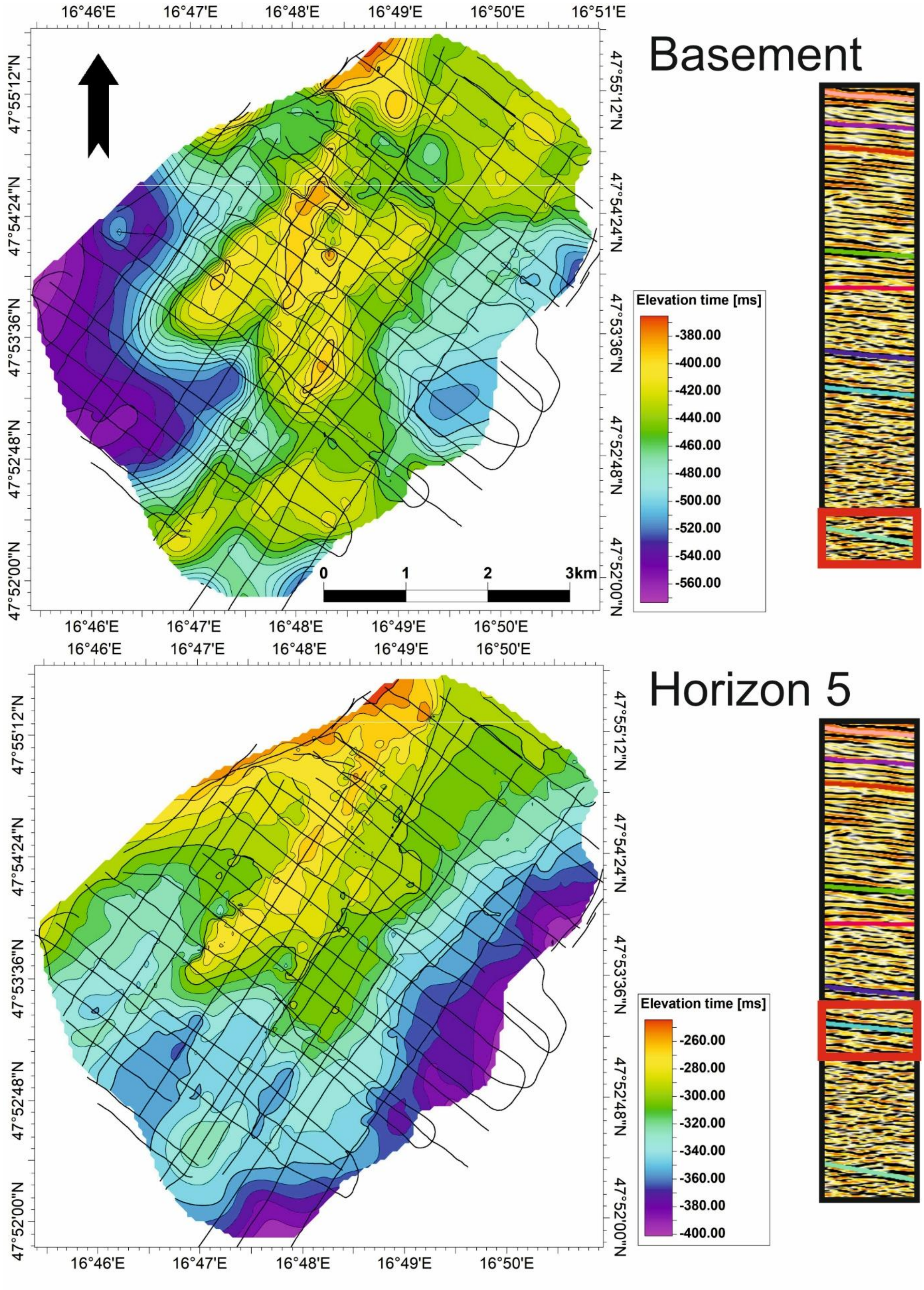

Figure 13. Map view of the interpreted Basement and Horizon 5 surfaces, colour-coded by elevation time (ms). Seismic sections on the right highlight the respective interpreted horizons. Note the contrasting dip directions: the Basement surface deepens to the west and slightly to the east with an elevated high separating the two lows, while Horizon 5 dips with the general trend to the southeast.

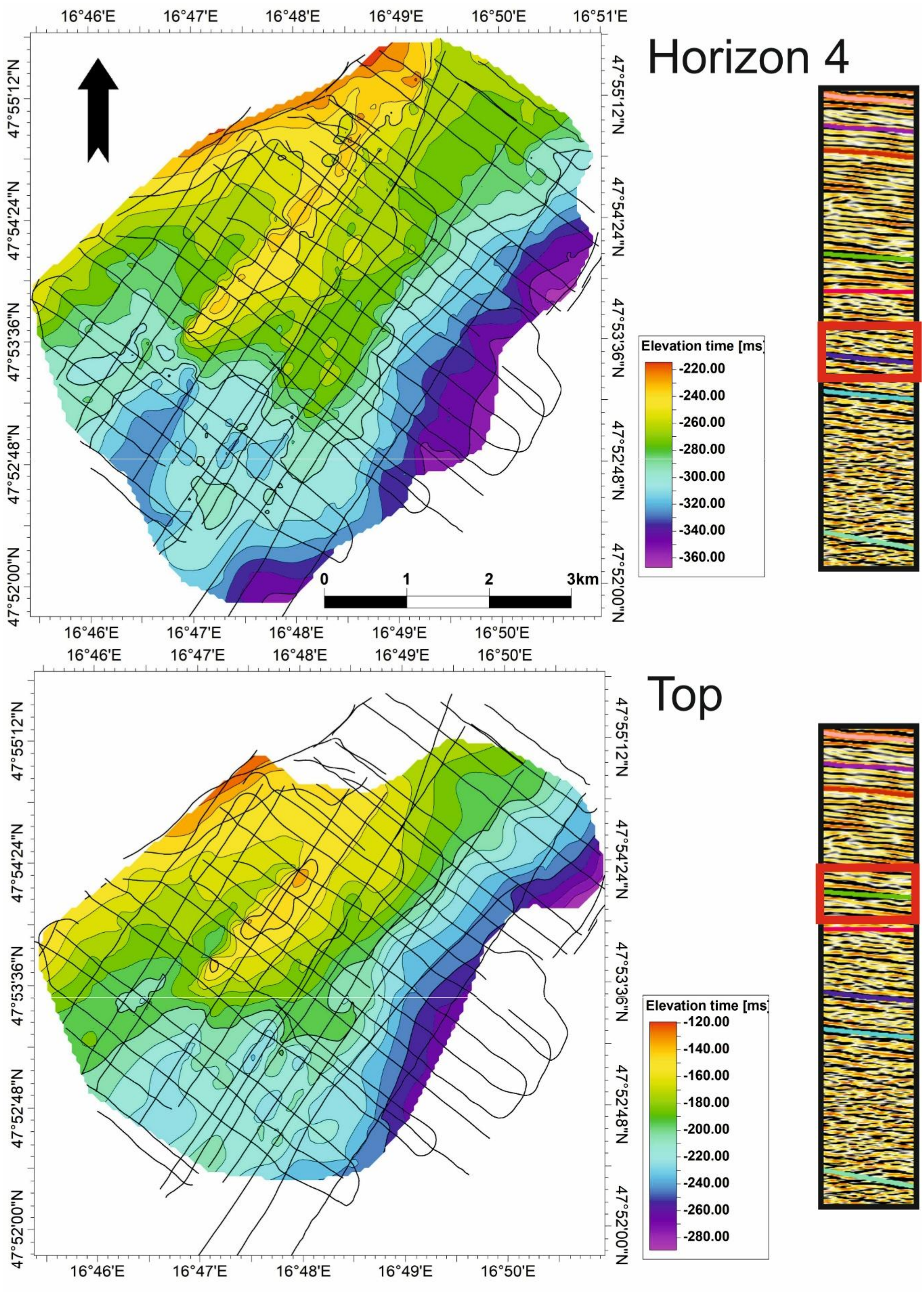

Figure 14. Map view of the Horizon 4 and "Top" surfaces, colour-coded by elevation time (ms), both following the general deepening trend towards the southeast. Seismic sections on the right highlight the respective interpreted horizons. The "Top" surface was defined to represent the upper boundary of a clinoform package discussed in Chapter 4.4.

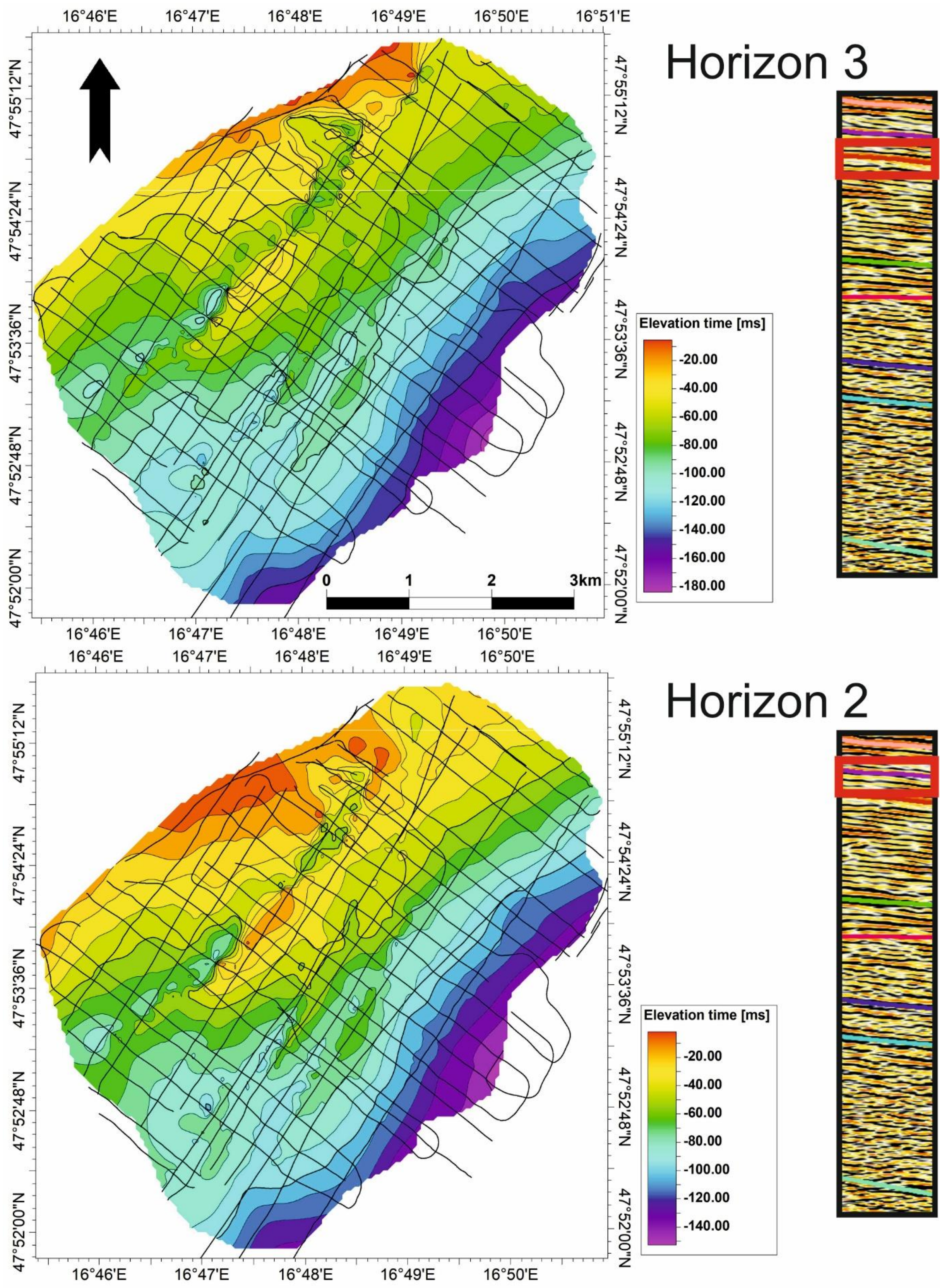

Figure 15. Map view of the Horizon 3 and Horizon 2 surfaces, colour-coded by elevation time (ms), both following the general deepening trend towards the southeast. Seismic sections on the right highlight the respective interpreted horizons.

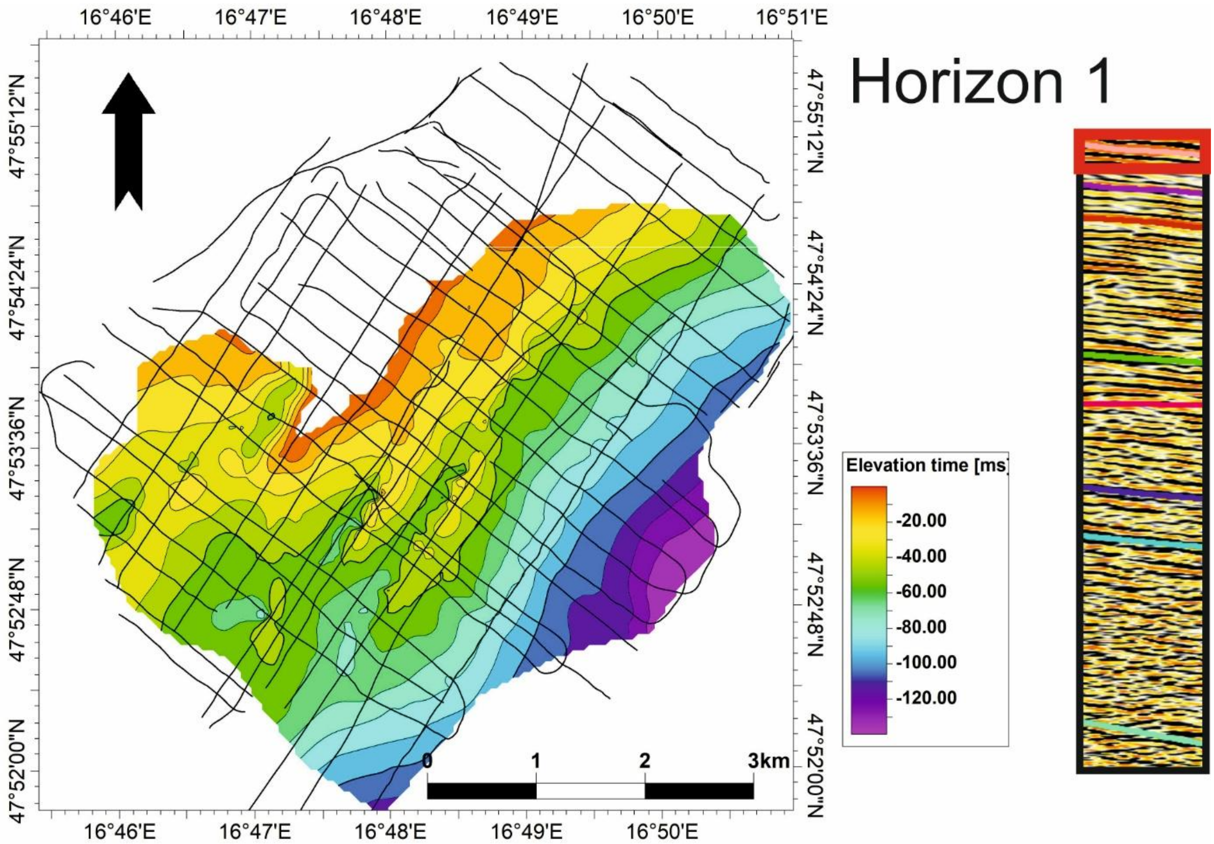

Figure 16. Map view of the Horizon 1 surface, colour-coded by elevation time (ms), following the general dipping trend towards the southeast. Seismic sections on the right highlight the respective interpreted horizons. Note a cut-off of the northwestern part of the horizon due to erosion.

The general azimuth of dip direction toward the southwest is observed in all Horizons 1-5 (Figures 13-16), with the exception of the Basement horizon, which exhibits a more complex morphology. The basement horizon map illustrated in Figure 13 displays central fault-controlled, NE-SW trending high, which is also imaged on the other horizon maps as structural high. In addition, the basement topography shown in Figure 13 indicates another trending basement high in the south, with possible N-S trend, though seismic coverage is not good in that area. Notably, this structural high is not imaged on overlying constructed horizon maps and is prominent at the basement level. The interpreted fault pattern becomes progressively clearer and more detailed toward the top of the seismic data, with the highest Horizons 1 and 2 providing the best structural resolution.

4.2. Faults

Of approximately 60 interpreted faults, 52 faults have sufficient lateral extent and were viable for the creation of a structural framework. An overview of these faults, mostly interpreted in the multichannel seismic data, is shown in Figure 17. A general SE-NW trend is observable throughout the whole seismic survey, with northeasterly located faults predominantly dipping to the southeast and faults in the southwestern region dip to the northwest. Structural framework together with horizon maps is documented in Figures 18-21. Fault density generally increases with increasing depth, with most complex fault pattern being observed at the level of Horizons 4 and 5 (Fig. 20) and also in the northernmost part of the multichannel seismic survey (Figs. 19 and 20). Additionally, to the dominant NE-SW trending faults, roughly NNE-SSW trending faults occur in the central part of the studied area and are well defined mainly at the basement level (Figure 21) but are also visible at younger mapped horizons, where the NNW-SSE trending faults cross-cut the NE-SW faults in the north to northwestern area (Figs. 19 and 20).

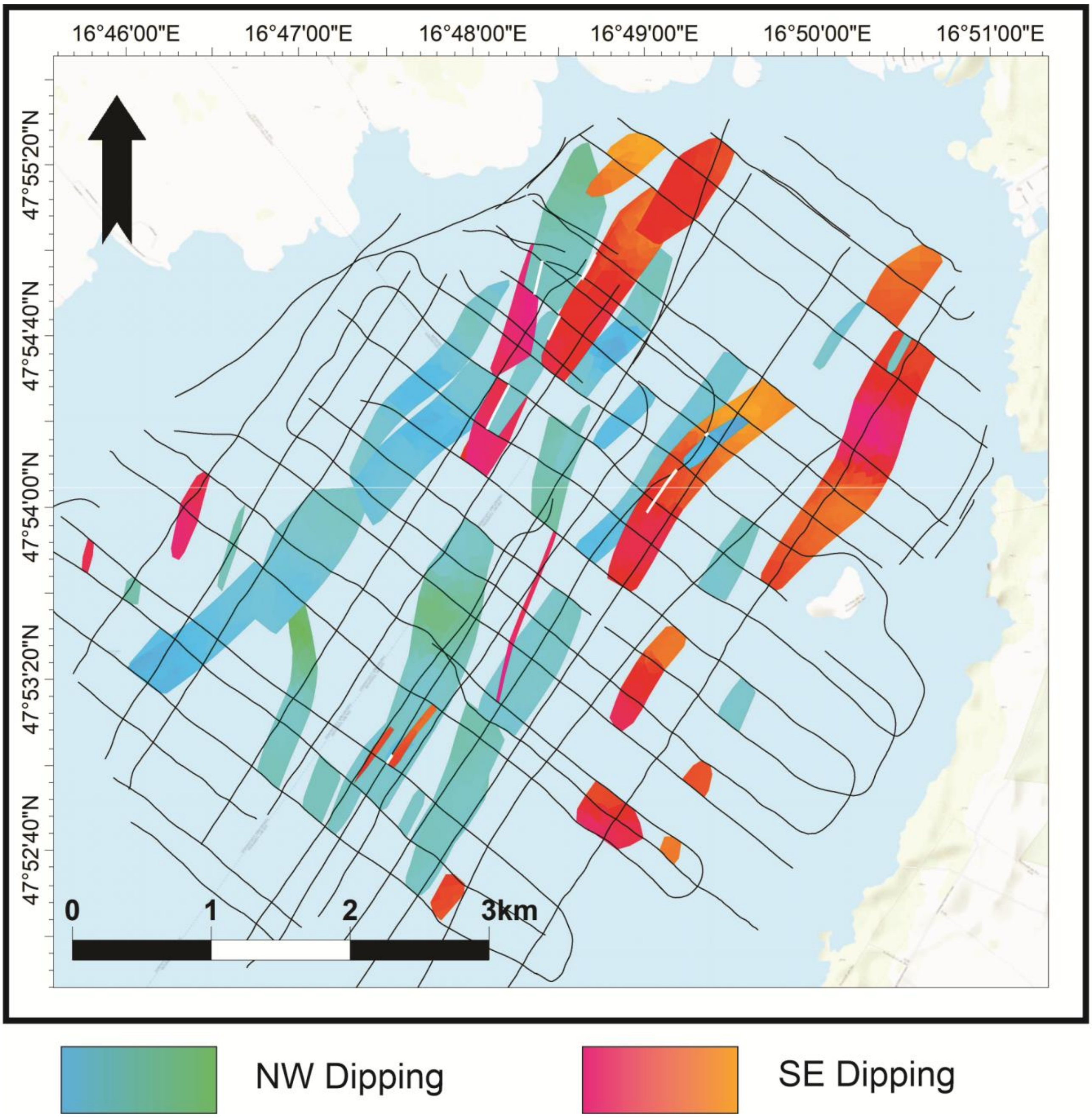

Figure 17. Overview of the mapped faults. Colours show dip direction of each fault. Black lines represent multichannel seismic survey lines. Faults in the northeastern and eastern portion of the study area predominantly dip toward the southeast, while faults in the southwestern and western region show a dip to the northwest.

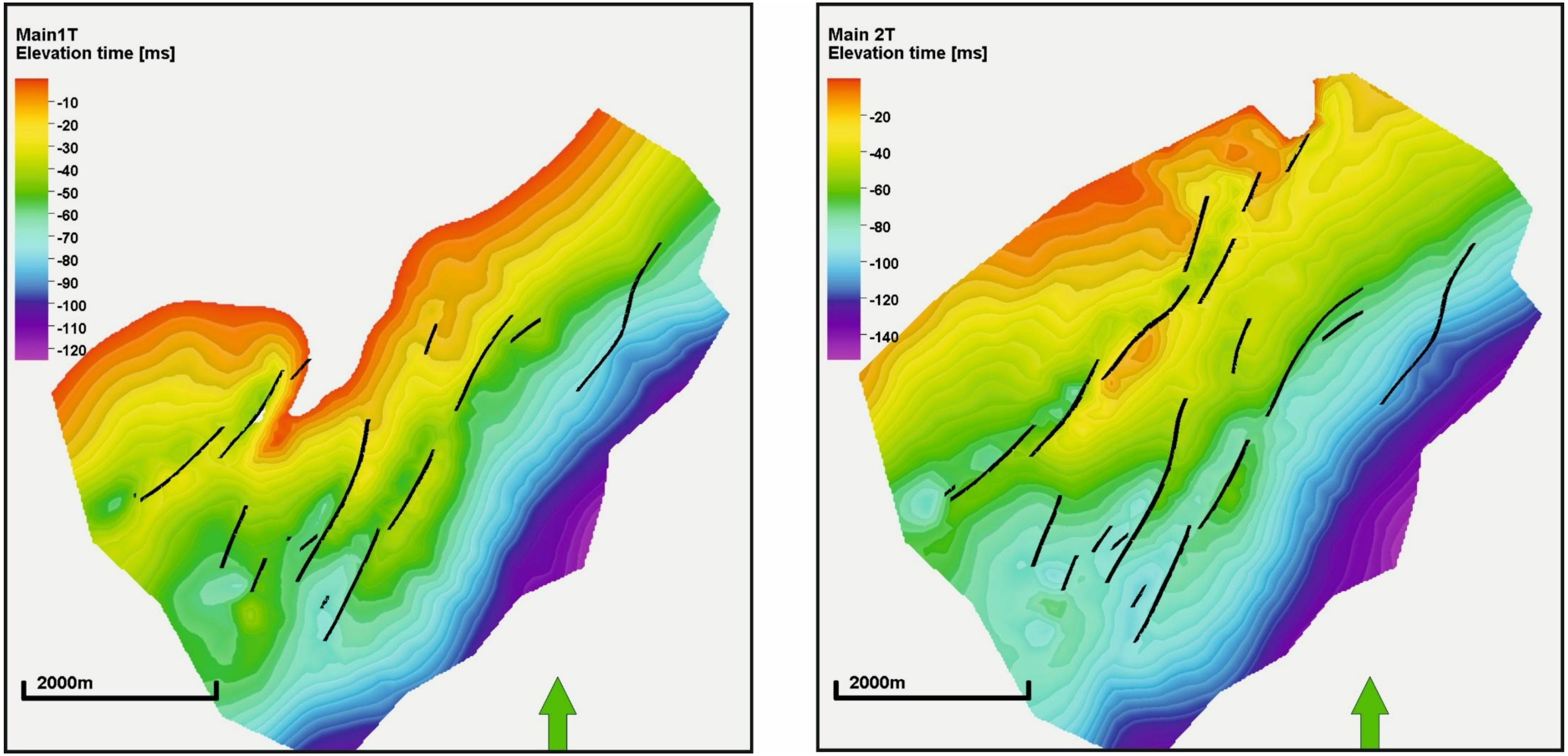

Figure 18. Black lines representing the fault framework intersections with Horizon 1 and Horizon 2. Modelled surfaces for the 2 horizons show erosion in the northern part of the study area. Colours show elevation in ms TWT. A clear SW-NE striking fault trend is observable.

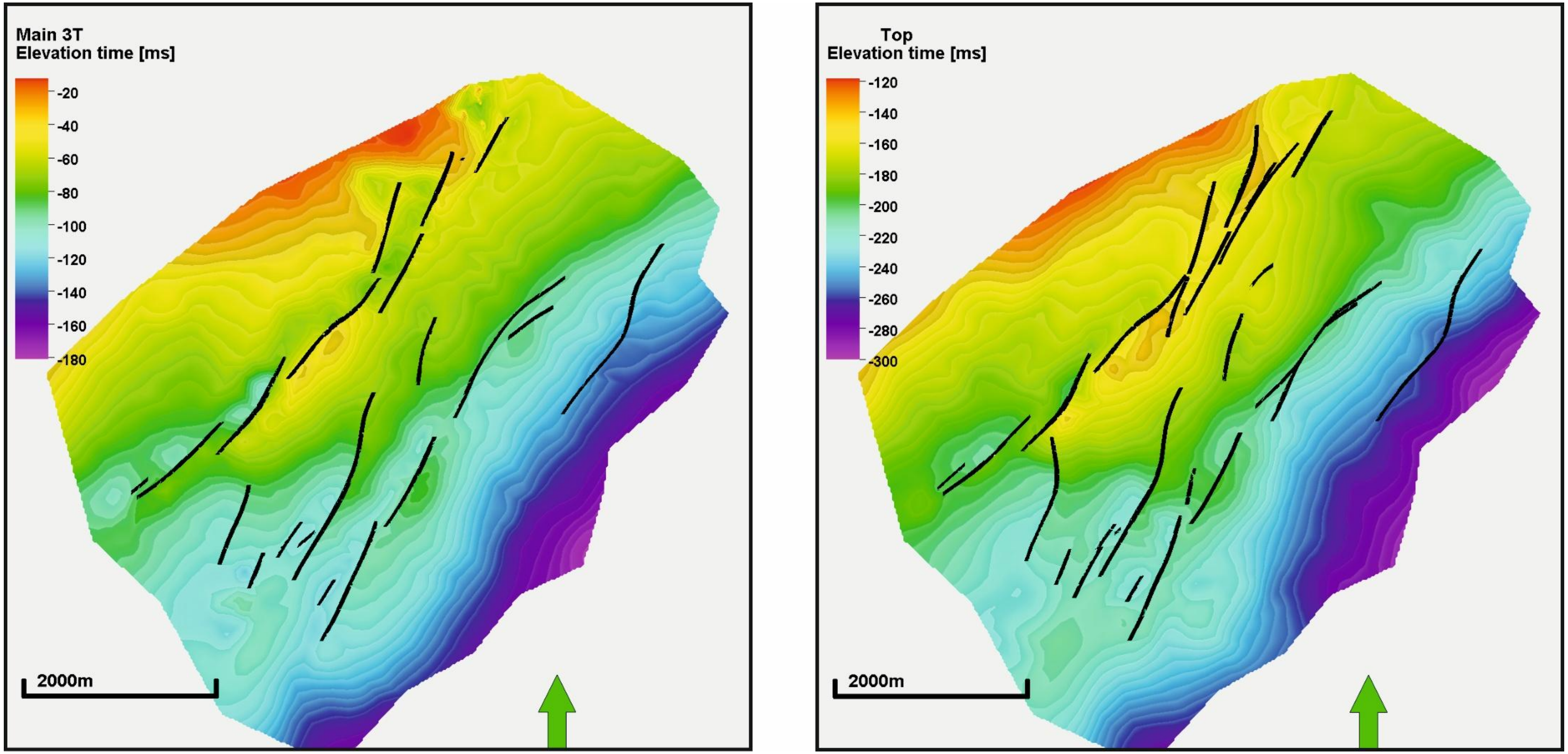

Figure 19. Black lines representing the fault framework intersections with Horizon 3 and "Top" Horizon. Colours show elevation in ms TWT. Note an increased fault density, starting with the "Top" Horizon.

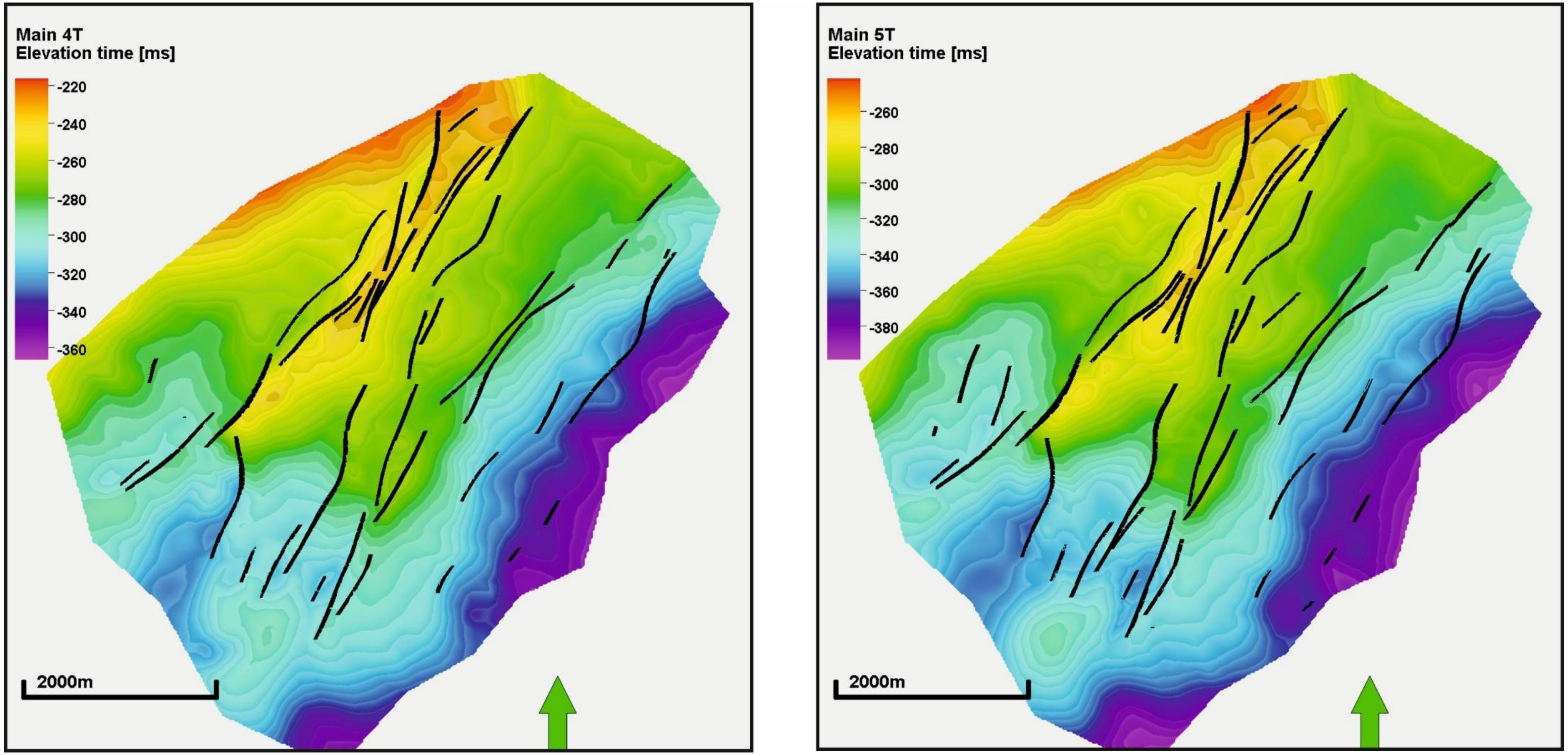

Figure 20. Black lines representing the fault framework intersections with Horizon 4 and Horizon 5. Colours show elevation in ms TWT. Note a further increase in fault density and complex fault pattern in the northern area.

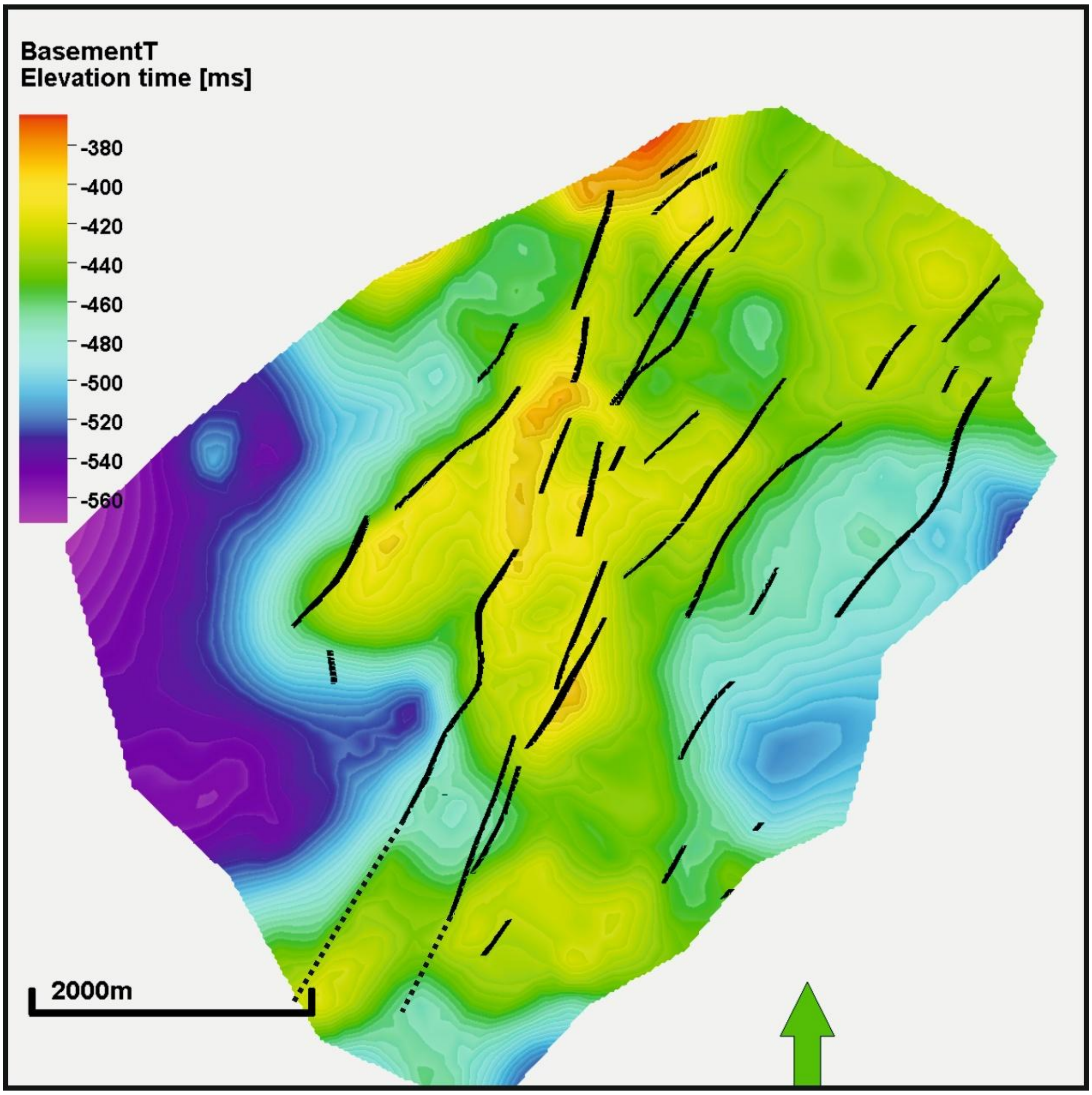

Figure 21. Black lines representing the fault framework intersections with the acoustic basement horizon. Colours show elevation in ms TWT. A decline in fault density is observable. Faults mapped at the basement level record syn-sedimentary activity during the deposition of the oldest seismic package. Dotted lines represent potential continuations of faults.

A clear fault pattern is observable throughout the whole seismic survey (Figures 22-24). Two major NE-SW oriented normal fault zones dominate the analyzed area. In general, faults locally form stepping pattern, and both main fault zones exhibit changes in fault dip.

The westerly located fault zone (Figures 18-21) is formed by a number of normal faults. In the southwest, the faults have predominant NW-dip (Figure 23). In the northernmost segment of this fault zone, where the NE-SW trend is offset by the NNE-SSW faults, faults have variable dips and the only reverse fault (F52) is documented as localized feature in the entire survey (Figure 22). The decrease in fault intensity at the Basement horizon, is probably connected to lower resolution of the seismic images (Fig. 21). However, well defined basement elongated highs in the southeast of the studied area as well as depocenter to the west is be observed (Fig. 21) and is not displayed at the overlying horizon maps (Figures 18-20). Figure 24 illustrates syn-sedimentary stratal growth of Package 1 and thickness changes across the faults indicating a syn-sedimentary fault activity. Further, Figure 24 displays decreasing fault offsets upward through the seismic section, suggesting reactivation of some of the NE-SW trending faults.

The easterly located second main fault zone marks significant drop in depth to the east as shown on the horizon maps (e.g., Figure 18). Faults that belong to this zone dip solely to the southeast. A structural high is located in the footwall of these faults (e.g., Fig. 19).

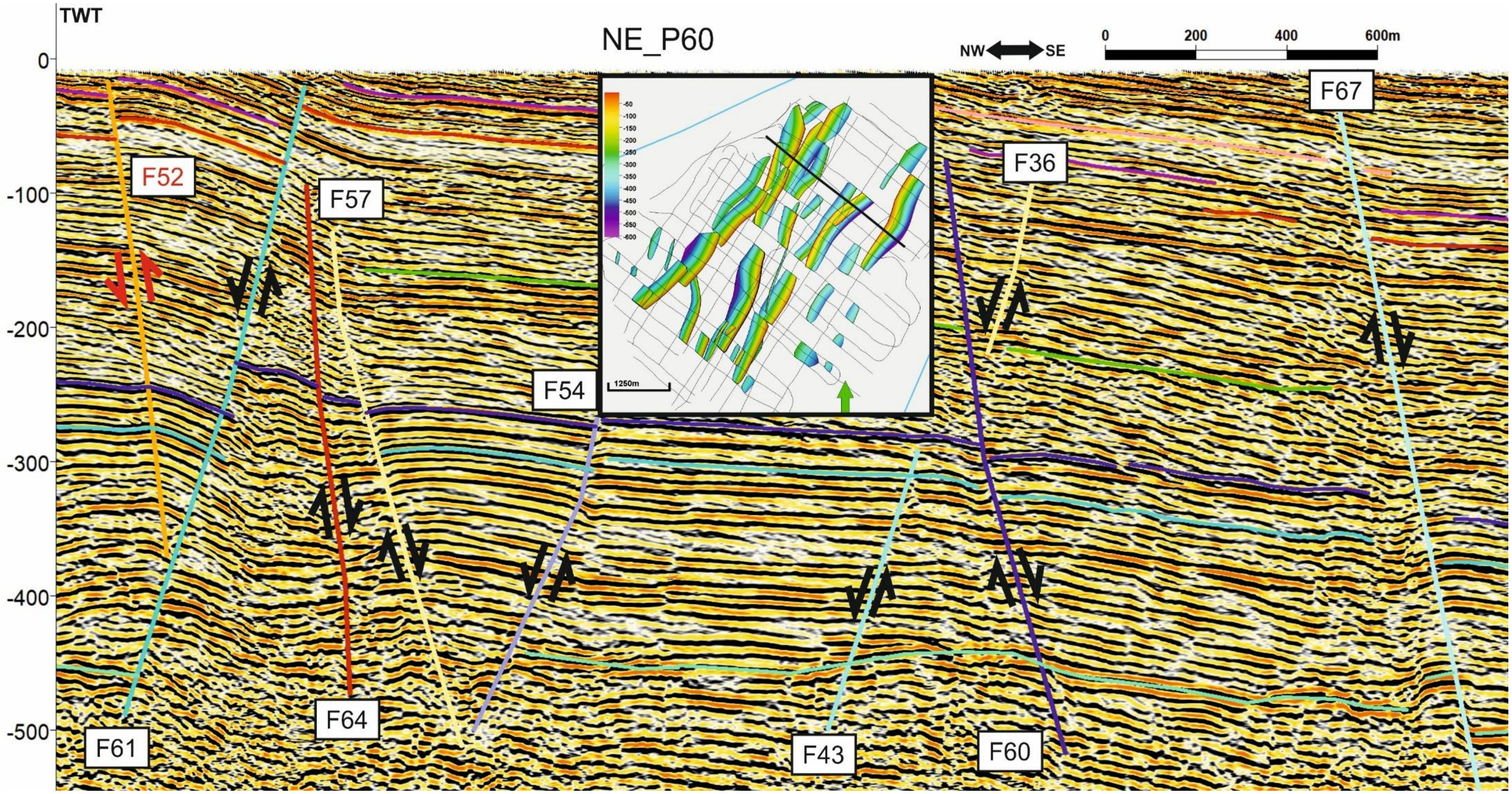

Figure 22. An interpreted seismic line in the north showing the structural configuration of the area. Most major normal faults that belong to the eastern fault zone, are dipping to the southeast (F67, F60). The structure of the western fault zone is more complex, including variably dipping normal faults (F61, F64, F57, F54) and Fault 52, which represents the only reverse fault observed in the seismic survey. The western segment of the seismic lines displays the most complex fault pattern.

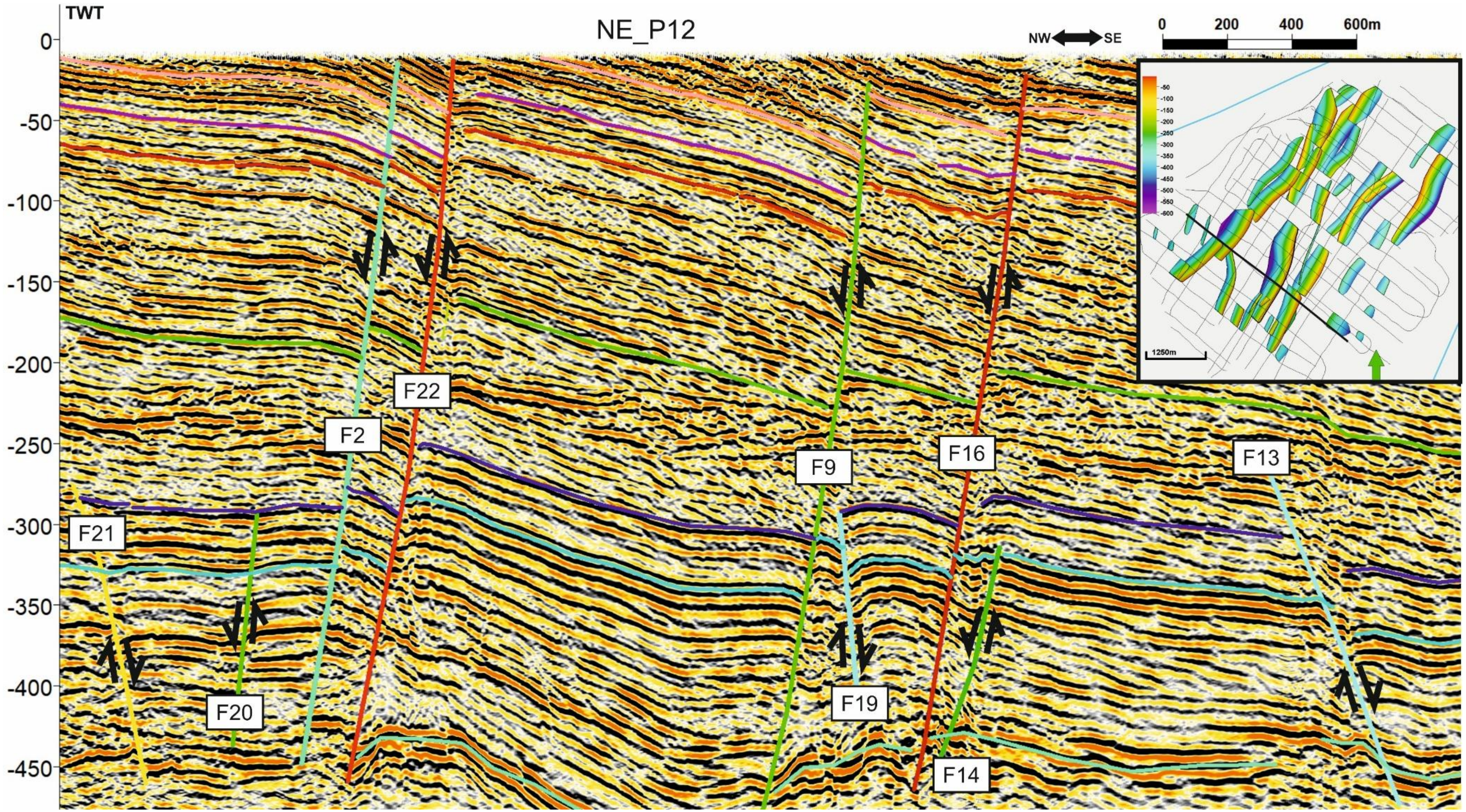

Figure 23. Southern example of an interpreted seismic line. Majority of the interpreted faults are dipping to the northwest (e.g., F2, F22, F16, F9). Note minor faults that occur mostly between the Basement and Horizon 5. SE-dipping Fault F13 belongs to the eastern fault zone.

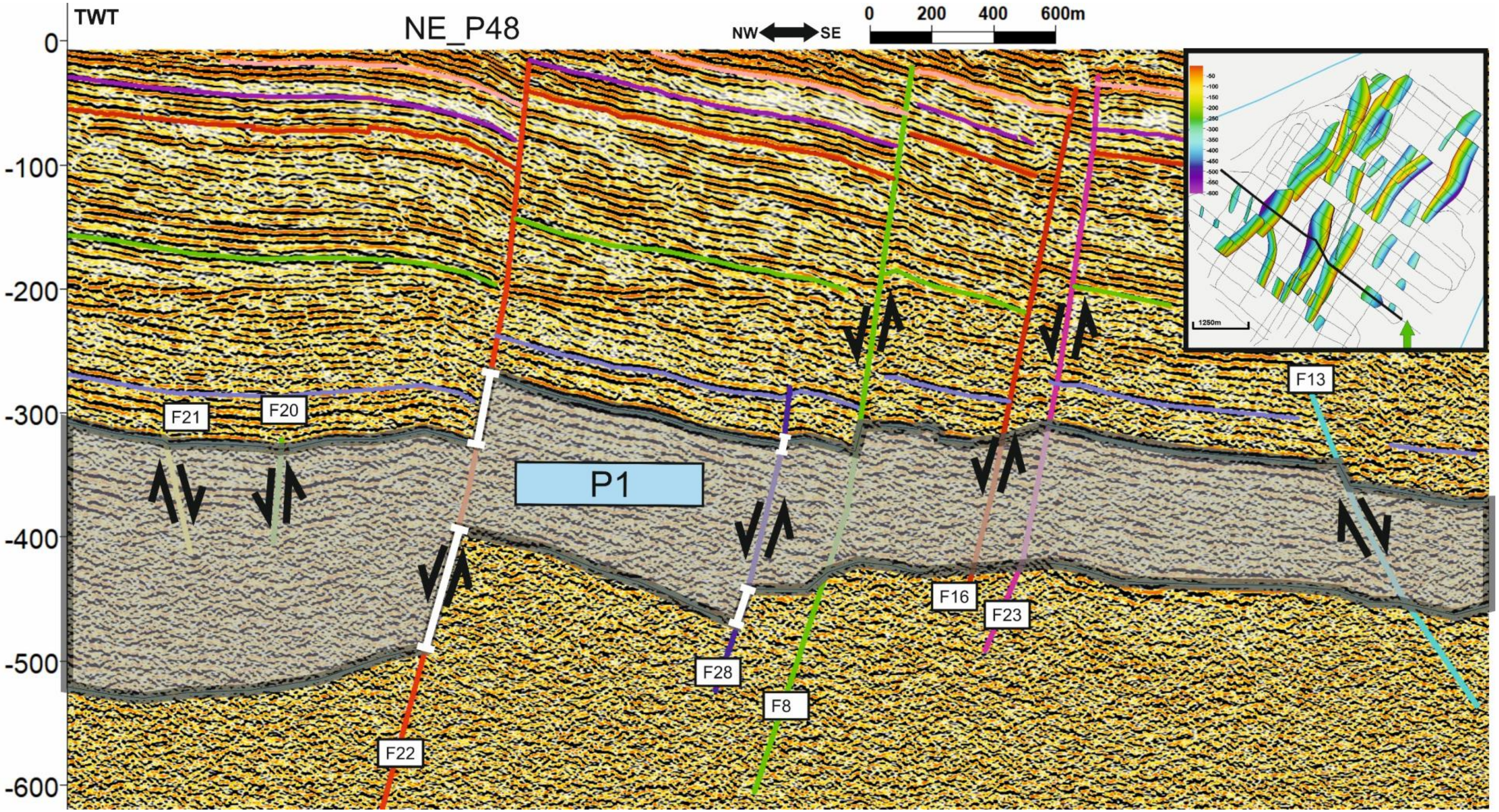

Figure 24. Example of an interpreted seismic line in the southernmost area showing thickness changes and syn-sedimentary growth of strata belonging to Package 1 (shown in grey). Note different fault offsets indicated by white lines.

4.3. Seismic Packages

Seismic packages were defined by the earlier established bounding horizons based on parameters such as lateral continuity, seismic character, and external and internal seismic geometry. Using these criteria, six packages were interpreted. A list of all packages, their apparent thickness, and key characteristics is presented below in Table 2.

Package Name	Thickness (ms TWT)	Character	Bounding Horizons
P6	0-57	Continuous seismic reflectors, almost no thickness change, eroded in the NW, highest package, fluvial channels.	Horizon 1 (top)- Horizon 2 (base)
P5	0-40	Continuous seismic reflectors, almost no thickness change with small variations along the middle ridge, eroded in the NW.	Horizon 2 (top)- Horizon (base)
P4	53-142	Continuous seismic reflectors, thickening towards the southeast, small-scale clinoforms.	Horizon 3 (top)- „Top“ Horizon (base)
P3	48-116	Visible large-scale clinoforms (50-100 ms), thickening towards the northwest.	„Top“ Horizon (top)- Horizon 4 (base)
P2	0-72	Continuous seismic reflectors, almost no thickness change	Horizon 4 (top)- Horizon 5 (base)
P1	56-293	Thickest package, thickening towards northwest, shows onlap onto basement. Small-scale clinoforms.	Horizon 5 (top)- Basement (base)

Table 2. An overview of interpreted seismic packages.

Analysis of generated time thickness maps reveal thickness variations across the packages as illustrated in Figures 25-27. Package 1 (Fig. 25), bounded at the base by the basement horizon, exhibits the most pronounced thickening of all interpreted packages. It shows stratal thickening toward the northwest and existence of a large depocenter, most probably due to syn-sedimentary faulting (Fig. 20). Package 2 (Fig. 25) demonstrates a relatively uniform thickness distribution with subtle thinning in the central study area, coinciding with a regional basement high and minor, but noticeable thickening to the NW. Package 3 (Fig. 26) follows a similar trend like Package 1, displaying significant northwestward stratal thickening and documenting an existence of westerly lying depocenter. This package is of particular importance as it contains large-scale clinoforms and represents the only stratigraphic unit above the basement that thickens towards the NW. The clinoforms are discussed in detail in the following Chapter 4.4. Package 4 (Fig. 26) follows the regional structural trend, dipping towards the east, showing thickness increases toward the southeast. Package 4 marks a profound change in the tilt of the studied basin. Package 5 (Fig. 27) displays moderate thickening in the central portion of the study area, controlled most probably by active faulting, while Package 6 maintains the most uniform thickness among all analyzed packages (Fig. 27). Additionally, Package 1 contains abundant channel-like features that are discussed separately in Chapter 4.5.

A structural 3D static modelling was carried out based on the seismic interpretation and generation of the thickness maps. A final model of the packages is shown in Figure 28a, highlighting the erosional nature of the two uppermost packages indicating tilt and uplift of the basin. Figure 28b integrates seismic packages in transparent mode combined with the fault model to present their spatial relationship and also location of the studied area.

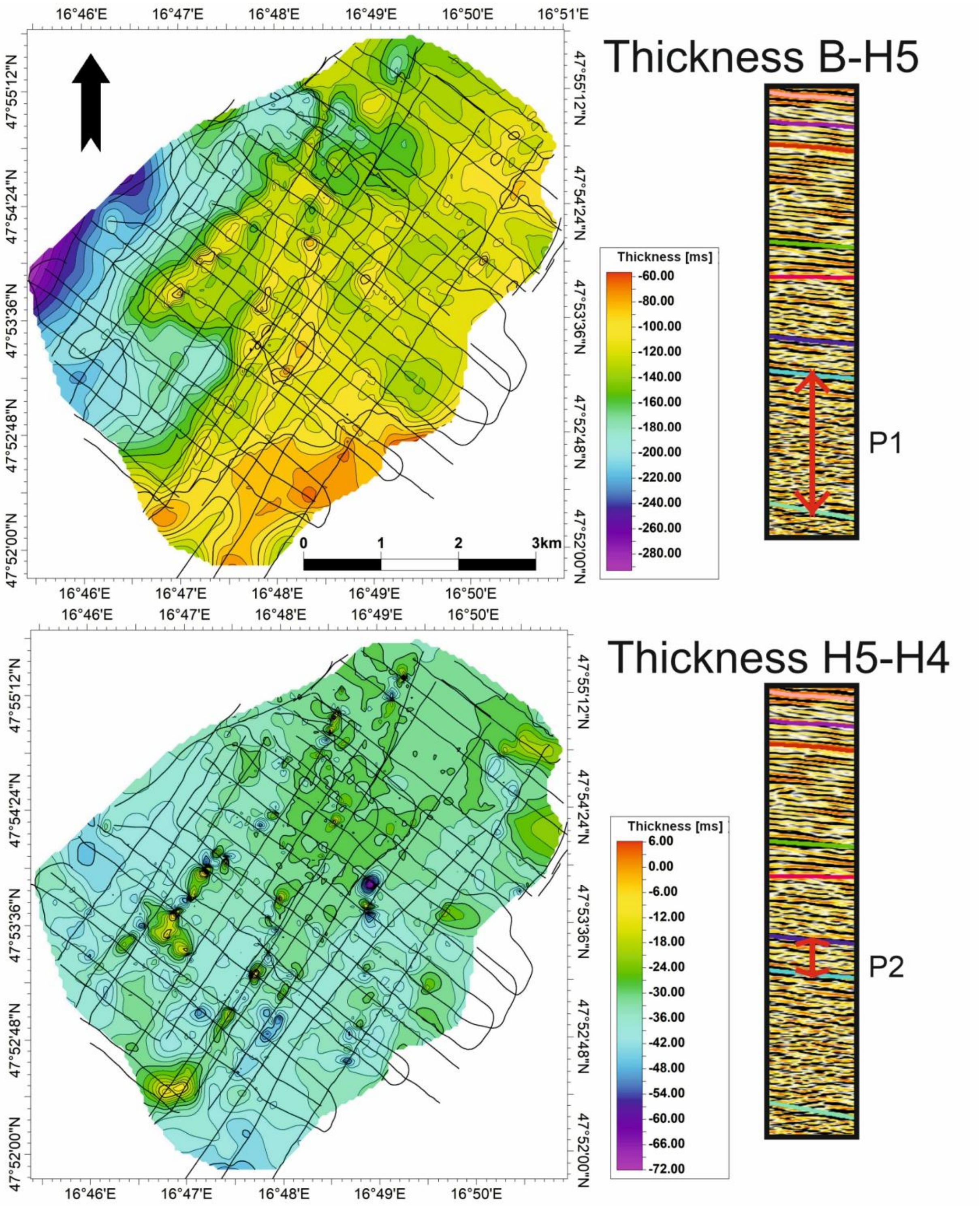

Figure 25. Time thickness map (in ms) of seismic packages 1 and 2. Package 1 is bounded by Basement and Horizon 5 (upper), while Package 2 is bounded by Horizon 5 and Horizon 4 (lower). Seismic sections on the right highlight the respective package intervals and seismic character. Note that Package 2 has very locally positive values, an error introduced due to faulting and data processing. Package 1 thickens significantly towards the northwest, while thin Package 2 retains relatively constant thickness, with minor but noticeable increase to the NW.

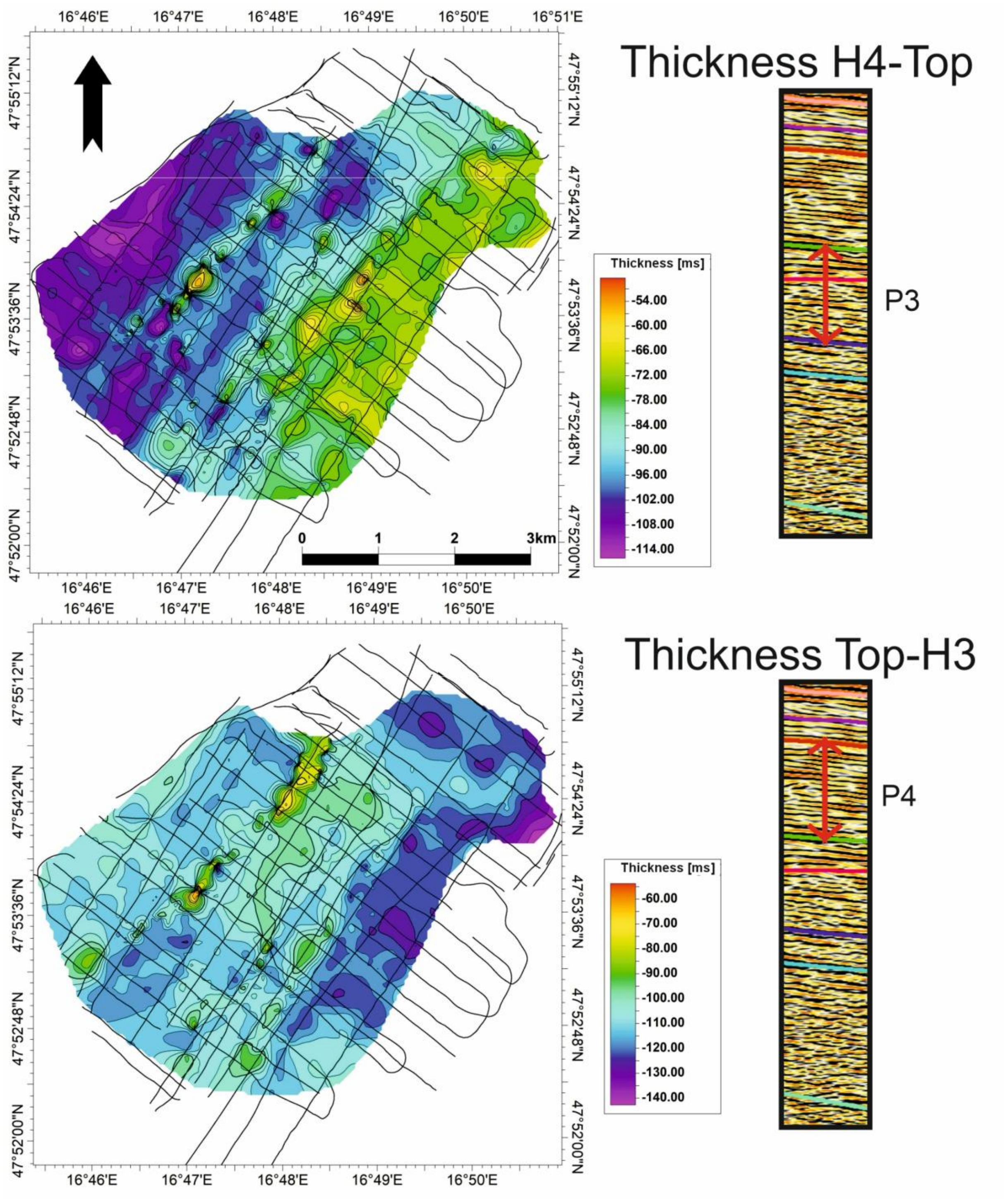

Figure 26. Time thickness maps of seismic packages 3 and 4. Package 3 is bounded by Horizon 4 and "Top" (in ms, upper), while Package 4 is bounded by horizons "Top" and Horizon 3 (in ms, lower). Seismic sections on the right highlight the respective package intervals and their seismic character. Package 3 thickens towards the northwest, while overlying Package 4 thickens towards the southeast. Note that Package 3 contains large-scale clinoforms and shows a similar northwest thickening pattern as Package 1.

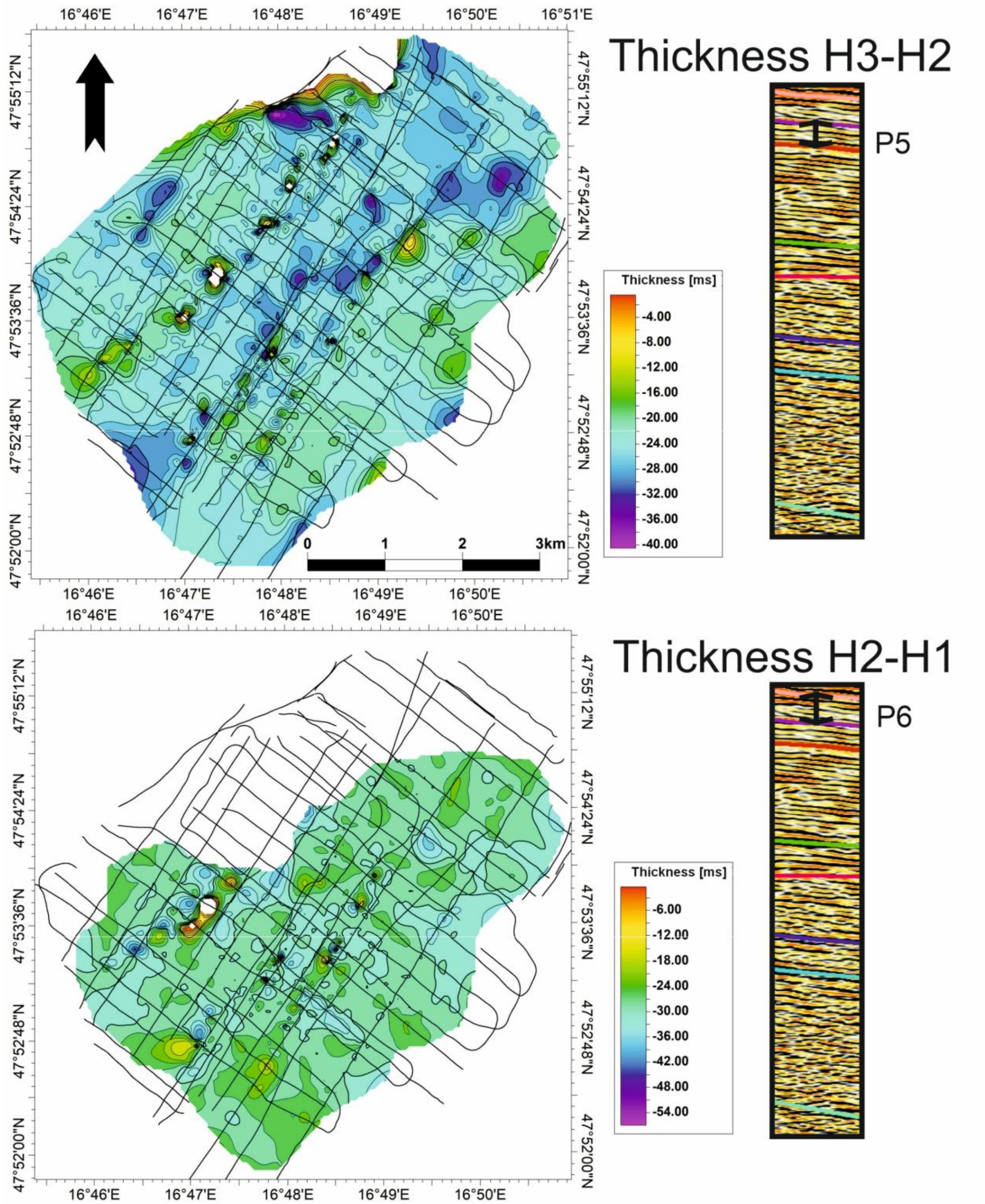

Figure 27. Time thickness maps of packages 5 and 6. Seismic package 5 (in ms, upper).is bounded by Horizon 3 and Horizon 2. Seismic package 6 is bounded by Horizon 2 and Horizon 1 (in ms, lower). Seismic sections on the right highlight the respective package intervals and its seismic character. Both packages retain relatively constant thickness.

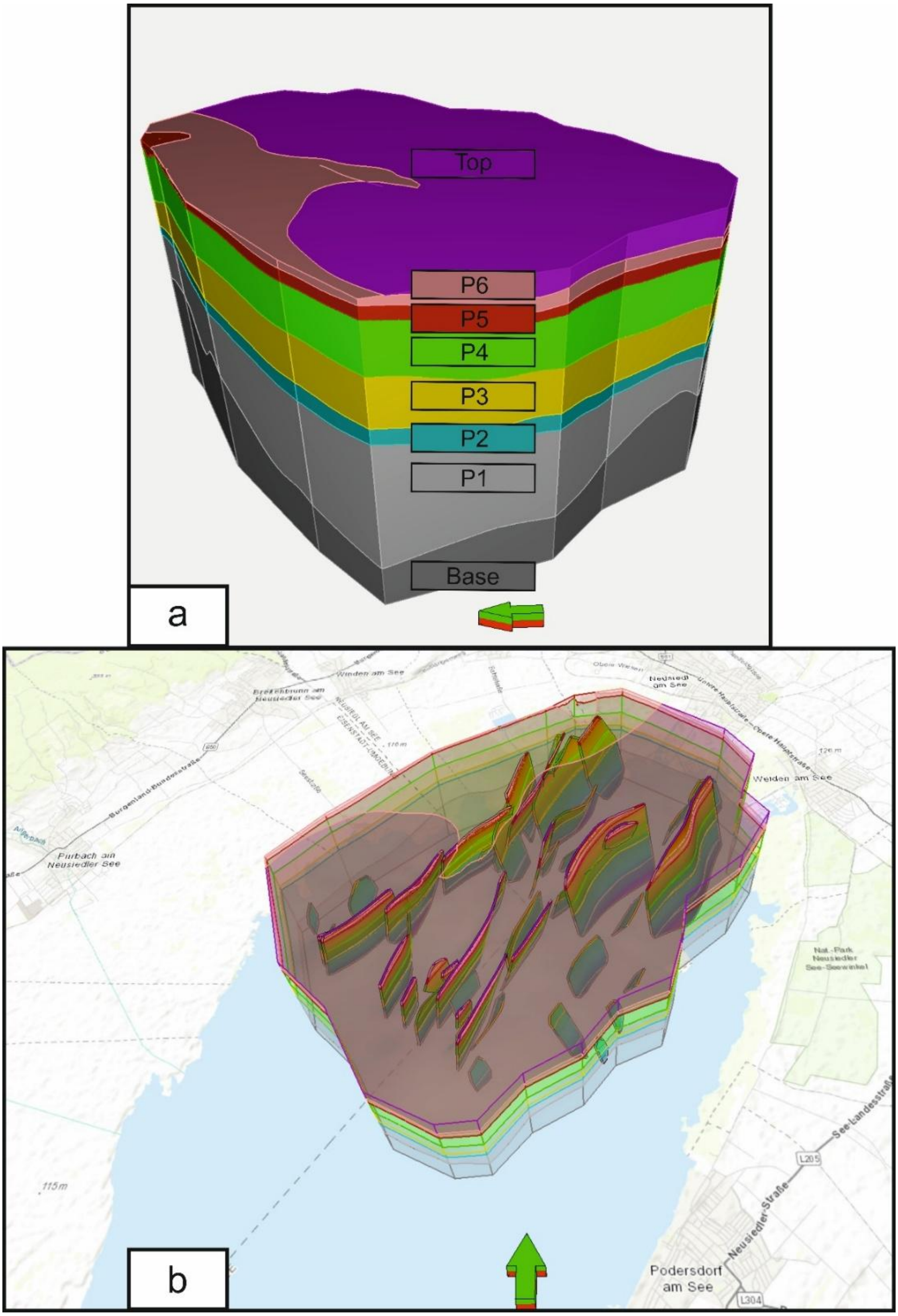

Figure 28. (a) 3D static model of the data based on established seismic horizons and packages. Note the thickness changes, especially visible in P1 to the southwest, and less pronounced in P3. (b) Transparent 3D model combined with modelled faults, shifted vertically above the top of the model to visualize the general spatial context.

4.4. Deltaic Structures

A detailed analysis of the multichannel seismic survey revealed occurrences of seismic packages displaying clinoforms, which are mostly progradational and less commonly aggradational (Figs. 29, 30 and 31). These packages occur at different depths and display variable thicknesses (Figure 32) and are described below in detail.

The most prominent clinoform package occurs vertically roughly in the middle of the multichannel survey and is observed in the entire study area (Figs. 29, 30 and 32). As shown in Fig. 29, this clinoform package is bounded by the "Top" horizon at the top and by Horizon 4 at the base. Horizon 4 was first interpreted as one of the marker horizons and only later found to be aligned with the base of the clinoform package. The "Top" horizon was interpreted specifically to represent the upper boundary of the clinoform package. Throughout the survey, Horizon 4 is located in depths between 200 and 400 ms TWT, while "Top" horizon appears between 90 and 312 ms TWT. The thickness of the clinoform package decreases gradually, following the general stratal dip from northwest to southeast, from approximately 100 to 70 ms TWT (e.g., Fig. 32). Notably, the survey's resolution declines towards the SW, making thickness measurements more challenging (Fig. 32).

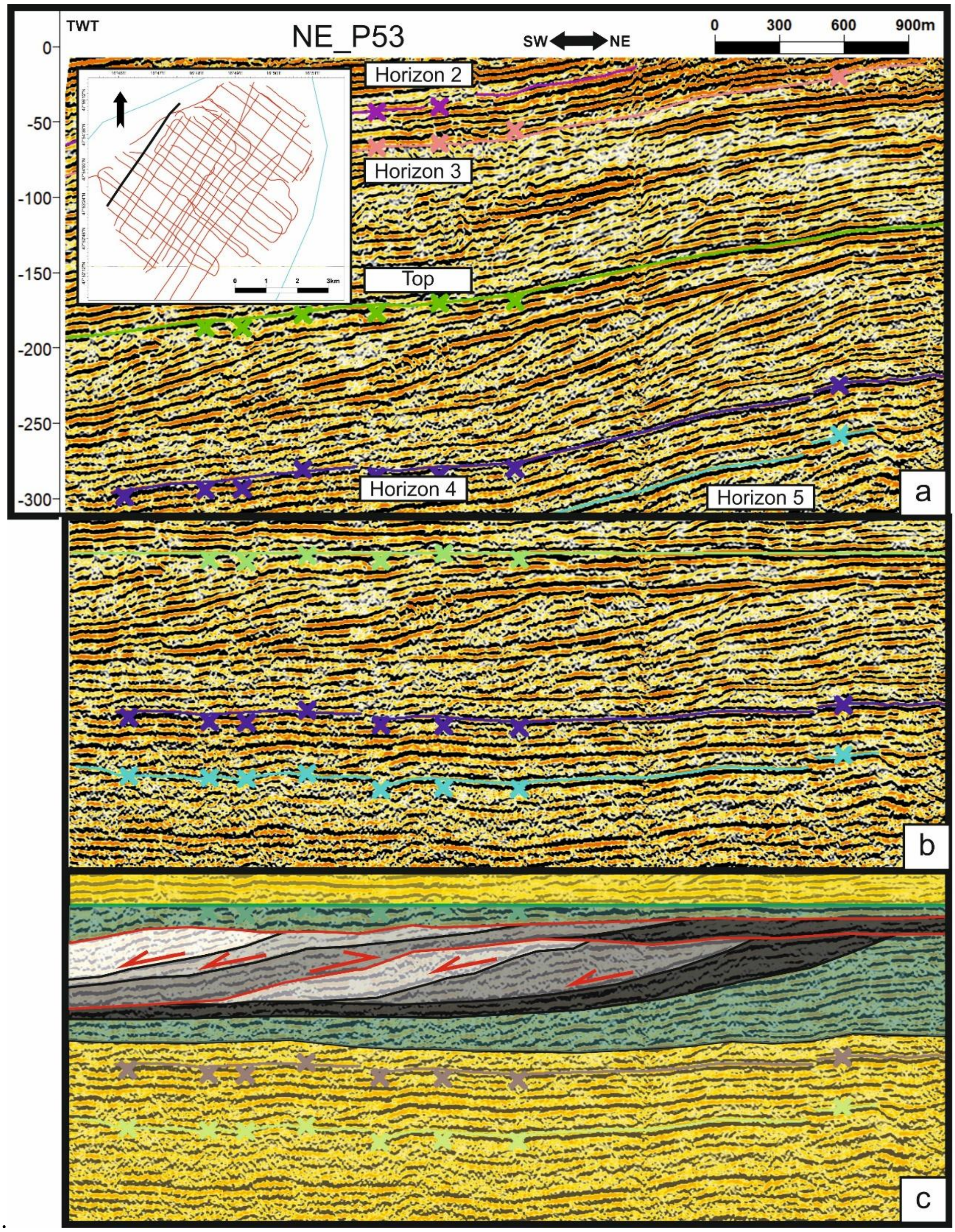

Figure 29. (a) Seismic section NE-P53 located in the NW study area showing a distinct seismic package with internal progradational clinoforms. The seismic package with depths of up to 300ms TWT. (b) The same section with the "Top" horizon flattened. (c) Colour-coded sections with different inclines and internal morphology, highlighting a clinoform package alternating between aggradation and propagation. Arrows indicating toplap and downlap. Vertical exaggeration (VE): 7.

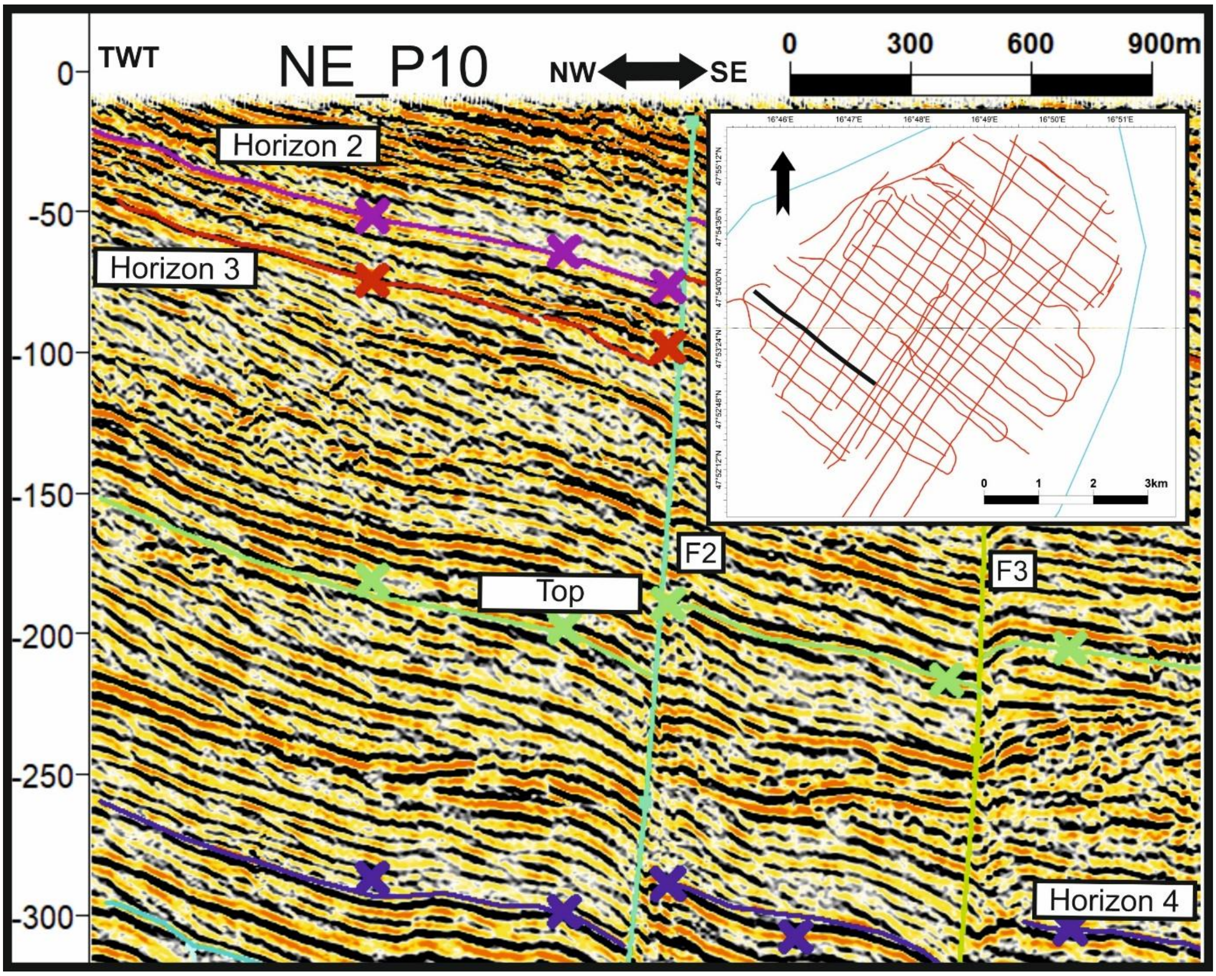

Figure 30. Seismic section located in the SW area showing that the main clinoform package below the green 'Top' horizon is faulted. Mapped horizons (2-4 and Top) and faults are labeled. VE: 7

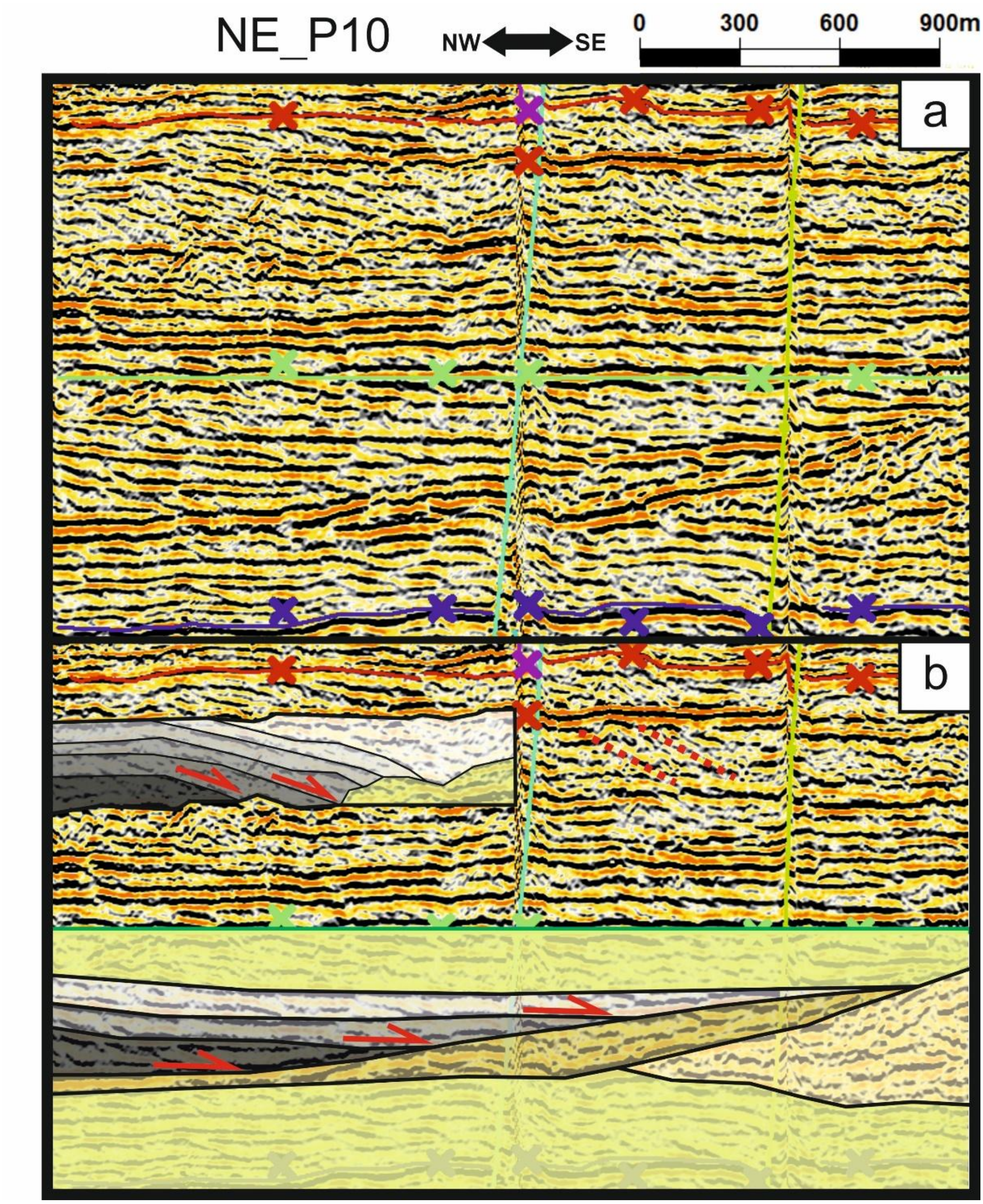

Figure 31. (a) The same seismic section as in Fig. 30 with the "Top" horizon flattened. (b) Colour-coded sections of interest. Arrows in the upper package indicate downlap (top left) in a prograding succession. Dotted red line representing a likely continuation of the upper progradational body. The lower package displays onlap (bottom). VE: 7

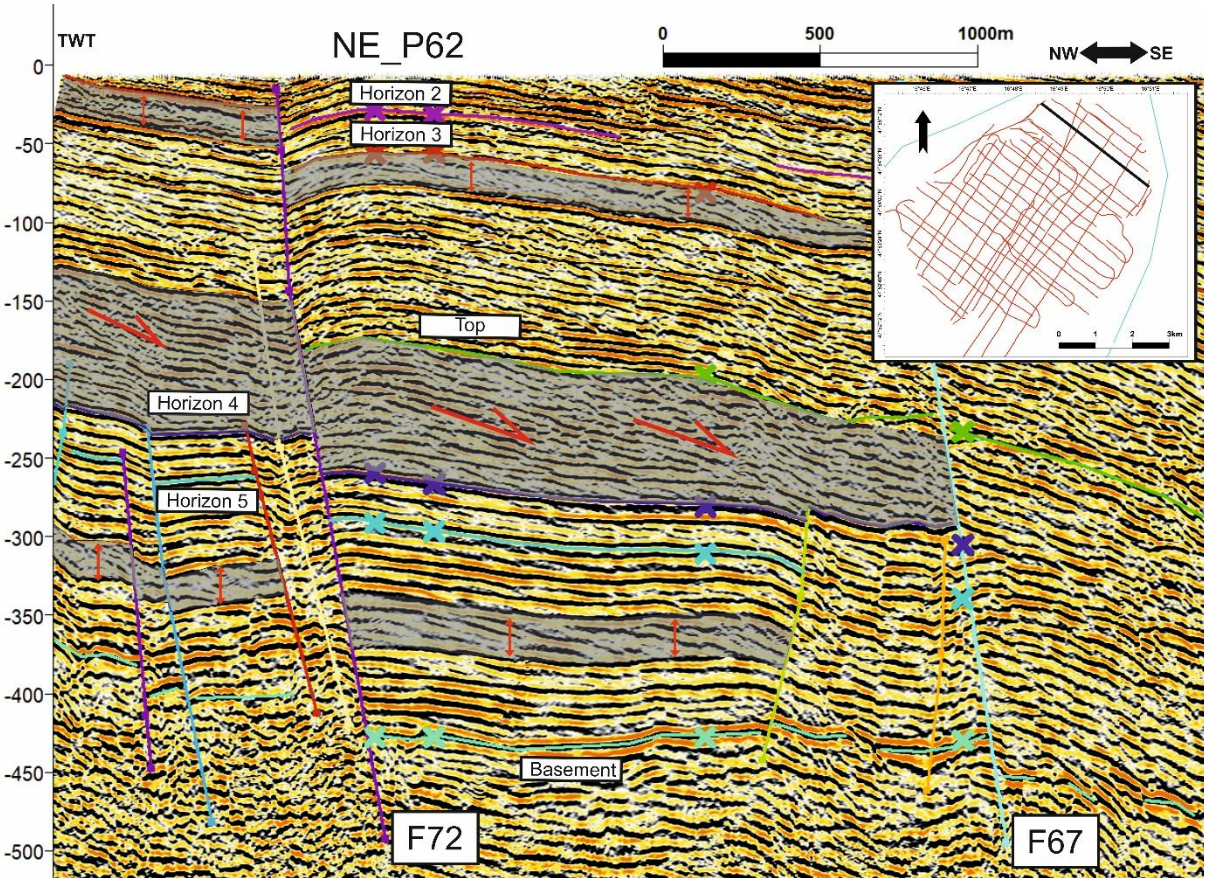

Figure 32. Faulted seismic section NE-P62 located in the NE part of the survey showing depth to basement at 360 to c. 460ms TWT. Mapped horizons (2-4, Top and Basement) and major faults are labeled. Grey shading indicates three packages with clinoforms. The central section depicts the thickest clinoform package. Red arrows indicate progradation direction. The lower and upper thinner packages with smaller clinoforms are marked by double arrows. VE: 5

Flattening the "Top" horizon with the “flatten horizon” function in Petrel to eliminate general dip and faulting proved especially effective for generating extensive, coherent horizons, as seen in Figs. 29 and 31, which is otherwise difficult to follow in unflattened seismic data (Fig. 30). Additionally, Figures 30 and 31 reveal another, higher package with clinoforms at depths between 50 to 100 ms TWT. The clinoforms are mostly progradational, either parallel or sigmoidal in geometry and do not consistently dip in the same direction, but rather change orientation, as evident in Figs. 29, 31 and 32 in different areas of the studied survey. The main clinoform package also locally shows onlap and aggradation onto older sedimentary layers and parallel reflectors on towards the top of the package (Fig. 31). Figure 32 also shows two other thinner packages which contain parallel clinoforms, particularly nicely developed in the seismic package between basement and Horizon 5. The youngest, regionally observed package occurs just below Horizon 3. The main clinoform package is also very well imaged in the survey's southeast sector, where it is disrupted by a chimney feature (Figure 33). Onlapping of the strata onto the basement is also visible in this area, indicating possible syntectonic deposition (Figure 33). A fault, which accommodates the sedimentation, ceased activity before the deposition of the main clinoform package (Horizon 4), as this horizon is not offset.

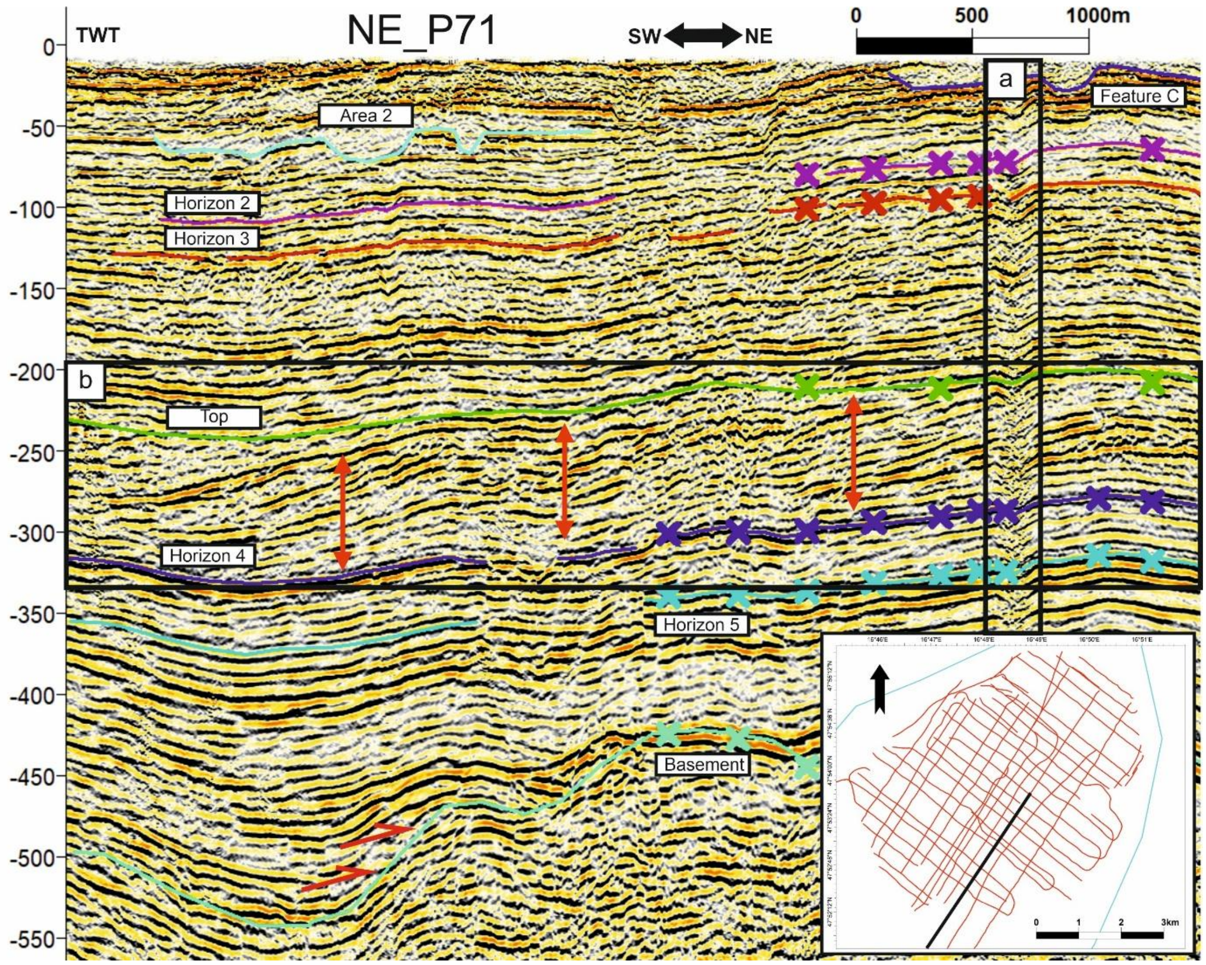

Figure 33. Seismic section from the SE area of the survey reaching depth to Top Basement at 550ms TWT. Note onlap of the oldest seismic package onto the basement. Mapped horizon Top (in green) marks the top of the clinoform package (marked by double arrows). Area 2 and feature "c" mark channel-like structures discussed in Chapter 4.5. (a) Acoustic anomaly that is interpreted as part of a chimney-system described in Chapter 4.6. (b) Area of the most prominent clinoforms, with red arrows showing their vertical extent. Additional red arrows near the basement indicate onlap surfaces onto the basement. VE:.7

To better understand the progradation direction of these strata, the top of one clinoform package was mapped as a horizon, and dip azimuth points were calculated. The same workflow was applied to other marker horizons above and below, using the same polygon to maintain consistent areal extent. The dip azimuths of each horizon were then plotted against their frequency, revealing a bimodal distribution of dip direction within the clinoform horizon (Fig. 34). This bimodal pattern is only observed in the clinoform horizon, implying two possible progradational directions for the foresets within the thickest clinoform packages bellow the Horizon “Top”.

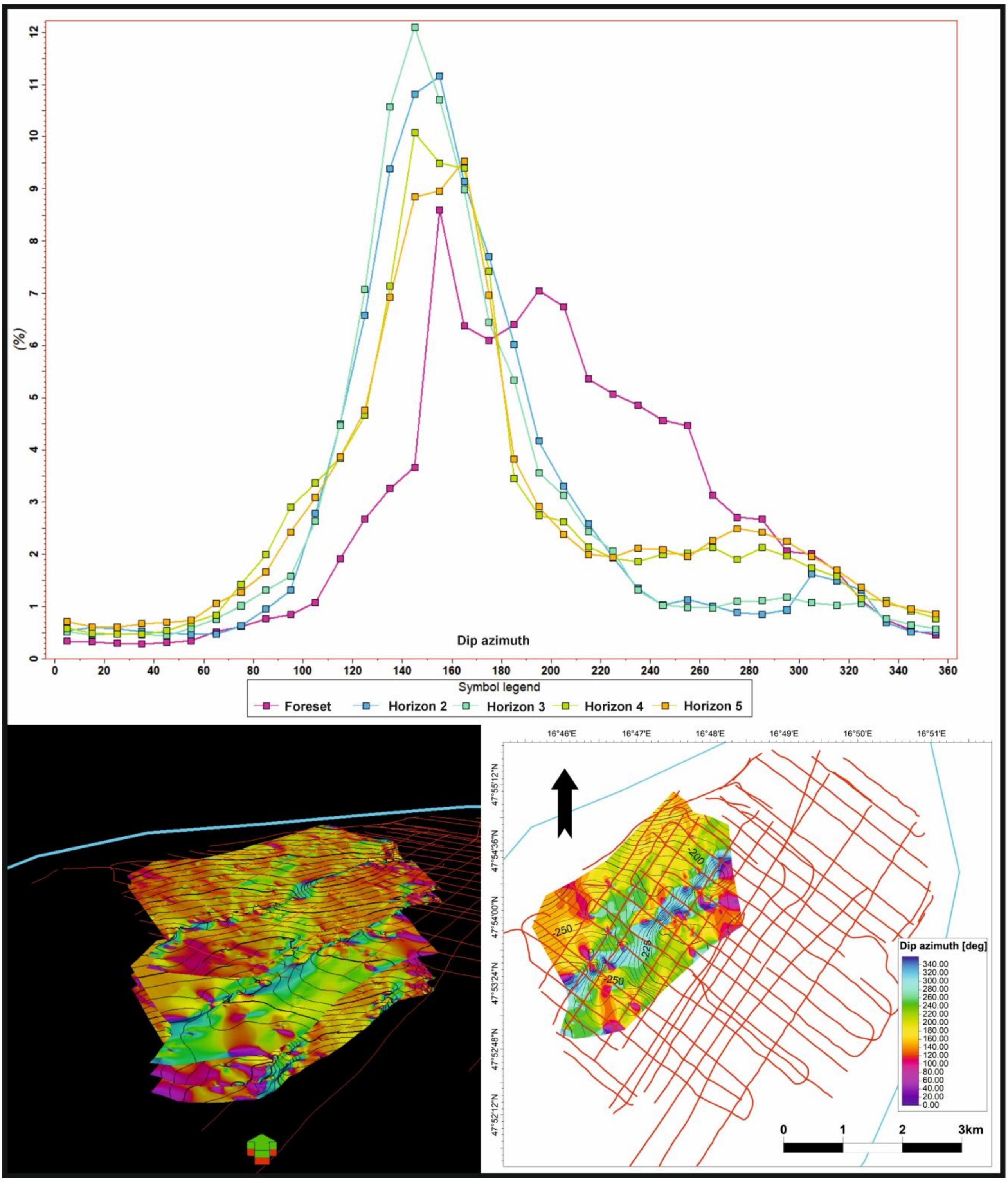

Figure 34. Graph illustrating the distribution of dip azimuths for points on mapped horizons. Most horizons display a primary dip direction close to 150°, reflecting regional dip direction. The analyzed area contains a mapped top clinoform horizon (purple), whose distribution is bimodal, suggesting the presence of a partly superimposed secondary inclination within the clinoform package. Lower left: Overview of all horizons used in the histogram; Lower right: Top view of the foreset of "Mid" horizon.

4.5. Channels/Erosional surfaces

Analysis of the uppermost parts of the seismic lines (down to ~50ms TWT) revealed the existence of erosional features of various continuity and morphology. Due to its higher seismic resolution, almost all of these erosional features were identified in single-channel seismic survey (Fig. 35). As some of these features are vertically superimposed and spatially clustered, categorization into 3 areas with Area 1 being divided into 2 sub-areas was established for better visualization.

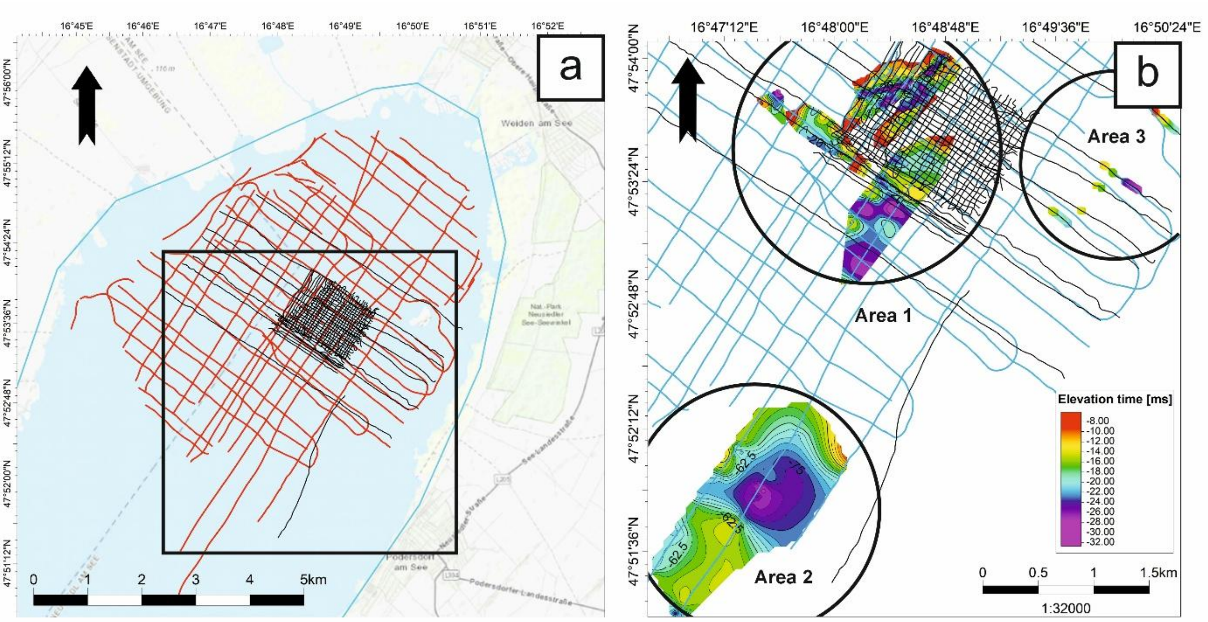

Figure 35. (a) General overview of seismic surveys used in this study. Black square delimits the area, where erosional channel-like features have been mapped. (b) Based on morphology and size of individual erosional features, the studied region is divided in 3 areas. Blue lines represent multi-channel seismic lines. Black lines represent single-channel seismic lines.

Area 1

This area contains the highest concentration of erosional features and was therefore further subdivided into Area 1.1 and Area 1.2 for visualization purposes (Fig. 36). Prominent and continuous erosional features, which are continuous at least through 3 subsequent seismic lines were identified, labeled A–G, and subsequently analyzed. Features A–C represent laterally extensive surfaces, while features D–G are more localized (Fig. 36).

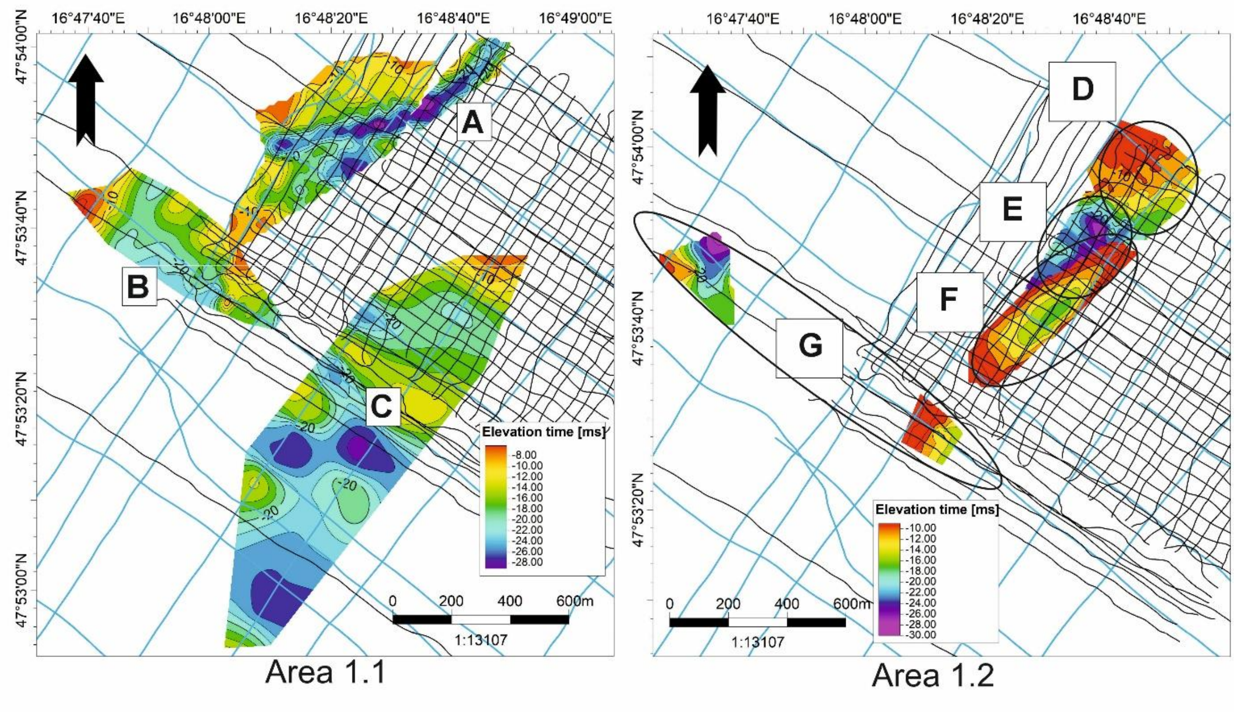

Figure 36. Overview of Area 1. Due to the presence of superimposed features, Area 1 has been subdivided into two distinct sub-areas for detailed analysis. Erosional features A-C represent laterally prevalent and most significant surfaces, while features D-F are more localized.

Within Area 1.1 (Fig. 36), feature A represents the longest and the best-preserved erosional channel-like structure. Its length is approximately 800 m, with the deepest point reaching 31 ms TWT. Fig. 37a provides a slightly oblique perspective of feature A, highlighting its narrow and deeply incisional geometry. Internally, a possible secondary erosional event, indicated by dotted lines in Fig. 37a, has been recognized, overlying the more seismically reflective lower succession of the feature A. The strata above this younger erosional reflector are seismically poorly resolved and appear homogeneous. Further to the southeast, Fig. 37b shows multiple superimposed erosional features (labelled as A, E, D and F), with feature A occupying the lowest stratigraphic position on the seismic line and retaining its narrow and deeply incisional character.

As seen in Fig. 38a, interpreted feature B represents a laterally extensive and faulted erosional surface, with a length of approximately 850 m and depth reaching up to 23 ms TWT. The northwesternmost part of the seismic line in Fig. 38a shows a small localized channel-like structure, which was initially considered a possible continuation of the feature A. However, the depth difference of about 15 ms TWT and its higher stratigraphic position (compared to feature A) does not conform with the structural setting in the area. Further, feature B is crosscut by the large-scale Fault 9 (Fig. 38a), implying fault activity postdating formation of feature B.

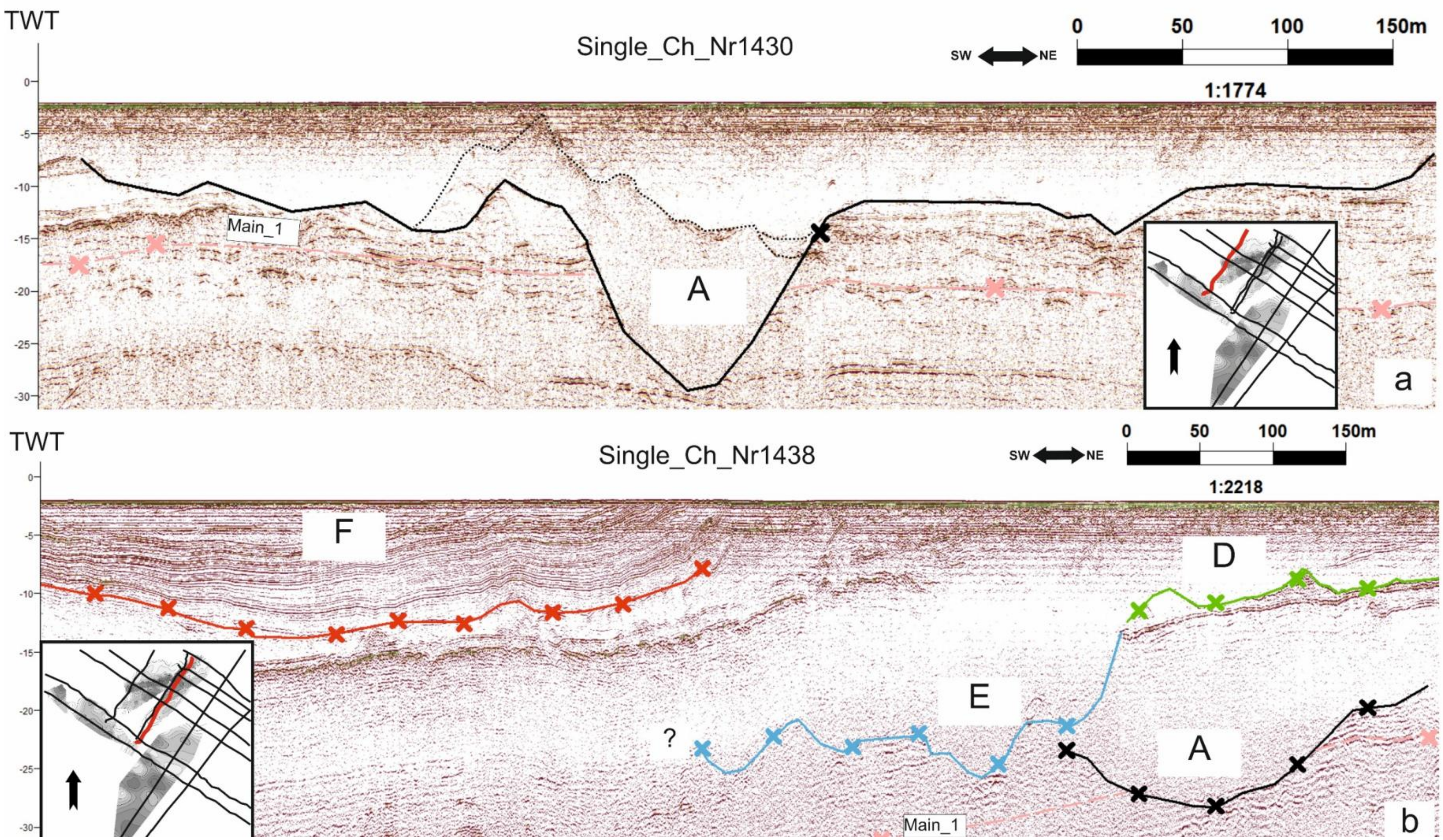

Figure 37. (a) Seismic line obliquely intersecting Feature A. Main Horizon 1 is crosscut by channel-like feature A. Dashed lines indicate a subsequent erosional event. (b) Seismic line illustrating multiple erosional features (A, D, E, F). Due to seismic noise, the lateral extent of Feature E cannot be clearly determined as well as its relationship with Feature D. Feature A cross-cuts Main Horizon 1. Note that the cross-cutting geometries of these features provide relative chronological information by cross-cutting relationships and suggest gradual lateral shift of channel belt. Feature F is depicted in near-perfect alignment with its longitudinal axis clearly showing stratification. VE: 5

In comparison with feature A, feature B appears more indicative of wide-spread, laterally extensive erosion with small distributed scours as shown in the central and eastern parts of the seismic line (Fig. 38a).

Feature C represents another laterally extensive erosional surface, which was interpreted in Area 1 and is observed exclusively in multichannel seismic lines (Fig. 38b). Due to the inherently lower seismic resolution of the multichannel data and the location of feature C very close to the top of the seismic line, it remains uncertain, whether feature C is a genuine erosional surface or a possible seismic artefact. Nevertheless, it most likely represents a real erosional surface as it is consistently observed on three separate multichannel seismic lines. Feature C reaches maximum depth of 30 ms TWT and can be mapped laterally for approximately 1600 m. This feature occurs above the main interpreted Horizon 1 (Fig. 38b) and is therefore regarded as the highest erosional surface within Area 1.

As shown in Figure 36, the northeastern part of Area 1 also contains two less extensive features, D and E. Feature D, stratigraphically positioned above the main channel represented by feature A, is characterized by relatively flat erosional base atop a high reflective seismic reflector (Fig. 39). The erosional base does not cut through the seismic reflector and older sedimentary strata are locally preserved bellow the base (Fig. 39). Unlike other erosional surfaces in the area, feature D is less vertically extensive, exhibiting a variation of only 5ms TWT. Its length is approximately 300 m, with maximum depths reaching 18 TWT. Dashed lines in the upper part of the feature D mark cross stratification, which might be a result of fluvial bar deposition (Fig. 39).

Feature E is shown in Figures 37 and 39 as an undulating erosional surface. The full lateral extent of Feature E remains unclear due to low seismic resolution of the seismic data. Its minimum observed length is 400 m, with maximum depths reaching 28ms TWT.

Unlike Feature A, Feature E does not form a single-channel but rather consists of multiple, channel-like incisional features (Fig. 39). As shown in Figures 37 and 39, Feature E is located either above or adjacent to the main channel of Feature A, in some places partially eroding it (Fig. 37). Due to a seismically blank area, it cannot be resolved if the Feature E is a continuation of Feature D or if these two are separate events of different age (Fig. 37).

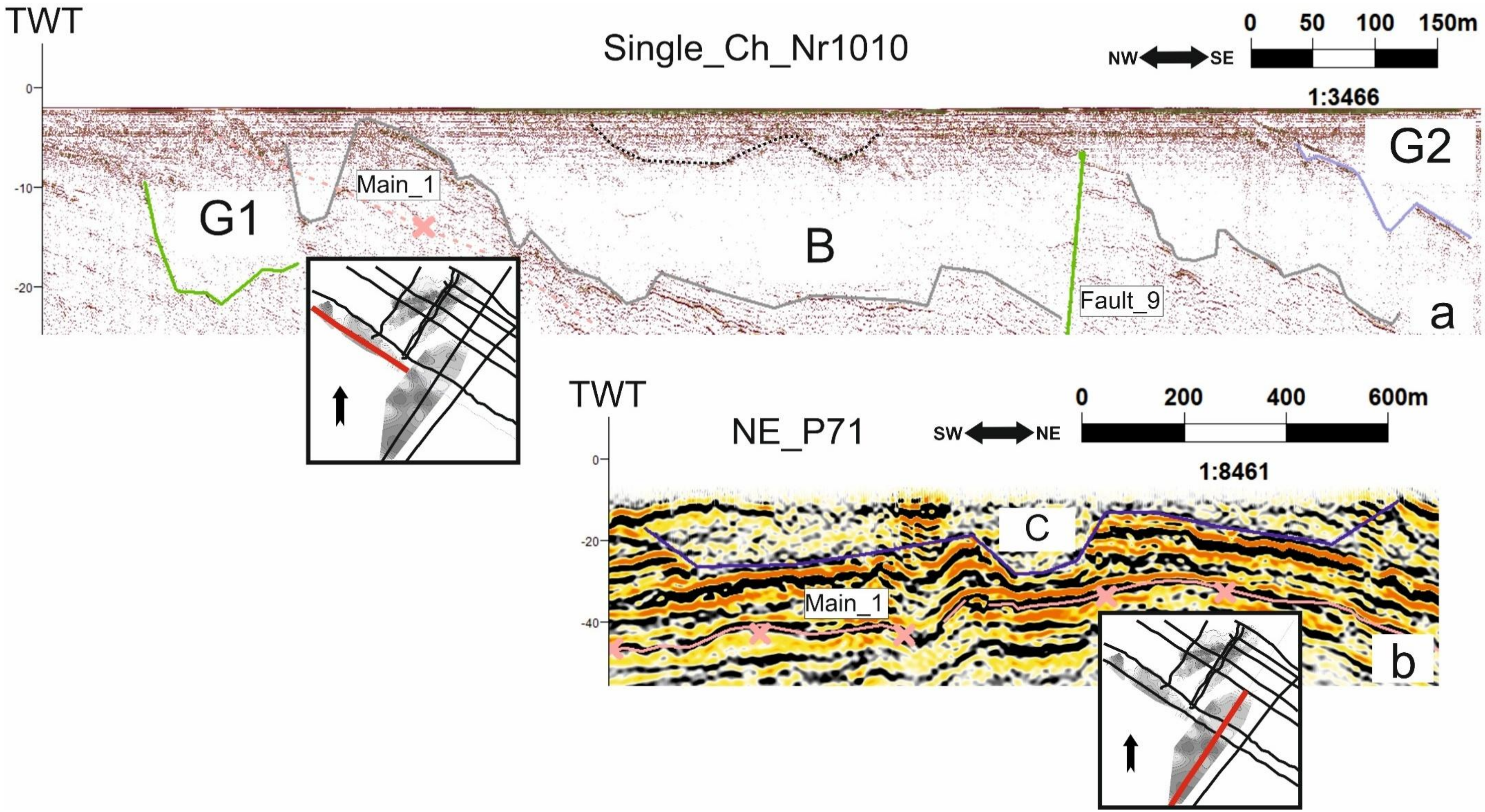

Figure 38. Two perpendicular seismic lines (a, b) displaying Features B, C, and G. Reference horizon Main_1 is crosscut by feature B, lies above feature G1 and occurs below features C and G2. (a) Feature B is one of the most prominent and the longest features. Note a narrow channel-like structure occurring in the northwest of the seismic line. Two features G1and G2 represent highly localized erosional features, each visible only in two seismic lines. (b) Feature C is the only erosional feature observed in the multichannel survey in Area 1. VE: 8

Another feature interpreted in Area 1, as seen in Fig. 36 is Feature F. This feature is located in the middle of Area 1 and appears to be fundamentally different from all others identified, primarily because it lacks typical indicators of erosion and instead shows well-defined sedimentary layering and thickening of the strata towards the northeast (Figs. 37 and 40). The stratal thickening is clearly visible in Fig. 37 especially at its lower part. The red mapped horizon represents the presumed base of the feature F (Fig. 37). In map view, the feature has an elliptical shape (Fig.36), extending over a length of 700m and reaching a maximum depth of 18ms TWT, with its highest points reaching up to the lake floor. The uppermost section of the feature is eroded. Evident weak internal folding is interpreted as post-depositional and is well observed along its long axis (Fig. 37). However, along its short axis, Feature F exhibits synclinal geometry, that does not appear in the underlying strata (Fig. 40).

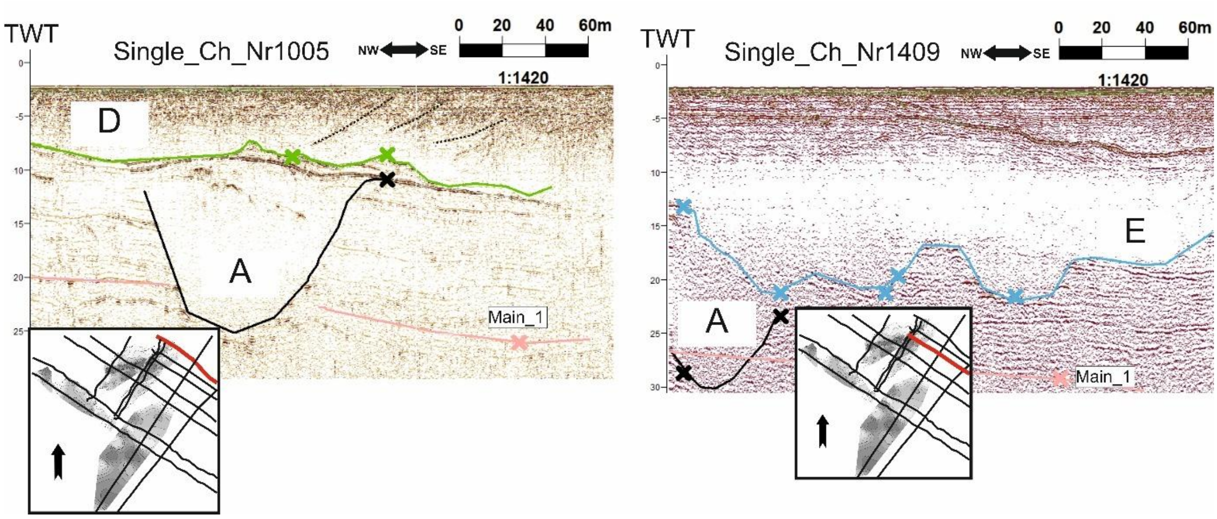

Figure 39. Two NW–SE oriented single-channel seismic lines illustrating Features A, D, and E. Feature A exhibits a pronounced channel-like geometry. Feature D, one of the shallowest features, displays characteristic uneven, erosional base, which runs along and does not cut through a strong seismic reflector. Dashed lines represent cross stratification, which might result of fluvial bar deposition. Feature E, which occurs above Feature A, shows some resemblance to fluvial structure with number of discrete channels; however, its geometry is not clearly defined. VE: 5

The last feature in Area 1 consists of two separate localized incisions (G1, G2 in Fig. 38a). Stratigraphically lower feature G1 displays a distinct channel-like morphology and is situated below the NW part of Feature B (Fig. 38a). Feature G2 that is located stratigraphically above the SE part of Feature B is characterized by a broader lateral extent and exhibits less pronounced erosional relief.

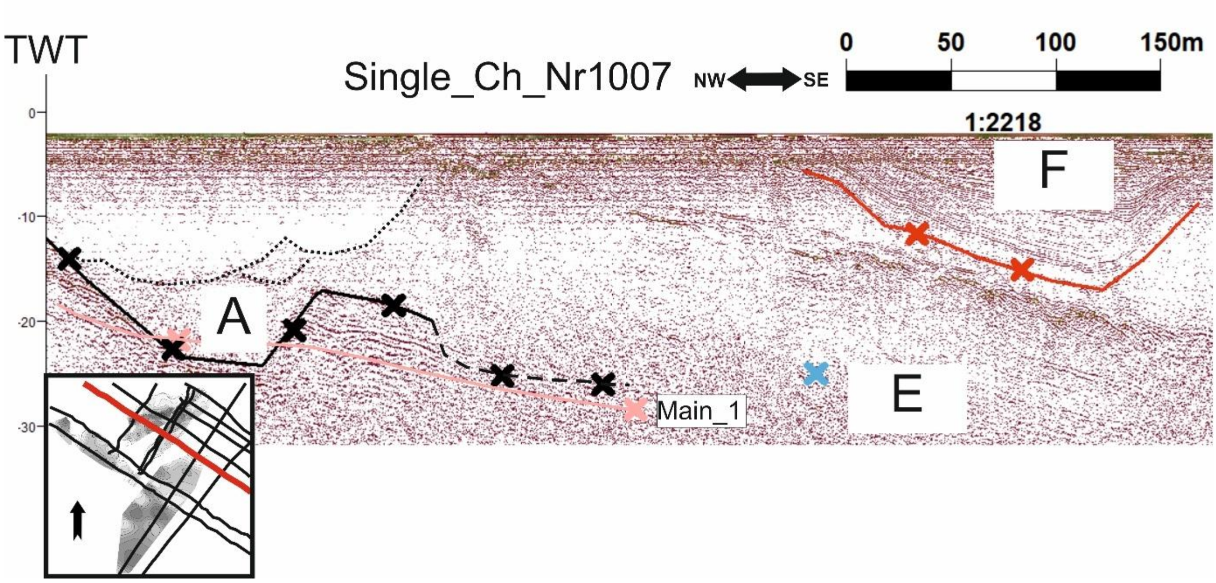

Figure 40. Seismic line illustrating Features A, F, and E. Feature A exhibits its distinct narrow channel-like geometry, although its full extent to the SE cannot be mapped due to seismic noise. Dotted lines within Feature A indicate subsequent erosional event. Feature E is not interpreted fully on this line. Feature F is observed from a perpendicular perspective relative to its long axis. VE: 5

Summary

Analysis of the relative stratigraphic relationships of individual features documented in the single-channel seismic data is shown in Figure 36 and indicates that Features A and G1 represent the oldest erosional events, while Feature F the youngest one. Features E and D are both younger than Feature A, with feature E directly eroding feature A while feature D is overlying channel-like feature A. Due to insufficient well data, their absolute ages remain uncertain. As mentioned before, one plausible interpretation is that Features E and D are two segments of a single erosional surface, with feature E forming the deeper part and feature D corresponding to a shallower part of the system. Localized feature G2 is younger than features E and D and probably slightly older that feature F.

Area 2

Area 2 represents the southeasternmost feature identified in the studied region (Fig.35). Due to the absence of single-channel seismic lines in this area, the features are observed exclusively on multichannel seismic lines (Fig. 41). It is the largest erosional surface interpreted in the upper sedimentary succession lying above the main Horizon 1, with dimensions of 2300×900 m and depths reaching up to 80ms TWT. The channel-like features are visible only on the three seismic lines available in this area, but probably extends beyond the current survey boundaries.

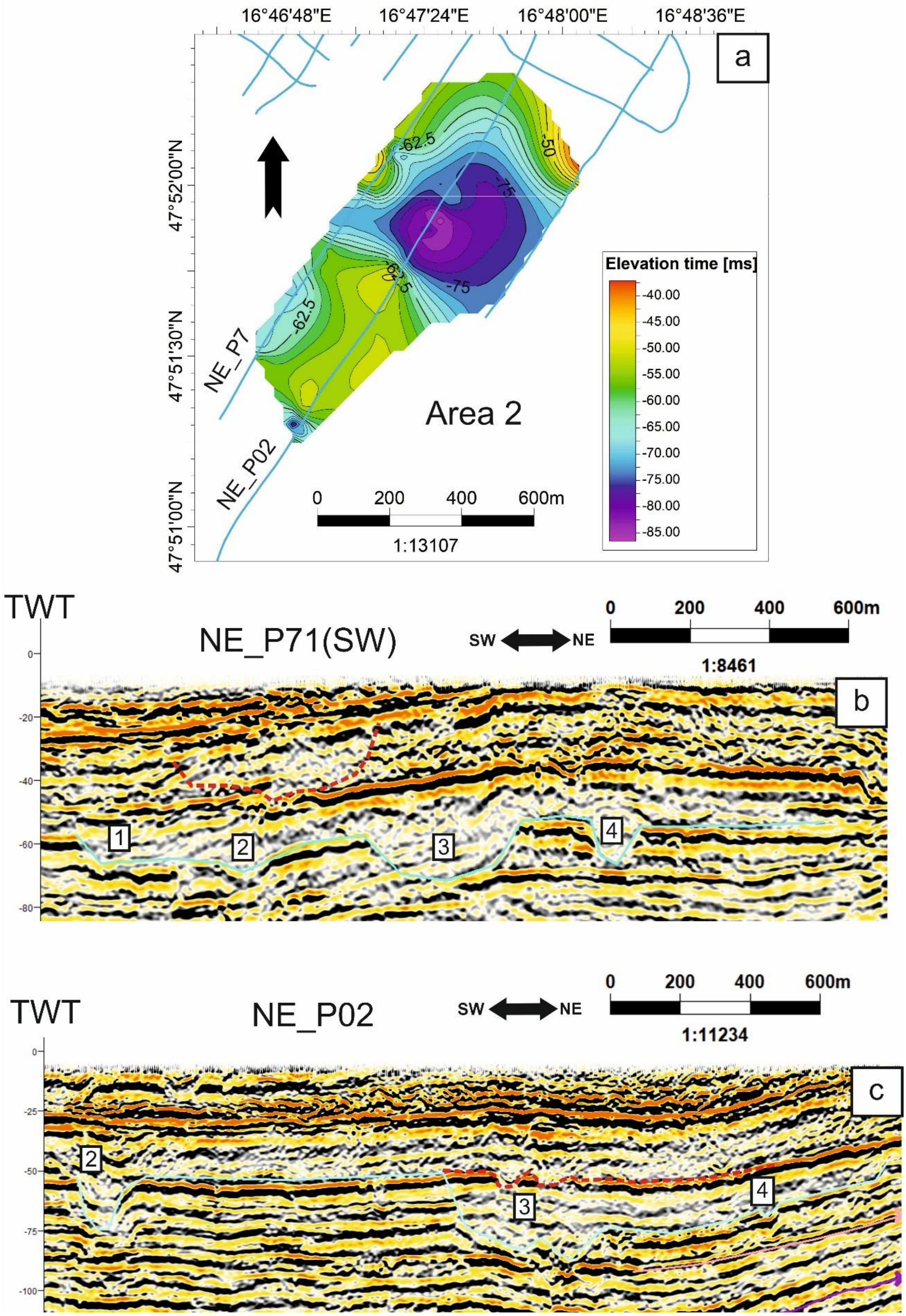

Figure 41. (a) Overview of Area 2.The horizon map is based on three multichannel seismic lines, two of them shown in (b and c).The seismic multi-channel lines show two channelized units. The older channel unit (in light blue) is shown as seismic surface in (a). Individual interpreted channels are numbered 1-4, with 2, 3 and 4 being laterally more continous. The shallower red dotted line represents a younger erosional event. VE: 7

Area 3

The final area containing shallow erosional features is depicted in Figure 42a and b. Area 3 is characterized by semi-connected, sometimes localized and vertically restricted (not deep) erosional features, that are shown in Fig. 42 and numbered 1-3. Given the limited lateral extent of individual features and the sparse line density in this area, no horizon map was constructed (Fig. 42c). Youngest erosional channel-like feature (1) is depicted in Fig. 42a. The most prevalent erosional surface in the easternmost part of the studied area is marked by 2 and involves up to 3 individual incisions (Fig. 42a, b). In one example, internal architecture and lateral migration of channel can be seen (Fig. 15b). Additionally, Figure 42b shows a distinct surface marked by (3) with erosional base up to 10 ms TWT that might represent a channel belt. Locally, convex-up seismic reflectors occur below the erosional base of the surface 3 (marked by 4 in Fig. 42). These reflections are interpreted as preserved remnants of fluvial bar or channel levee.

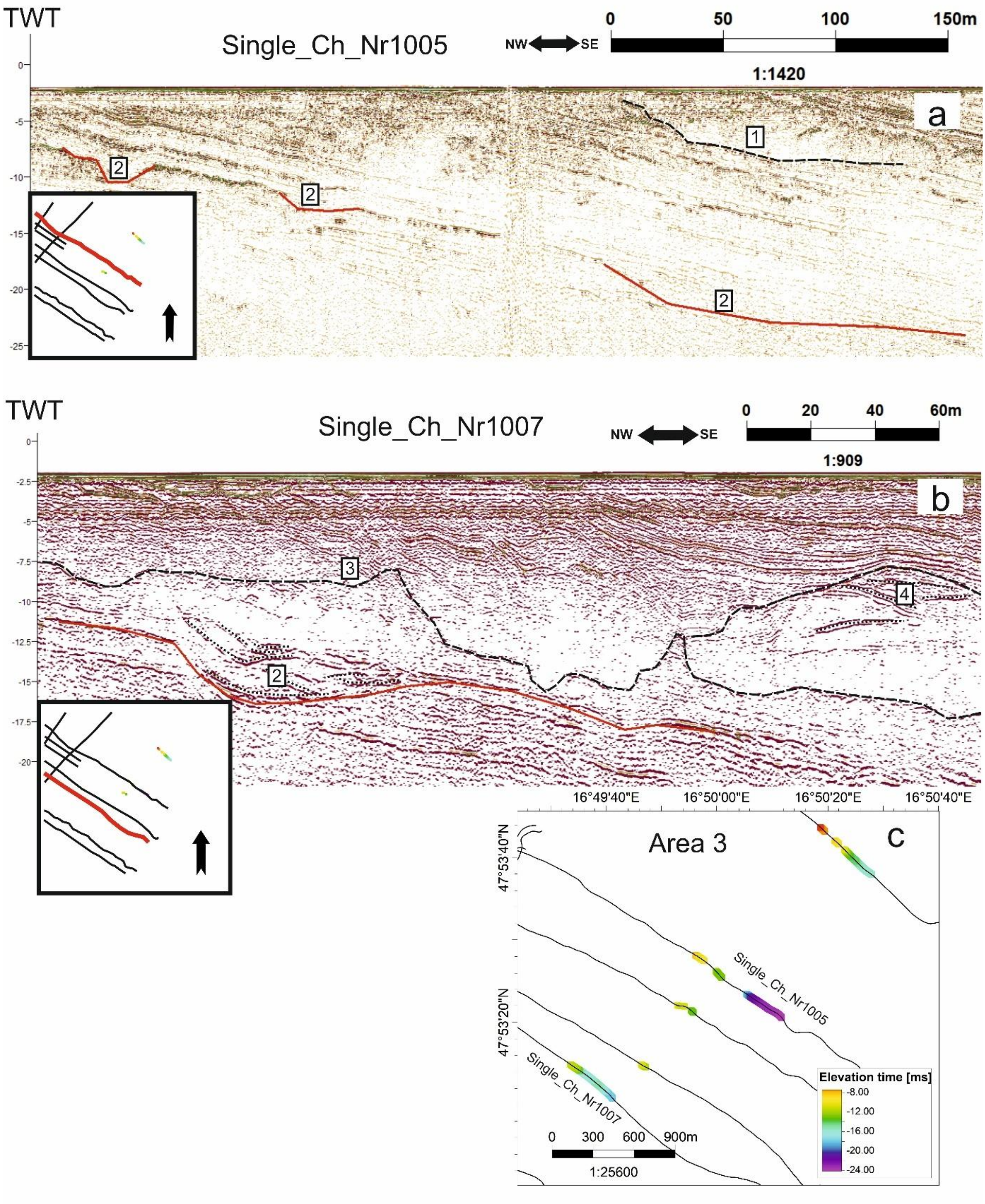

Figure 42. Two representative single-channel seismic lines (a, b) are presented in this figure: (a) Seismic line displaying two erosional features (1) and (2). (b) Seismic line illustrating erosional features (2) and (3) at a sub-10m scale. Feature (2) with individual channel incisions is tracked on several seismic lines suggesting that they are part of a single erosional feature. Notably, more pronounced channel-like morphology and internal structure is observed within (2). Feature (3) marks a prominent erosional feature, likely representing a channel belt, while (4) might represent a remnants of a fluvial bar. (c) Overview of Area 3. The features identified in this area lack sufficient spatial continuity to be assigned to one surface. VE: 7

4.6. Chimneys

Both single- and multi-channel seismic lines exhibit vertical acoustic anomalies that generally persist through all interpreted reflectors, often extending down to the acoustic basement (Figs. 43 and 44). Importantly, the fact that the chimneys occur in both seismic surveys suggests that these are most probably not seismic artefacts. These narrow seismically blank zones typically show a characteristic geometry of being widest at their base and thinning toward the surface. In this study, the vertical seismic anomalies were mapped using the horizon mapping tool in Petrel (Fig. 44). V-shaped outlines were used to map the anomalies, with the maximum width of the V shape representing the width of each anomaly at the uppermost part of seismic sections.

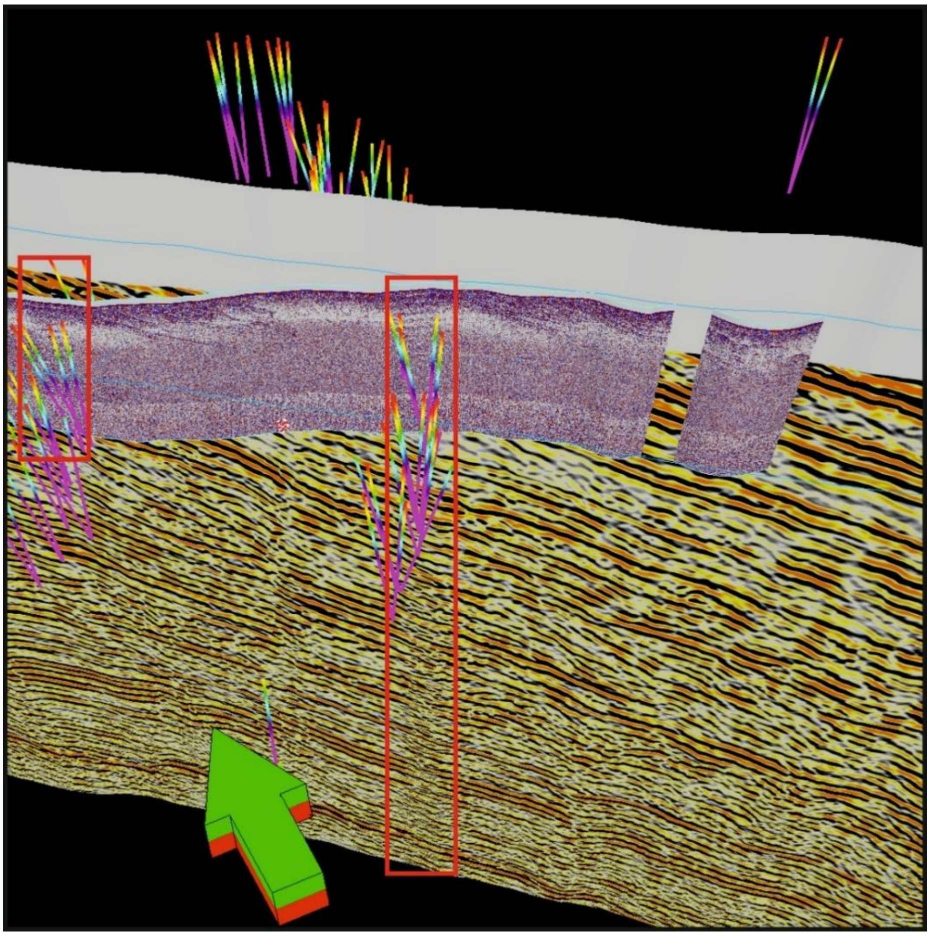

Figure 43. An oblique view of a selected single-channel line and multi-channel line, each containing features interpreted as chimneys (highlighted by red rectangles). The coloured V shaped outlines were drawn using Petrel horizon drawing tool to outline the location of the chimneys. Note that the mapped

structures (delimited by red rectangles) show clear continuity between multi-channel and single-channel lines. The fact that the chimneys are displayed in both seismic surveys suggest that these are not seismic artefacts.

The initial analysis of the seismic data by (Loisl et al., 2018) suggested that the observed anomalies might correspond to so-called "Kochbrunnen"—a local term used for natural gas seeps in Lake Neusiedl, well observable during winters when the lake is frozen. Additional studies in the region (Rank et al., 1985; Tanzberger, 2005; Bähr, 2024) have mainly investigated the chemistry and distribution of such gas seeps, generally concluding a predominantly shallow biogenic gas origin. Nevertheless, it remains uncertain whether minor contributions from deeper, more mature sources might also be present (Rank et al., 1985).

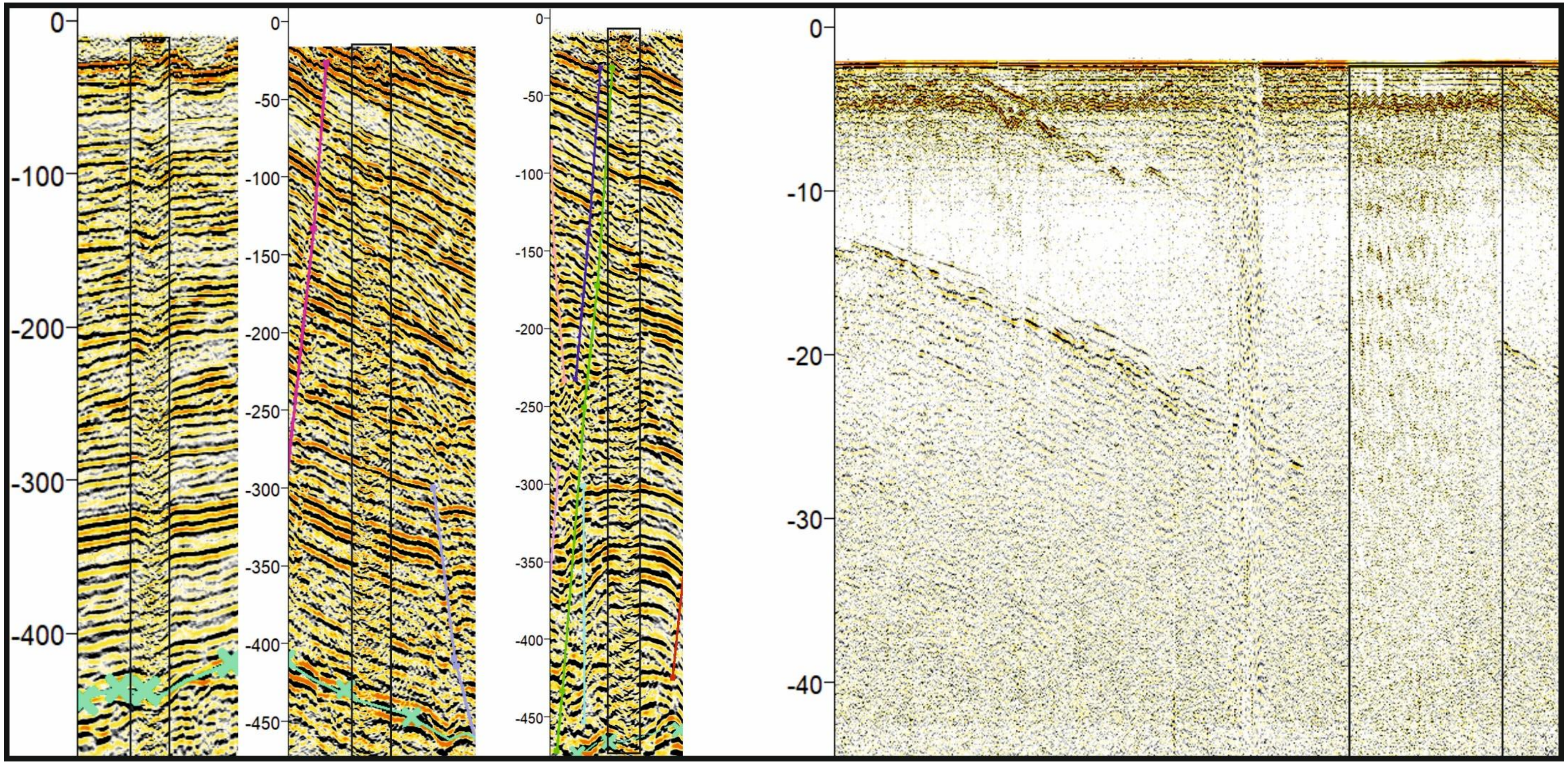

Figure 44. Examples of seismic lines displaying prominent vertical acoustic anomalies (seismically blank areas), interpreted as gas chimneys and highlighted by black boxes. The multi-channel lines are shown on the left, including the mapped acoustic basement (in green). The single-channel line is displayed on the right.

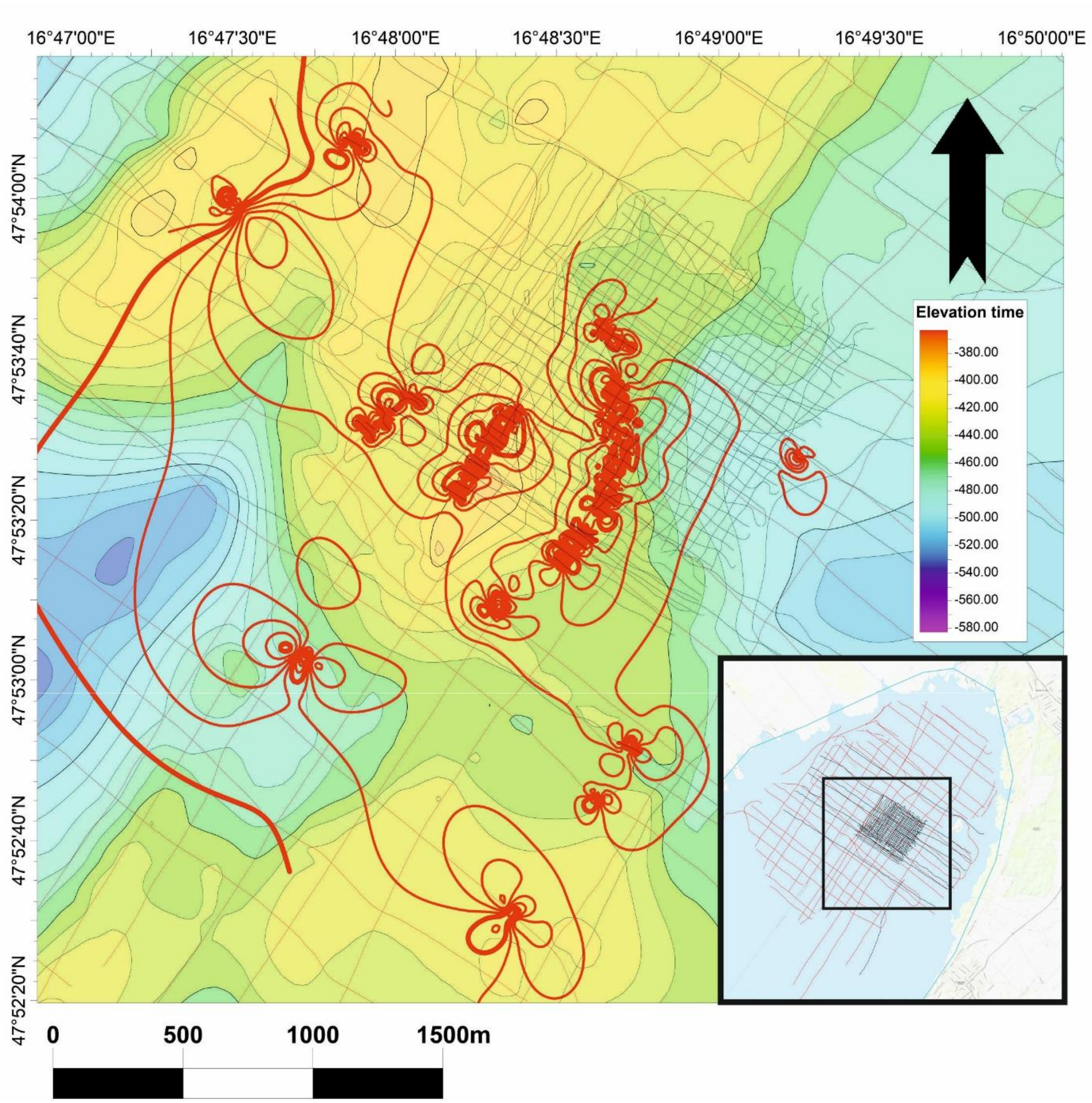

Figure 45. Overview of mapped chimneys depicted in red shows areas with isolated occurrences and elongated, laterally continuous chimney structures. Black and red lines in the inset indicate SC and MC seismic lines. The chimneys extend even below the acoustic basement level, which is shown as a surface in this figure. Note that majority of chimneys, especially laterally extensive ones, are located above a regional roughly NE-SW trending basement high.

The distribution of all mapped chimneys is presented in Figure 45**.** Most of the chimneys are predominantly concentrated in the central portion of the lake (see inset in Fig. 45). Moreover, almost all of the more laterally extensive chimneys are located above a basement high, which is shown as seismic surface in Figure 45. The chimneys are predominantly appearing in a linear arrangement and only rarely as isolated circular features (Fig. 45). The mapped chimneys do not appear to originate from any specific depth interval on the seismic sections (Figs. 44 and 46); rather, they penetrate the full vertical extent of the sections. Uninterpreted and interpreted multi-channel seismic section NE_P46 displays an example of two chimneys that coincide with occurrence of normal fault in depth of c. 430 ms. The vertically offset horizon acoustic basement (shown in green in Fig. 46) supports the existence of the fault, although the seismic resolution is low. In fact, documented chimneys appear often adjacent to or even superimposed on interpreted normal faults. The inset in Figure 46 shows that some chimneys are elongated. A single-channel seismic profile Ch-Nr1510 runs along the long axis of the largest identified elongated chimney (Fig. 46) suggesting that NE-SW trending faults play an active role in formation of chimneys.

The origin of the chimneys remains unclear and cannot be deciphered based on seismic data only. On one hand, geochemical data suggest shallow biogenic origin of the gas, on the other hand, deeper source cannot be ruled out. For example, late Miocene strata contain coal layers, which could be the source of the observed chimneys. This is, however, not supported by the seismic data. The basement is not an ideal candidate for gas production, although it seems that the chimneys are in many cases related to basement faults. It is noted, that the penetrative nature of the chimneys and their existence in the deepest levels needs to be treated with caution, because it could be a seismic artefact caused by shallower structures.

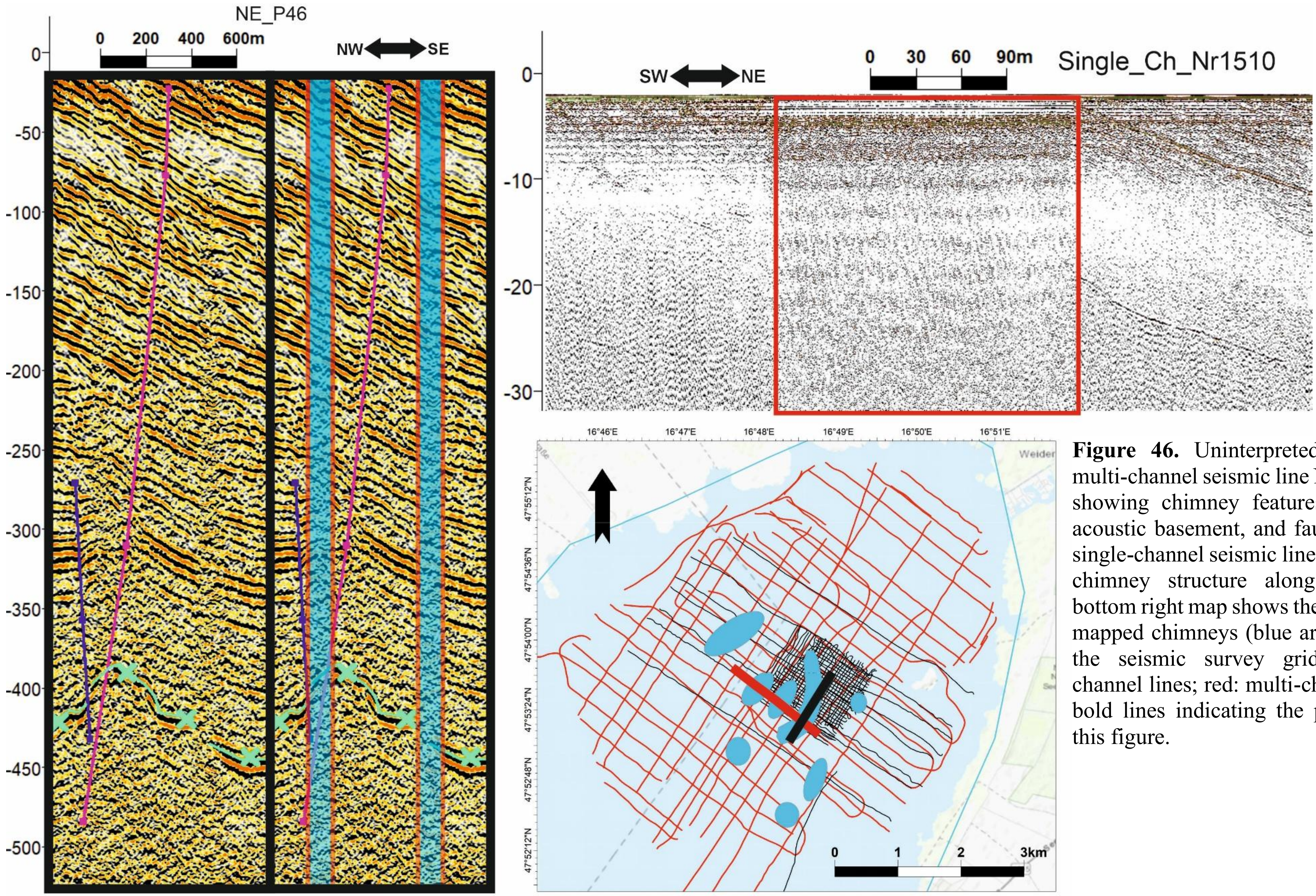

Figure 46. Uninterpreted and interpreted multi-channel seismic line NE_P46 to the left showing chimney features (blue), mapped acoustic basement, and faults. The top right single-channel seismic line Nr_1510 displays chimney structure along its strike. The bottom right map shows the distribution of all mapped chimneys (blue areas) in relation to the seismic survey grid (black: single-channel lines; red: multi-channel lines), with bold lines indicating the profiles shown in this figure.

5. Discussion

The westernmost part of the Danube Basin, adjacent to the Leitha Mountains, still presents an exploration challenge (Fig. 47). While regional well data and outcrop information exists in surrounding areas (Fig. 48, 49), no direct stratigraphic control is available within the studied central region. Given the absence of age constraints within the seismic survey area, regional interpretation relies primarily on seismic features and structural analysis. The approach therefore integrates multiple lines of evidence including visible seismic structures, external and internal geometries, syn-tectonic growth patterns in the strata, differential fault offsets, and thickness variations of individual seismic packages to reconstruct regional evolutionary trends.

The study area is located in the transition zone between the Eastern Alps and the Danube Basin, which formed as part of the broader Pannonian Basin complex. Basin formation initiated between 15-20 million years ago during the early to middle Miocene, characterized by fluvial and marine environments with the deposition of Badenian and Sarmatian sediments during the latter. These sediments are preserved as carbonate platforms in the Leitha Mountains region and are also proposed to exist in the area of Seewinkel (Häusler et al., 2010; Loisl et al., 2025). The absence of Badenian and Sarmatian sediments in the Podersdorf-1 well suggests that the Podersdorf High remained above sea level during this period (Fig. 51). The existence of high, or an elevated area in general, is further supported by the geometry of Badenian and Sarmatian strata in the Seewinkel region, where they onlap and thin towards the Podersdorf High. Faults within the Badenian and Sarmatian strata that are documented in the Leitha Mountains (Wiedl et al., 2014b and citations therein) indicate ongoing extensional tectonic activity, albeit of limited intensity .

Throughout the studied Miocene stratigraphic sequence, an extensional regime with normal faulting was dominant, with all mapped faults from oldest to youngest generally maintaining a clear NW-SE trend (Fig. 47).

As documented in the Frauenkirchen well data, Badenian and Sarmatian sediments exist in the vicinity of the seismic survey, with onlapping geometries observed at 1200ms TWT. However, these strata occur at significantly greater depths compared to the seismic survey coverage, which reaches a maximum basement depth of approximately 600ms TWT. Assuming these strata would exhibit morphologically similar characteristics to those observed in the Frauenkirchen well and vintage seismic line B03, any Badenian-Sarmatian deposits within the survey area would be of very limited extent. The clearest indication of onlapping sedimentary package onto basement is observed in the deepest part of the southwestern portion of the survey (Fig. 33). Given the scarcity of such features, it is concluded that sediments of this age occur only in isolated pockets, if at all, within the seismic survey area, with more extensive deposition occurring further west toward the Leitha Mountains, where fault geometry and orientation would favor their preservation at depth.

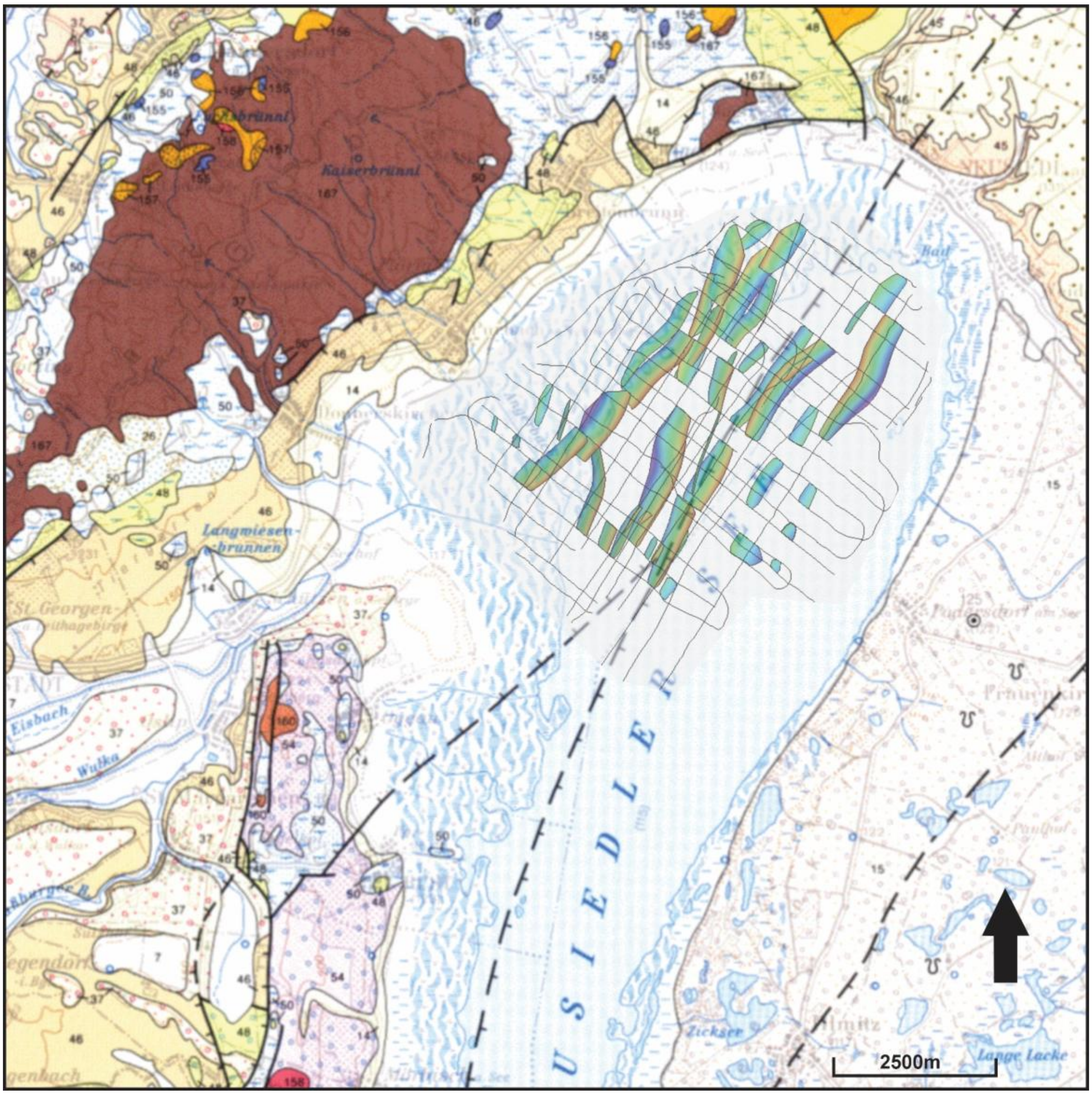

Figure 47. NE-SW trending fault systems mapped from seismic data. Fault traces overlain on regional geological map (Fuchs and Grill, 1984). Note a high-resolution of the mapped faults.

Through analysis of seismic package thickness variations, changes in fault activity can be observed and fault induced dip directions inferred. The studied stratigraphic sequence reveals an initial period of westward thickening, followed by a brief interval of relative tectonic quiescence, succeeded by a second, milder phase of westward thickening of the strata. This pattern, which is represented by the oldest packages 1 to 3 (Fig. 28a) is interpreted to reflect fault-controlled basin formation. It is likely, that normal faults existed in the area between the Leitha Mountains and the area of the seismic surveys, serving as the primary structural control.

Early clinoform development is also evident within the lowermost seismic package 1, although these features remain sparse as documented in Figure 32.

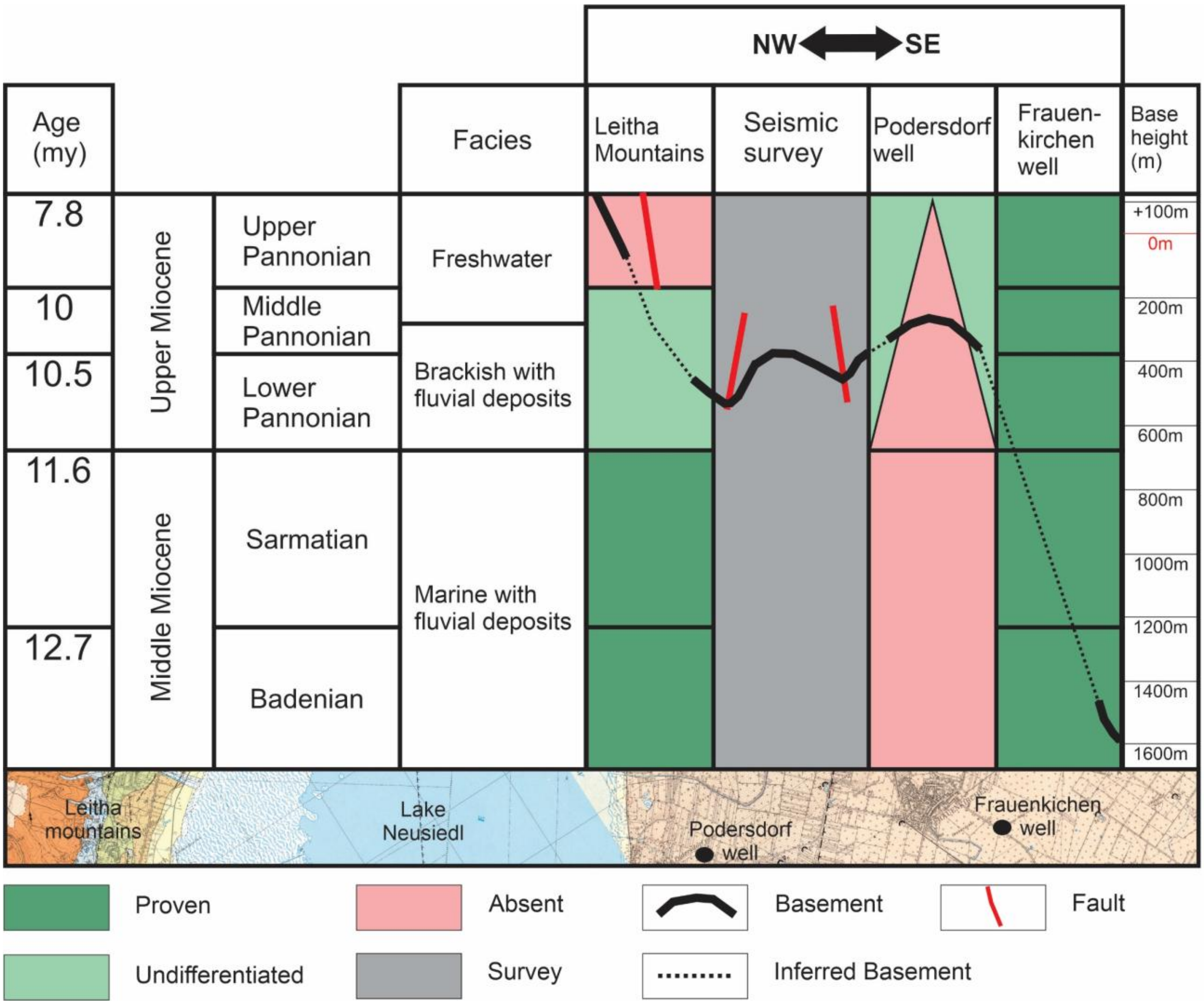

Figure 48. Geochronological chart of the studied area, derived by data from well logs, outcrops, and morphology (Häusler et al., 2018 and references therein). Pink: absent, light green: undifferentiated, green: proven, grey: seismic survey coverage. The pink triangle at Podersdorf indicates the missing sub-divisions of the strata, as it was designated only as undifferentiated "Pannon" in the well log data. Overlain is also the true depth of the top basement: black lines represent proven data; dotted lines indicate inferred connections. Red lines represent proven faults.

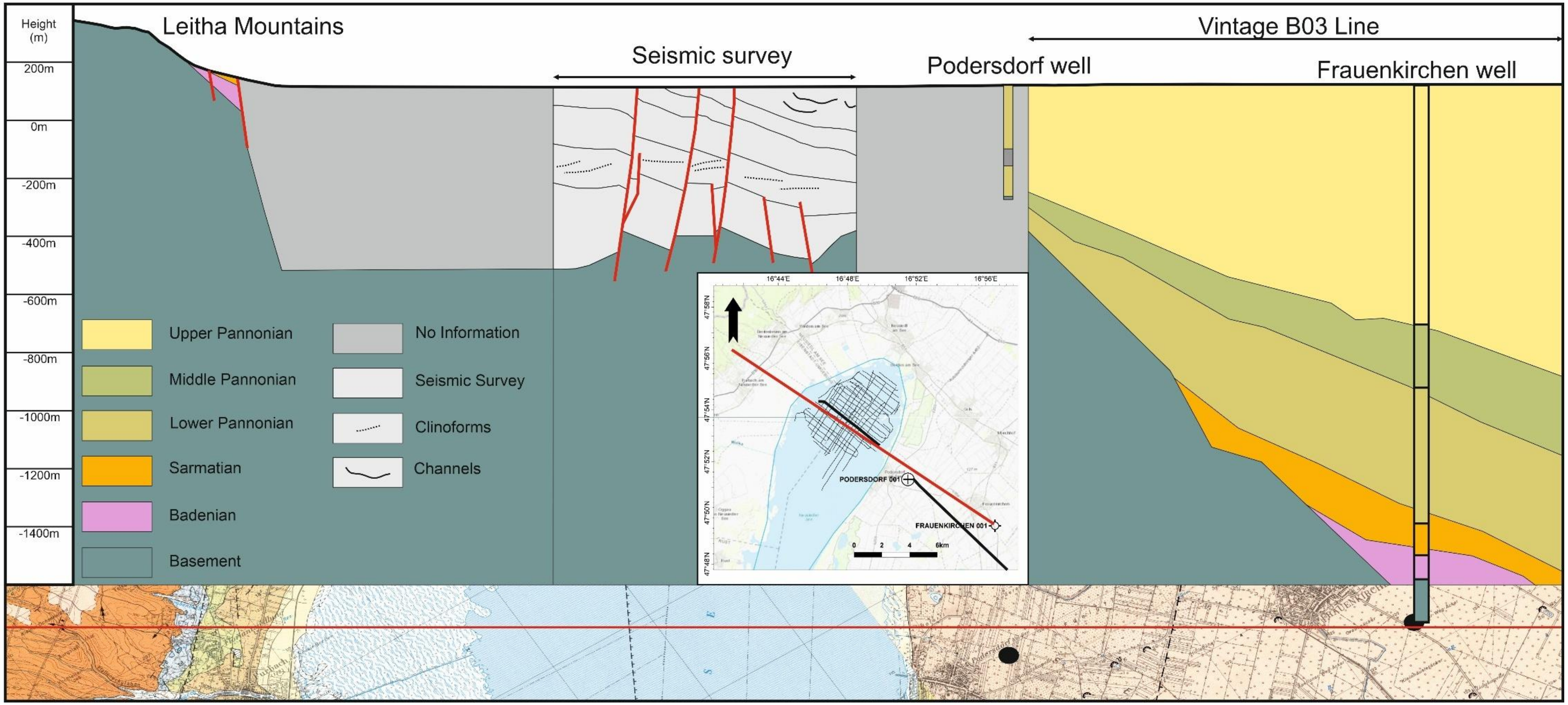

Figure 49. Cross-section running from the Frauenkirchen well in the east to the Leitha Mountains in the west. It shows only proven observations derived from seismic data, well logs and outcrop analysis. The multichannel seismic line “NE_P46” and the vintage seismic line “B03” were projected onto the section for tectono-stratigraphic context. Light grey indicates the extent of seismic survey coverage, whereas dark grey delimits areas with no available data.

The first major observation relevant for establishing the relative age of the undated succession documented in the seismic surveys is the presence large-scale regionally occurring clinoforms in Package 4 that are interpreted as prograding deltaic deposits, most likely associated with the decreasing size of Lake Pannon, water level oscillation and sediment supply fluctuation. Magyar et al. (2013) dated similar clinoforms found in the broader vicinity of the study area as part of the prograding paleo-Danube system, roughly between 10-9 Ma. Although the clinoforms observed in these regional studies exhibit greater thicknesses and dimensions, linking the features identified in this study to the general progradational trend of the Danube delta system is reasonable. This correlation establishes a broad temporal framework for the observed strata with clinoforms (package 4) within the studied area. As documented in the previous chapter, the clinoform dip directions exhibit a bimodal distribution. While Loisl et al. (2018) previously identified clinoforms following the general southeastern trend, this study reveals that some clinoforms within the same package dip toward the southwest, in the direction towards the Leitha Mountains and presumed active fault(s), as demonstrated in the histogram shown in Figure 34. This bimodal pattern, combined with the previously described westward thickness increase, indicates a more complex depositional history than simple unidirectional progradation.

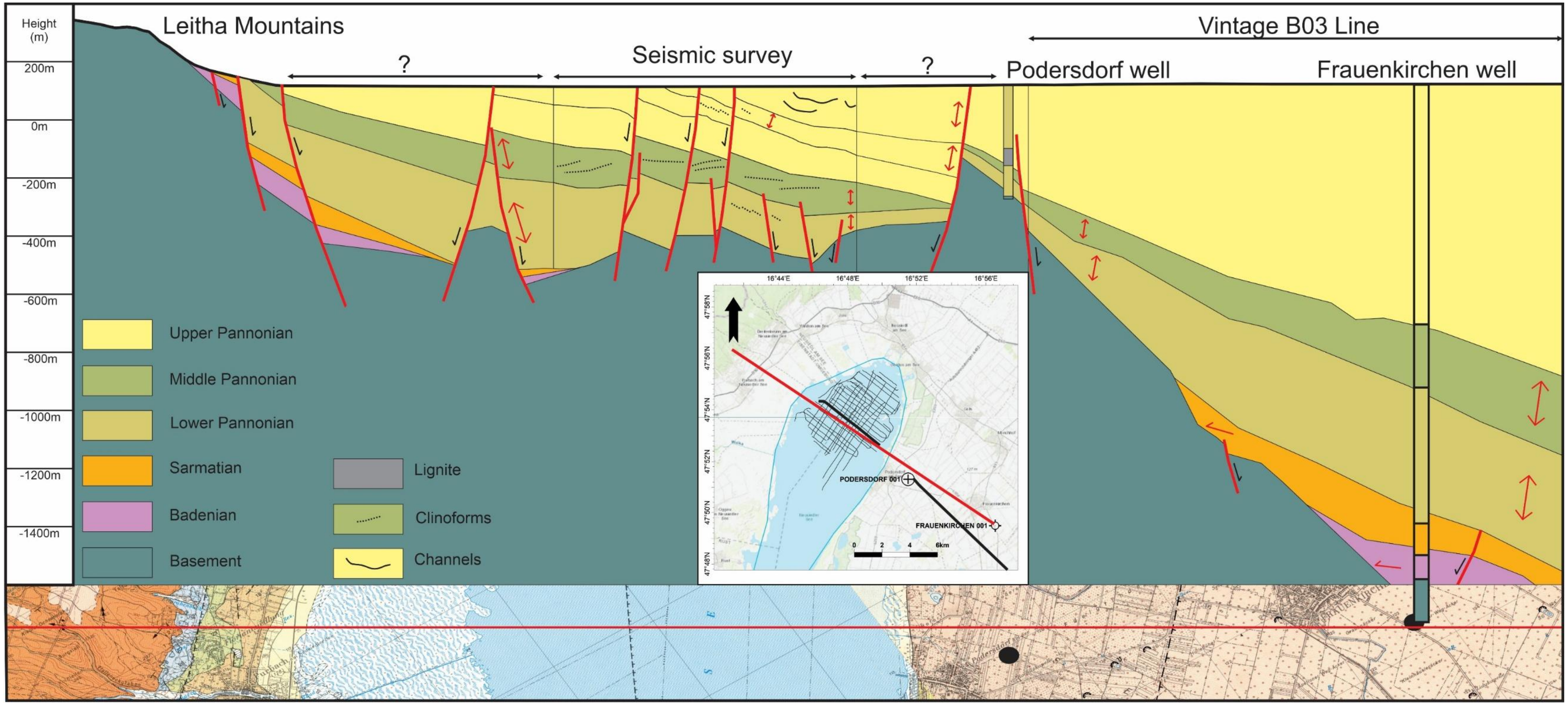

Figure 50. Interpreted version of the cross section presented in Figure 49. The interpretation includes an introduction of a major fault of presumed Upper Pannonian age close to the Podersdorf high and major fault of Lower to ?Upper Pannonian age close to the Leitha Mountains. Small pockets of Badenian and Sarmatian succession are further interpreted to exist in the NW, as result of topographic infill and fault-controlled deposition. Question marks indicate zones of geological interpretation based on structural coherence and regional trends, where data coverage is absent. Double-arrows indicate stratal thickening.

Loisl et al. (2025) pointed out that stratigraphic correlation of existing wells is challenging and with uncertainties. Due to discrepancies in stratigraphic age interpretations derived e.g., from the Frauenkirchen well logs and its correlation with vintage B03 seismic data, and also due to the fact that Pannonian succession in the Podersdorf well is undifferentiated, the age constraints of the observed clinoforms remain uncertain. In Figure 50, specific ages of Lower, Middle and Upper Pannonian age are assigned to undifferentiated strata shown previously in Fig. 49. This represents an attempt of stratigraphic correlation across the Podersdorf High, rather than a definitive framework. Precise definition of Pannonian sub-stages west of the high is not feasible given the available seismic data, absence of well data and empirical control points in the vicinity, therefore, the stratigraphic framework presented here represents one possible scenario.

The Upper Pannonian strata (seismic packages 4-6) exhibit a pronounced southeastern thickening trend, indicating a shift in basin tilt from the NW to the SE. This SE to E strata tilting is interpreted as a result of either ongoing or renewed tectonic activity in the study area and possibly also east of the Podersdorf High, but mainly result of thermal subsidence of the central Pannonian basin. A fault adjacent to the Podersdorf high is introduced to accommodate this thickness variation while maintaining the structural high (Figure 50). During Upper Pannonian deposition, a further transition toward fully fluvial conditions is inferred and agrees with regional studies (e.g., Magyar et al., 2013; Sztanó et al., 2025). This interpretation is reinforced by the presence of paleochannels preserved in the uppermost portions of the seismic survey, as documented in the chapter 4.5. Given that regional basin inversion occurred at approximately 6 Ma, this provides an upper age constraint for these strata and paleochannels. The actual age may be somewhat older considering potential erosion of overlying strata, as evidenced by the truncated nature of Package 6.

As already explained in the previous chapter, the chimneys are well known and studied, but the source of the gas remains unclear - whether it is purely biogenic or involves also deeper sources

(Häusler et al., 2010). One new observation from this work is that majority of the documented chimneys do not appear to be circular and restricted in their locations as traditionally expected, but rather extensive and often linear. This suggests that they do not seep from very limited point sources but rather stretch along fault zones, which is sometimes directly observable through stratigraphic offsets occurring exactly where the chimneys are located (Fig. 46).

In summary, seismic data analysis, complemented with published literature have led to a construction of a geological profile, using only proven age data from well logs and outcrop observations, establishing thus the factual foundation for the regional stratigraphic framework (Fig. 49). Subsequently, the gaps between these empirical constraints were interpreted through integration of seismic data and structural analysis, and regional geological context (Fig. 50). Finally, these interpretations were synthesized into a comprehensive tectono-stratigraphic model that illustrates the basin development in the study area from early/mid to late Miocene through the transition from marine to lacustrine and finally to fluvial environment (Fig.51).

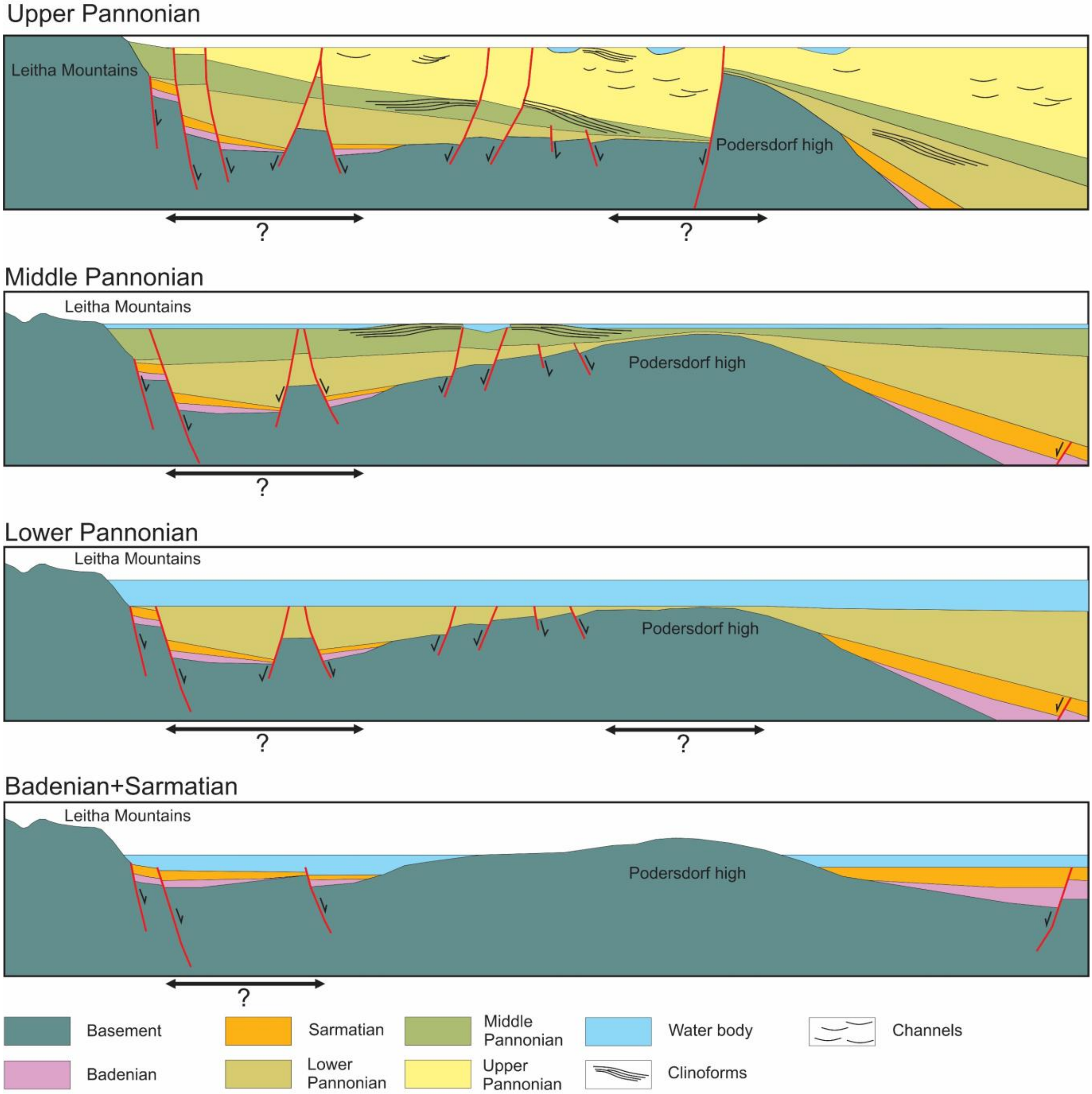

Figure 51. Four schematic drawings illustrate the tectono-stratigraphic evolution of the study area. Badenian+Sarmatian: Initial basement subsidence and segmentation due to syn-sedimentary faulting, geometry of strata also indicates role of palaeotopography, with the Podersdorf high remaining above the water table. Marine conditions. Lower Pannonian: Continued subsidence of the region with the Podersdorf high sinking below the water table; enhanced fault activity in the western part resulted in westward thickening of strata. Middle Pannonian: Further subsidence and fault activity accompanied by the introduction of large-scale clinoforms in the upper Middle Pannonian interval, as observed in seismic data. Upper Pannonian: General eastward subsidence and stratigraphic thickening, with the introduction of fluvial channels indicating a transition from lacustrine to fluvial environment. Small-cale clinoform development persist in the lowermost Upper Pannonian. Overall southeast dip of the strata is interpreted as result of regional subsidence of the Pannonian Basin as well as active faulting along the Podersdorf high.

6. Conclusion

1. Revision of the lake seismic datasets revealed a vertical offset between single and multichannel seismic as well as internal vertical offset in the multichannel seismic. These offsets were corrected prior to the seismic interpretation.
2. Thickness changes of interpreted seismic packages imply fault-controlled activity at different times in different areas (i.e., Badenian, Sarmatian and Lower Pannonian) and reactivation of older structures during the Upper Pannonian and Pliocene.
3. Three packages with clinoforms were identified. Complex depositional pattern of the largest clinoforms interpreted as deltaic in origin and as Middle to ?Upper Pannonian in age suggest at least two directions of propagation. The deltaic clinoforms possibly link with the progradation of the paleo Danube.
4. An existence of normal fault(s) along the western side of the Podersdorf High is proposed. However, the magnitude and lateral continuation of this fault as well as of the high remains unclear due to lack of seismic data.
5. Fluvial channels of presumed Upper Pannonian age and several other erosional features have been documented in the area.
6. Chimneys, defined as vertical distortions on the seismic data do not appear always as localized circular features, but commonly exhibit elongated appearance. In some cases, their positions roughly correlate with deep seated faults.
7. This study links observations from the adjacent Leitha Mountains and Seewinkel area to the seismic surveys for broader tectono-stratigraphic context.

7. Bibliography

Bähr, C., 2024, Systematic analysis of sediments, gas seeps and sludge gas at Lake Neusiedl: M.S. thesis, Montanuniversität Leoben.

Böhme, M., Winklhofer, M., and Ilg, A., 2011, Miocene precipitation in Europe: Temporal trends and spatial gradients: Palaeogeography, Palaeoclimatology, Palaeoecology, v. 304, p. 212–218, doi:10.1016/j.palaeo.2010.09.028.

Csontos, L., and Vörös, A., 2004, Mesozoic plate tectonic reconstruction of the Carpathian region: Palaeogeography, Palaeoclimatology, Palaeoecology, v. 210, p. 1–56, doi:10.1016/j.palaeo.2004.02.033.

Draganits, E., Weißl, M., Zámolyi, A., and Doneus, M., 2022, Lake Neusiedl Area: A Particular Lakescape at the Boundary Between Alps and Pannonian Basin, *in* Embleton-Hamann, C. ed., Landscapes and Landforms of Austria, Cham, Springer International Publishing, World Geomorphological Landscapes, p. 207–222, doi:10.1007/978-3-030-92815-5_13.

Fuchs, R., and Schreiber, O.S., 1985, Das Pannonien im östlichen Burgenland (Seewinkel), in Papp, A., ed., M6 Pannonien (Slavonien und Serbien): Akadémiai Kiadó, Budapest, p. 68–72.

Fuchs, W., and Grill, R., 1994, Geologische Karte von Wien und Umgebung, scale 1:200,000: Vienna, Geologische Bundesanstalt.

Harzhauser, M., Kranner, M., Mandic, O., Coric, S., and Siedl, W., 2022, High resolution Late Miocene sediment accommodation rates and subsidence history in the Austrian part of the Vienna Basin: Marine and Petroleum Geology, v. 145, article 105872.

Harzhauser, M., Kranner, M., Siedl, W., Conradi, F., and Piller, W.E., 2026, The Neogene of the Vienna Basin – a synthesis, in Tari, G.C., Kitchka, A., Krézsek, C., Lucic, D., Markic, M., Radivojevic, D., Sachsenhofer, R.F., and Šujan, M., eds., The Miocene Extensional Pannonian Superbasin, Volume 1: Regional Geology: Geological Society, London, Special Publications, v. 554, https://doi.org/10.1144/SP554-2023-168.

Häusler, H., Figdor, H., Hammerl, C., Kohlbeck, F., Lenhardt, W., and Schuster, R., 2010, Erläuterungen zur Geologischen Karte 78 Rust: Geologische Karte der Republik Österreich 1:50000, Geologische Bundesanstalt, Wien.

Häusler, H., Chwatal, W., Scheibz, J., and Gallistl, J., 2018, The Winden Syncline – a tectonic half-graben in the transition between the Lower Austroalpine and the northwestern Pannonian Basin (northern Burgenland, Austria): Zeitschrift der Deutschen Gesellschaft für Geowissenschaften, v. 169, p. 3–25, doi:10.1127/zdgg/2017/0122.

Heine, E., Loiskandl, W., Briese, C., Eberhöfer, C., and Csaplovics, E., 2016, Hydrografische Vermessung des Neusiedler Sees: Vermessung & Geoinformation, 2016(1), p. 9–24.

Hodits, B., 2006, Interpretation hochfrequenter Seeseismik und 3-D Strukturmodellierung im Neusiedlersee (Österreich): Diploma thesis, University of Vienna, 70 p.

Löffler, H. (Ed.), 1980, Neusiedlersee: The Limnology of a Shallow Lake in Central Europe: Dordrecht, Springer Netherlands, Monographiae Biologicae, v. 37, doi:10.1007/978-94-009-9168-2.

Loisl, J., Dax, F., Siedl, W., and Tari, G.C., 2026, Neogene sedimentation in the Austrian Danube Basin (Seewinkel, northern Burgenland): Geological Society, London, Special Publications, v. 554, p. gslspecpub2024-97, doi:10.1144/gslspecpub2024-97.

Loisl, J., Tari, G., Draganits, E., Zámolyi, A., and Gjerazi, I., 2018, High-resolution seismic reflection data acquisition and interpretation, Lake Neusiedl, Austria, northwest Pannonian Basin: Interpretation, v. 6, p. SB77–SB97, doi:10.1190/INT-2017-0086.1.

Magyar, I., Krezsek, C., and Tari, G., 2020, Clinoforms as paleogeographic tools: Development of the Danube catchment above the deep Paratethyan basins in Central and Southeast Europe: Basin Research, v. 32, p. 320–331, doi:10.1111/bre.12401.

Magyar, I., Radivojević, D., Sztanó, O., Synak, R., Ujszászi, K., and Pócsik, M., 2013, Progradation of the paleo-Danube shelf margin across the Pannonian Basin during the Late Miocene and Early Pliocene: Global and Planetary Change, v. 103, p. 168–173, doi:10.1016/j.gloplacha.2012.06.007.

Mitchum, R.M., Vail, P.R., and Thompson, S., 1977, Seismic stratigraphy and global changes of sea level, Part 2: The depositional sequence as a basic unit for stratigraphic analysis, in Seismic Stratigraphy applications to hydrocarbon exploration, American Association of Petroleum Geologists Memoir, p. 53–62.

Rank, D., Tschulik, M., Papesch, W., and Dolezel, P., 1985, Untersuchungen an den "Kochbrunnen" im Neusiedlersee bei Rust: BFB-Bericht, 55, p. 45–49.

Schmid, H., 1968, Das Jungtertiär an der SE-Seite des Leithagebirges zwischen Eisenstadt und Breitenbrunn (Burgenland): Wissenschaftliche Arbeiten aus dem Burgenland, 41, p. 1–74.

Šujan, M., Braucher, R., Kováč, M., Bourlès, D.L., Rybár, S., Guillou, V., and Hudáčková, N., 2016, Application of the authigenic 10Be/9Be dating method to Late Miocene–Pliocene sequences in the northern Danube Basin (Pannonian Basin System): Confirmation of heterochronous evolution of sedimentary environments: Global and Planetary Change, p. 35–53.

Šujan, M., Rybár, S., Kováč, M., Bielik, M., Majcin, D., Minár, J., Plašienka, D., Nováková, P., and Kotulová, J., 2021, The polyphase rifting and inversion of the Danube Basin revised: Global and Planetary Change, v. 196, p. 103375, doi:10.1016/j.gloplacha.2020.103375.

Székely, B., Zámolyi, A., Draganits, E., and Briese, C., 2009, Geomorphic expression of neotectonic activity in a low relief area in an Airborne Laser Scanning DTM: A case study of the Little Hungarian Plain (Pannonian basin): Tectonophysics, v. 474, p. 353–366.

Sztanó, O. et al., 2025, Sedimentology, lithostratigraphy, paleogeography and water level changes in a lacustrine basin: the depositional model of Lake Pannon: Geological

Society, London, Special Publications, v. 554, p. SP554-2024–72, doi:10.1144/SP554-2024-72.

Sztanó, O., Kováč, M., Magyar, I., Šujan, M., Fodor, L., Uhrin, A., Rybár, S., Csillag, G., and Tőkés, L., 2016, Late Miocene sedimentary record of the Danube/Kisalföld Basin: interregional correlation of depositional systems, stratigraphy and structural evolution: Geologica Carpathica, v. 67, p. 525–542, doi:10.1515/geoca-2016-0033.

Tanzberger, A., 2005, Die "Kochbrunnen" des Neusiedlersees/Ein kurzer Überblick über neue Untersuchungen: B.S. thesis, University of Vienna.

Tari, G., 1996, Neoalpine tectonics of the Danube Basin (NW Pannonian Basin, Hungary), in Ziegler, P.A., and Horváth, F., eds., Peri-Tethys Memoir 2: Structure and Prospects of Alpine Basins and Forelands: Mémoires du Muséum national d'Histoire naturelle, v. 170, p. 439–454.

Tari, G., Bada, G., Király, Á., Koroknai, B., Kovács, G., Lemberkovics, V., and Tóth, T., 2024, The Pannonian Basin: regional geology of a back-arc basin, in Chiarella, D., Scarselli, N., and Adam, J., eds., Regional Geology and Tectonics, 2nd ed., Elsevier, p. 1–25, https://doi.org/10.1016/B978-0-444-64136-6.00005-1.

Wiedl, T., Harzhauser, M., Kroh, A., Ćorić, S., and Piller, W.E., 2014a, From biologically to hydrodynamically controlled carbonate production by tectonically induced paleogeographic rearrangement (Middle Miocene, Pannonian Basin): Facies, v. 60, p. 865–881, doi:10.1007/s10347-014-0408-2.

Wiedl, T., Harzhauser, M., Kroh, A., Ćorić, S., and Piller, W.E., 2014b, From biologically to hydrodynamically controlled carbonate production by tectonically induced paleogeographic rearrangement (Middle Miocene, Pannonian Basin): Facies, v. 60, p. 865–881, doi:10.1007/s10347-014-0408-2.

Zámolyi, A. et al., 2017, Latest Pannonian and Quaternary evolution at the transition between Eastern Alps and Pannonian Basin: new insights from geophysical, sedimentological and geochronological data: International Journal of Earth Sciences, v. 106, p. 1695–1721, doi:10.1007/s00531-016-1383-3.